Uzair Maqbool

NUMERICAL ASSESSMENT OF FRICTION DAMPERS UNDER QUASI-STATIC AND IMPACT LOADING

February, 2018

UNIVERSIDADE DE COIMBRA

Numerical Assessment of Friction Dampers Under Quasi-Static and Impact Loading

Author:

Uzair Maqbool

Scientific Supervision:

Professor Doctor Aldina Maria da Cruz Santiago

DEPARTAMENTO DE ENGENHARIA CIVIL

FACULDADE DE CIÊNCIAS E TECNOLOGIA

UNIVERSIDADE DE COIMBRA

ACKNOWLEDGEMENT

ABSTRACT

Steel structures are most widely used form of construction in various types of applications around the globe in recent years. To make the built environment sustainable, steel construction is considered as the nodal intervention in the construction industry. Whereas, in steel frame structures joints are considered to play the most significant role in providing ductility, sufficient rotational capacity and adequate dissipation under extreme conditions. However, the accidental loadings such as blast, fire and impact, may instantaneously causes rupture of the elements that are located within the vicinity of the impact, in some situation leading to a disproportionate failure of structural components or even to the failure of complete structure.

Therefore, to make the built environment safe and to ensure that buildings remain operational and more importantly do not collapse under extreme loading conditions, this work aims at investigating a new innovative design strategy of "FREEDAM" (Free from Damage Connections) connection under accidental conditions. This connection was initially design as a sustainable connection, able to withstand without any damage in the rotation demands due to seismic events.

The response of this type of connections subject to transient dynamic loads is uncertain and yet absent in current design guidelines. Such innovative beam-to-column connections are equipped with friction dampers which are located at the bottom flange level of the connected beam to dissipate the input energy. Therefore, the study addresses the issues by developing a validated three-dimensional finite element model of such a connection under impact and quasi-static conditions. Exploring numerical procedures to simulate non-linear behaviour of friction damper subjected to impact loads, the friction resistance is calibrated by accounting the number of bolts, their diameter and tightening torque governing the preloading. The flexural resistance results from the product between the damper friction resistance and the lever arm.

The friction damper numerical model is used to describe the behaviour of joint; i) "under quasi-static loading" and ii) "under impact conditions" presented in a beam-to-column moment resistant connection. The components of the friction damper are responsible in facilitating the dissipation of induced energy in joints and being able to provide sufficient ductility to a joint. Although, the friction damper model is a less intricate model, compared to the complete joint, yet its frictional behaviour incorporation to a joint's dissipation capacity is quite arduous. Equipped with a failure criterion describing the softening phase of the materials, the FE model

describes the failure modes observed experimentally in the displacing plate of the friction damper. Results exhibited that the transient loads application, induced elevated strain rate in the material, which enhanced the constitutive mechanical properties. Therefore, enabling the friction damper to resist the maximum load observed in quasi-static cases with reduced displacements. Parametric studies show that stiffer friction dampers are less prone to develop elevated strain rates and therefore less keen to strength enhancement; on the other hand, the ductility capacity is reduced for rather flexible dampers comparing the quasi-static with the impact response.

.

TABLE OF CONTENTS

LIST OF FIGURES

European Erasmus Mundus Master
Sustainable Constructions under natural hazards and catastrophic events
520121-1-2011-1-CZ-ERA MUNDUS-EMMC

ruscos

LIST OF TABLES

NOTATIONS

General (Sorted according to appearance)

a_w	Weld thickness
t_f	Flange thickness
t_w	Web thickness
E	Modulus of elasticity
f_y	Yield strength
f_u	Ultimate tensile strength
C_{WH}	Work hardening coefficient
ε	Strain
ε_{h1}	Derived modulus to strain hardening
ε_{h2}	Derived modulus to ultimate
ε_u	Strain at ultimate stress
ε_t	Total strain
σ	Stress
σ_{tru}	True stress
ε_{tru}	True strain
ε_{eng}	Engineering strain
ε_{pl}	Plastic strain
σ_{dyn}	Dynamic stress
σ_{static}	Static stress
$\dot{\varepsilon}$	Average strain rate
ε^n	Strain at the ultimate stress
T^*	Temperature related parameter

C_{steel}	Strain rate sensitivity parameter
η	Stress triaxiality
σ_{EQ}	Equivalent Von Mises stress
σ_H	Hydrostatic pressure stress
ε_0^{pl}	Equivalent plastic strain at the onset of damage
ε_f^{pl}	Equivalent plastic strain at failure
$\bar{u}_f^{pl}$	Effective plastic displacement
L_{char}	Characteristic length of the finite element
L_E	Element size
λ_E	Element type factor
D	Damage scalar variable
K	Stiffness matrix
u	Vector of unknown displacements
F	External force vector
M	Element mass matrix
C	Viscous damping
L_0	Initial gauge length
A_s	Tensile area of a bolt
α, β, γ	HHT algorithm parameters
τ	Period
Δ_t	Time-increment

Abbreviations (alphabetic order)

DIF – **D**ynamic **I**ncrease **F**actor

DLS – **D**amage **L**imit **S**tate

DST – **D**ouble **S**plit **T**ee

EN – **E**uro**n**orm

FEA – **F**inite **E**lement **A**nalysis

FEM – **F**inite **E**lement **M**ethod

FEMA – **F**ederal **E**mergency **M**anagement **A**gency

FFD – **F**ree **F**rom **D**amage

FREEDAM- **Free** from **Dam**age Connections

HHT – **H**ilber-**H**ughes-**T**aylor direct integration method

LVD**T** – **L**inear **V**ariable **D**ifferential **T**ransformer

MRF – **M**oment **R**esisting **F**rames

PEEQ – Equivalent Plastic Strain

RBS- **R**educed **B**eam **S**ection

SLS – **S**erviceability **L**imit **S**tate

SHBT – **S**plit **H**opkinson **B**ar **T**est

ULS – **U**ltimate **L**imit **S**tate

General steel material properties (Szuladziński, 2010):

Material	E GPa	ρ kg/m^3	v	G GPa
Steel	200	7850	0.3	76.92

1. INTRODUCTION

1.1   General Consideration

In past few decades robustness design of a structure was addressed with minor importance, but now due to the increase in frequency of accidental events (Koccaz et al., 2008), the design of structures under extreme loading conditions became of cardinal importance. Due to unexpected conditions such as, blast, terrorist attacks and any catastrophic events, the design consideration under accidental loading conditions became the dire need of the hour. In most of the design codes, these conditions are not addressed properly due to the lack of knowledge of specific conditions and the frequency of the occurrence of the events. In order to evolve the response of structures, their capacity building should incorporate the extended design for the life safety and to ensure the operation even under unforeseen conditions.

Steel Moment Resisting Frames (MRFs) have been extensively acknowledged for their better performance in past. In contrary, it has been observed in recent few catastrophic events, where they were unable to meet the demands (WTC 2001, Ronan Point 1968). Therefore, research for new and innovative techniques to mitigate the structural damages to buildings has attained immense importance recently. Furthermore, the robustness design of MRFs under accidental conditions became the motivation which united agency of resource in order to discern unique solutions aimed at enhancing the capacity in terms of dissipative mechanism of frame structures (FREEDAM, Mid-term Report, 2017).

Under extreme loading conditions, extensive inelastic deformations are expected, which are linked with intense ductility demands concerted in the region of joints within the vicinity of affected structural component in typical steel structures, particularly beam-to-column joints in steel frame structures. After the World Trade Centre (2001) collapse, it was stated that the response of the joint under impact needs to be investigated and evaluated (McAllister, 2002). Therefore, beam-column joints are considered to be the most critical component of the MRFs (Al-Rifaie *et al.*, 2017).

Dissipative zones in steel MRFs are usually located at beam ends where energy can be dissipated and structural elements may suffer significant degradation (Lemos, 2015). However, even if the sole purpose for the damages incurred to the structural components would result for the dissipation of certain amounts of induced energy, it can be prevented. The global technique for performance has been on a shift

towards the development and implementation of efficient damage resisting systems in order to reduce the economic effects of catastrophic incident. However, any probable minor damage may be retrofitted easily and cheaply thus preventing the ultimate collapse of the buildings or major structural components and ensuring effective means to make it immediately operational.

1.2   Motivation

The primary motivation is the European project "FREEDAM" derived from "Free from Damage Connections" was to develop an innovative mechanism within beam-to-column joint in Moment Resisting Frame, in a way that joint will behave to dissipate energy induced due to seismic loading conditions, so that there may not be any significant damage in the structural components of the structure (FREEDAM, Mid-term Report, 2017).

There has been some work done related to robustness design of MRFs, but still there is much to investigate particularly in relation to research interest of this European project. Joints are the most vulnerable elements which play significant role in providing ductility and sufficient rotational capacity for steel frame structures subject to accidental loading conditions; therefore, in order to make the connection free from damage and to ensure sustainable design of buildings, which remains operational even under sever conditions, the design of dissipative assembly becomes the need of the hour.

The inspiration for this dissertation was to figure out the response of the dissipative mechanism under accidental conditions and the formulation of suitable unique dissipative assembly by means of investigation through finite element analysis by calibrating and validating against experimental results. Finally, to conclude with parametric study the appropriate friction damping material along with most effective geometric configuration.

1.3   Objective

The main objective of this work is to study a new type of connection that prevents damage to all other structural components with the exception of the one component of the connection that is specially designed to dissipate the energy by means of the slippage long a friction material. Additionally, the friction component of the joint must fulfill certain requirements, such as: possess a steady performance as well as

provides enough energy dissipation capacity and ductility supply. In order to do that, the friction material must have a decent tribological action.

The above-mentioned study of the connection was proposed as a part of the European project named "FREEDAM", which is a joint venture of several European organizations: The University of Salerno (UNISA) as coordinator, the University of Naples (UNINA), the University of Coimbra (UC), the University of Liege (ULG) and the companies "FIP INDUSTRIALE" and "O FELIZ".

This study principally focuses on two different aspects, on one hand, to fully explore the behaviour of the friction interfaces and normal force acting in the form of preloading of bolts in the different dissipative assemblies; on the other hand, to assess the response of joints that are specially designed to dissipate the input energy due to quasi-static and impact loadings. More specifically, the research tackles on the following objectives:

- The development of a strategy for the numerical modelling of intricate frictional interface. The proposed approach should be able to describe the frictional behaviour of the damper installed in the bolted connection along with the development of stick-slip mechanism.
- Development of a ductile damage model to predict the failure mechanism under quasi-static response.
- Formulation of an appropriate 3D finite element modelling approach for incorporating preloading effect of bolts and development of complete numerical model using the finite elements method (FEM) with Abaqus Software (Abaqus, 2012). Additionally, development of numerical model of connection equipped with the friction interface, when subjected to quasi-static and impact loading conditions.
- Later, calibration and validation of finite element model using experimental result to access the behaviour of joint close to reality, along with the findings discerned from the results.
- Finally, parametric numerical studies are conducted, identifying relevant parameters responsible for the specific behaviour.

1.4   Structure of Dissertation

The complete thesis is outlined over six main chapters. In Chapter 1, the significance of the study herein presented are justified, the objectives of the work, motivation of the study and relation to research project "FREEDAM" are discussed, the methodology adopted is described and the global organization of this dissertation is briefly explained.

Subsequently, Chapter 2, evaluates the current resource in the field of MRF frames designed to have connections with a stable performance under extreme loading conditions and a wide range of energy dissipation capacity. In the end, some of the recent major research work in relation to this topic are discussed.

The Chapter 3 introduces the relevant material characterization required to perform dynamic non-linear analysis of friction dampers under static and impact loads. Material characterization for later use in the numerical model, including the high strain rate characterization with data gathered from the literature, and the damage behavior modelling, are also established.

Chapter 4 describes the fundamental principles required to perform analysis with the finite element method. Particularly, the solution algorithm and finite element selection are explored and the contact algorithm are presented. Later, the chapter focuses on the development of finite element model of the geometry of the friction damper incorporating the dynamic properties in the finite element model. Development of friction interaction and optimum bolt preloading modelling techniques are also included.

Chapter 5 evaluates the validation of the FE model under static and impact loading conditions against experimental results extracted from "FREEDAM" research project. Furthermore, the effects of different damper assemblies and friction materials are explored in a parametric study along with the efficient dissipative mechanism.

Finally, Chapter 6 presents the conclusions of the developed work, its findings, ongoing effort and future work recommendations.

2. LITERATURE REVIEW

2.1 Introduction

Public development and awareness regarding the safety measures have risen drastically in the last few years. Modern extremism has been the major cause for targeting people's working and living environment (as example World Trade Centre, New York, 2001), but there are also unforeseen events such as, accidental explosion, fire, natural disasters or terrorist attacks that may expose structure's vulnerability.

The major incidents mentioned in the Figure 2.1 have diverted the attention on deficiencies in our structural designs, these alarming incidents served to compel for immediate actions to re-examine our existing design strategies for extreme loads.

i) Ronan Point (1968) London-gas explosion (Ronan Point, 1968)	ii) WTC (2001) New York-attack (WTC, 2001)	iii) Setubal, Portugal (2007) Accident (Izzuddin, 2012)
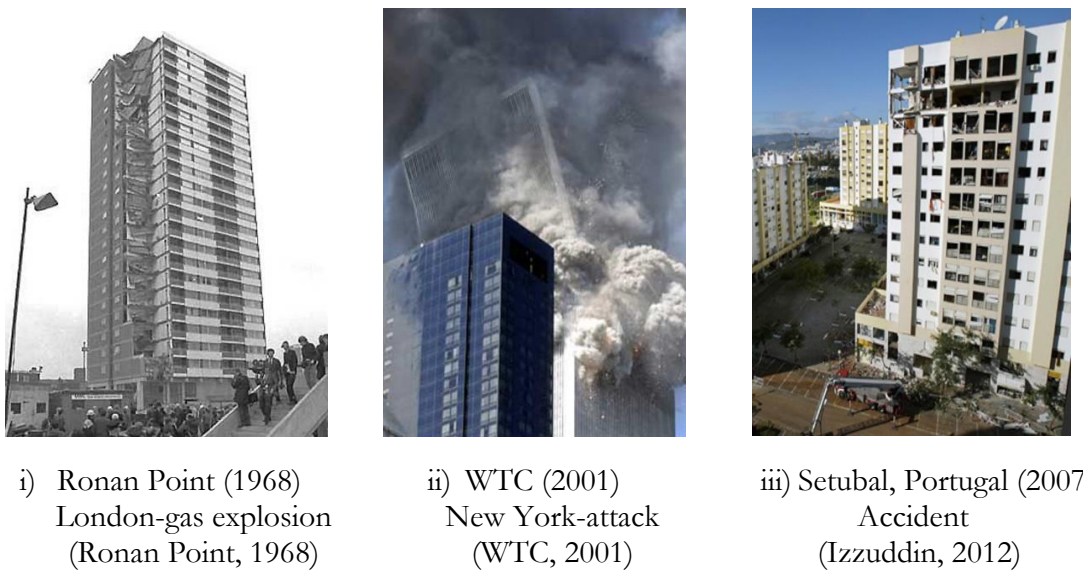
Figure 2.1 - Collapsed structure under catastrophic hazards i) accidental explosion; ii) terrorist attack; iii) accident.

However, some of these events in past led to a phenomenon known as *progressive collapse*, which actually occur due to the failure of primary structural elements, resulting into the collapse of adjoining structural components, ultimately leading to the complete building devastation. The accidental gas explosion of Ronan point (London, 1968) building incident eventually lead to the first approach for structures to be designed for removal of structural components under accidental conditions, with placement of minimum horizontal and vertical tying facilities, issued from the

authorities of UK Building Regulation, in 1970 (Cormie & Smith, 2009). The objective was to prevent any further *disproportionate collapse* of buildings, by integrating measures in the design that can restrict the effect of collapse exactly to its point of application.

In order to avoid disproportionate collapse, the connection performance under abnormal loading conditions should be critically assessed to certify its stability (Arup, 2011), (Cormie and Smith, 2009). Regardless, the real evidences as depicted in past hazardous events, even the recent research studies have discerned, joints behave as the crucial component restraining structural ductility and deformability (FEMA), (McAllister, 2002). However, the current design codes merely provide information on stiffness and resistance of joints under quasi-static loading, (EN 1993-1-8, 2005).

Concerning the response of the complete building, Eurocode 1, (EN 1991-1-7, 2006) defines two different methods to limit the disastrous affects due to accidental conditions. First approach is based on identification of the source of accidental actions, either as internal explosions or external impact due to collision. Where the incident is characterized by an equivalent static force corresponding to the equivalent action affects in the structure. It requires strain rate effects to be considered on the description of the material properties of both, the impactor and the structure. However, on the other hand the second approach is based on restricting the extension of immediate failure. These design strategies should be adapted to the depending upon the importance of the structure according to the Annex B of the EN 1990 (EN 1990, 2002); for highly classified building a "*tie-force-based design*" is suggested to circumvent inconsistent collapse. Furthermore, few design approaches are described in (Cormie and Smith, 2009) namely, the "*key element design*", where a limited number of elements designed to resist severe loads and the "*alternate path method*" in which structural integrity to redistribute the load and provision of alternative load paths are addressed (EN 1991-1-7, 2006).

2.2 Beam-to-Column Joints Progressive Development to Extreme Loadings

Earlier in past, the use of rigid full-strength joint was conventionally considered as the best practice to mitigate the induced energy due to extreme events. Later, prime focus was shifted in providing dissipative zones at the beam ends and put effort to circumvent the plastic engagement within the beam-to-column joints (Mazzolani and Piluso, 1996) (Faella *et al.*, 2000) (Bruneau *et al.*, 1998).

Since past major seismic events, two design strategies have been evolved to augment the plastic rotation capacity of fully welded joints. One method is to enhance the quality of the welding practices, strengthening of critical zones subjected to fracture. The second method is based on the possibility of directing the energy dissipation within the beam, and designing it as dissipative member. This second approach is precisely focused on reducing the bending area of beams by cutting the flanges width in vicinity close to beam-to-column joint as shown in Figure 2.2, the method is known as RBS (Reduced Beam Section) (Moore *et al.*, 1999; FEMA 351, 2000; FEMA 351).
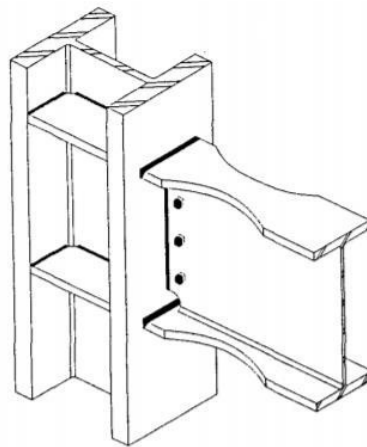
Figure 2.2 – Radius cut RBS moment connection (Moore *et al.*, 1990)

Later, a new system was developed for beam-to-column moment connection in line with a strategy principally focused on using bolts with minimum usage of welds, therefore, preventing shortcomings encountered in in-situ welding. This type of structural system is known as the '*weld free*' system. The mechanical evaluation of this damping system provided a steady seismic response (Koetaka *et al.*, 2004). Furthermore, as a consequence of the above-mentioned research, several types of connections had been proposed which were entirely concerted on the bolted type of joints, precisely articulated for the severe loading conditions. The real evaluation of such connections is very intricate in order to assess the inelastic behaviour of joint due to end-plate, bolts and T-stub behaviour. In addition, for these types of connections impressive work has been done in finite element analysis to evaluate their response.

Then a new design approach, which has been the focus of many studies from last few decades, has gained an increasing interest by researchers in recent years. The design of semi-rigid partial strength connections which can efficiently work for dissipation and provide adequate ductility compatible with the seismic demand. The

component approach (Jaspart, 1991) (Faella *et al.*, 2000) which is the study of semi-rigid steel joints, allows the moment-rotation response. The component method entails the precise classification (stiffness, resistance and ductility) of each active component. These components represent a specific part of a joint that makes an identified contribution to one or more of the structural properties. The Eurocode 3, part 1-8 (EN 1993-1-8, 2005) define strength and stiffness properties for different components that allow the calculation of a wide range of beam-to-column, beam-to-beam and column base joint typologies. Afterwards, the research was inclined on the assessment of the joint ductility (Simões da Silva *et al.*, 2002), (Girão Coelho and Simões da Silva, 2004).

Regarding, the joint ductility, double split tee (DST) is considered to be a great solution that could be simply employed in dissipative semi-rigid MRFs because they are easily replaced, leading to the sustainable design of connections, an essential requirement nowadays (Iannone *et al.*, 2011). Therefore, other researchers, such as Inoue *et al.* (2006), Kishiki *et al.* (2006), Oh *et al.* (2009), and Ramhormoziu and Clifton (2014) have been studying methods related to beam-to-column connections furnished with passive energy dissipation devices.

2.3   Dissipative Joints Equipped with Friction Dampers

The structures which are designed with a concept to withstand severe conditions, need to be facilitated in terms of strength, stiffness and ductility (Grecea *et al.*, 2004). Therefore, three limit states should be considered: Serviceability limit state (SLS) depends upon the stiffness measures; Damageability limit state (DLS) depends upon the ductility measures; and Ultimate limit state (ULS) based on strength criterion.

The innovative connection must be designed to prevent the abrasion of the friction pads under serviceability limit states and to be only triggered under severe loading conditions. Specifically, friction dampers can be used as a facilitator in displacement reducers at serviceability limit states (SLS) and as dissipative elements under ultimate limit states (ULS). Additionally, it is required that the components of the connection and structural elements do not reach a point of plastic engagement and do not under go any damages. The energy dissipation capacity is provided by the movement of the T-stub webs on the friction pads, which are preloaded by means of high strength bolts. Consequently, the slippage force depends on the magnitude of the normal force and on the friction coefficient.

Recently, Latour and co-authors (Latour *et al.*, 2015) introduced a novel type of dissipative concept for beam-to-column connection by using two dampers at the level of both the beam flanges as shown in Figure 2.3(a). Whereas, after the initial testing it was concluded that even the geometrical assembly was symmetrical still its response was asymmetric and the displacements attained on both flange levels were not similar. Therefore, an amendment in configuration of the joint was suggested by introducing only one damper at the lower beam flange level as depicted in Figure 2.3(b). With the second proposed layout, under bending actions, the joint is forced to rotate around the upper T-stub and the energy dissipation is addressed by the slippage of the lower beam flange on the interface of friction materials. Final proposed layout is equipped with additional haunch affixed with dissipative frictional dampers to dissipate the induced energy as represented in Figure 2.3(c). Moreover, with a classical fixed T-stub placed at the upper beam flange, concrete slab damage can also be easily prevented.
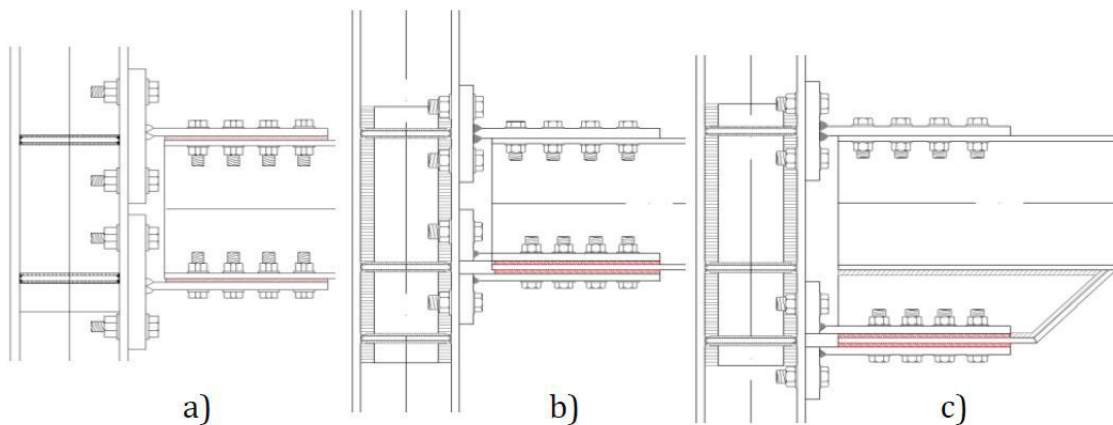
Figure 2.3 - Geometry of the connections (Latour *et al.*, 2014): a) Connection with two friction dampers; b) Connection with only one friction damper; c) Connection with one friction damper and with an additional haunch.

The research work carried out at University of Salerno comprises of two main programs. Initially, study was intended to characterize various frictional interactions, later, the same materials were used with the aim of energy dissipation in the DST joints. For the first part of the program, in order to accurately classify the tribological behaviour of the friction elements, several damping assemblies were subjected to static tension loading conditions (Latour *et al.*, 2014.a, b and Latour *et al.*, 2015). The tested specimens were constituted by an interface of a friction material overlaid between two plates made of S275 JR structural steel. Whereas to facilitate the relative movement of the plates over the friction material, the moveable inner plate was

equipped with slotted holes. The geometry of the tested specimens is depicted in the Figure 2.4
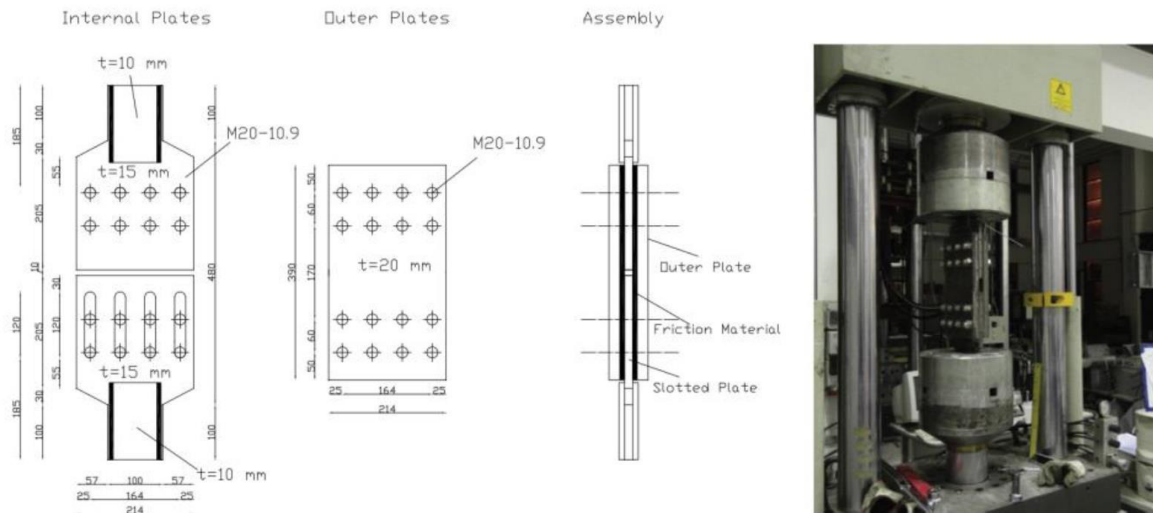
Figure 2.4 - Scheme of the specimen's geometry (Latour *et al.*, 2015).

Some parameters were changed during the experimental procedure in order to account for their influence on the friction coefficient and on the cyclic response of the specimen. These parameters were: the number of tightened bolts, the friction interface, the thickness of the friction interface, the tightening torque and the type of washer. Regarding the last variable, circular flat steel washers and cone shaped annular steel disc spring washers were analyzed.

In order to evaluate the influence of the friction material, the following interfaces were subjected to analysis: steel on steel; brass alloy on steel; sprayed aluminum on steel; rubber material M0 on steel; rubber material M1 on steel; and rubber material M2 on steel. The rubber materials are detailed in Latour *et al.*, (2014.b).

Tests were executed in the Universal Testing Machine, performed in order to obtain both static and kinetic friction coefficients, by varying the clamping force in a range suitable for structural applications. To do so, the experiments were executed in the Universal Testing Machine.

Further studies on the latter connection were proposed in the European project "FREEDAM".

2.4 Joint Behaviour Under Impact

Initially the study of steel connections subjected to dynamic loading conditions were mainly focused on seismic behaviour of the steel moment-resisting connections. However, since the September 11, 2001 incident, the concern for the impact loading condition became a serious issue over the sustainable construction of the building. Initially, Sabuwala and co-authors evaluated the performance of fully restrained steel joint by developing 3D finite element model to assess the behaviour of the joint under blast loading conditions (Sabuwala *et al.*, 2004). The studied connections were part of AISC Northridge Moment Connection Test Program (Report for AISC, 1994).

Lately, dynamic behaviour of single-sided bolted steel connections has been tested at the University of Sheffield. They developed a test rig used to carry out experimental testing of connection under high loading rates to assess their dynamic response (Davidson *et al.*, 2011). Three types of connections have been assessed; flexible end-plate joints (FEP), web-cleats angles joints (WC) and fin-plate joints (FIN). For flexible end-plate joints and fin plates joint, in general, as the rate of loading increases, the connections response becomes stiffer, reach a higher ultimate load and become less ductile. Furthermore, flexible end-plate joints tend to show more symmetrically failure modes when statically loaded. In addition, for higher thickness of the plates, the connection tends to show different failure modes for static and dynamic loading. However, for angle web cleats joints the influence of high strain rates are not significant (Rahbari *et al.*, 2014).

University of Coimbra also developed a test rig (Barata *et al.*, 2014). To carry out an extensive experimental program on the behavior of a T-stub component (Figure 2.5) under impact tangential loading and on single-sided end plate joints. For the T-stub, lower ductility and higher resistance was found from the impact tests when compared to the quasi-static ones; for the end-plate joint under impact loading, a reduction in the ultimate rotation of the joint, an increase of the plastic moment resistance and maximum resistance of the joint was observed. For both T-stub and end-plate joint, the failure mode mechanisms have been the similar for quasi-static tests and impact tests.
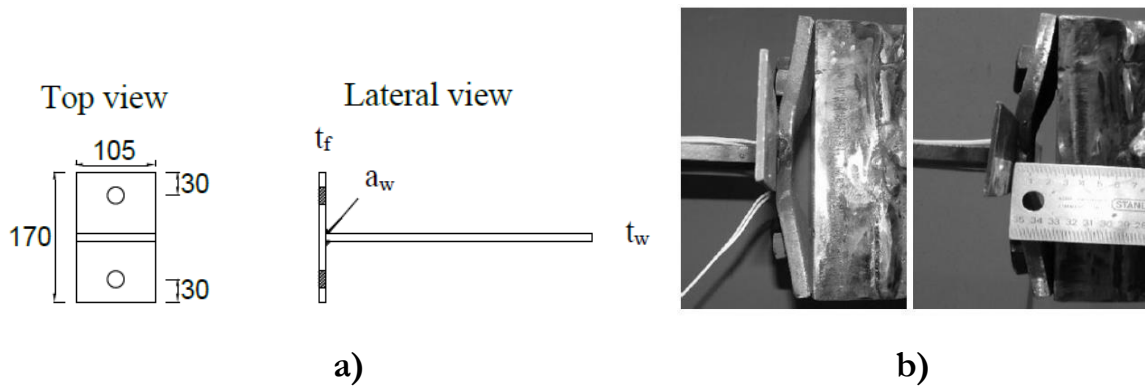
Figure 2.5 - T-stub component (Barata *et al.*, 2014): a) geometry, b) after impact loading

To increase the knowledge on the behaviour of connections exposed to severe loading, a double-sided beam-to-column connection assembly was tested at quasi-static and impact loading rates (Grismsmo *et al.*, 2015). The test specimens involved of H-section beams and columns, extended end-plates, and high-strength bolts. In both the quasi-static and impact tests, the fracture modes were bolt failure along with plastic deformation of the end-plates. Whereas, it was concluded that the connections absorbed significantly more energy before failure in the dynamic tests than in the quasi-static tests, partly due to changes in the deformation criteria at high loading rate. Also, the ductility of the joints seemed to increase for higher loading rates. Furthermore, the failure mode of the joint was not affected by the loading rate of the test.

2.5   Numerical studies on beam-to-column joints

Finite element modelling of structural component has been a common practice of mathematical approximation to evaluate the behaviour of diverse phenomena by altering model's characteristics with reduced cost. Due to the drastic increase in the computational capacity, finite element analysis has become a primary tool in providing solution to intricate structural phenomenon.

From last few decades, the performance evaluation of particular structural elements such as connections exposed to dynamic loading; cyclic loading, accidental loading and fire hazards has been under the prime focus of research studies for the last few decades by using finite element models. Primary objective of this research was to develop a calibrated model that truly depicts the experimental test results, and further assist in discerning the additional information by vary the parameters without having performed the actual experimental tests.

Regardless of the benefits of computational modelling particular to structural assessment and the detail information it ascertains to researchers, but still accurate finite element modelling is a laborious work which requires an extensive amount of knowledge to validate the model which accurately represents a real physical model.

Numerical simulation of steel connections has experienced a great development after the Bursi and Jaspart (Bursi and Jaspart, 1998) published their work focusing on basic issues encountered in simulation of extended end plate connections. In their study, an authentic procedure for the analysis of end plate moment resisting joint is established and an accurate 3-D finite element modelling technique is developed. Finite element modelling software ABAQUS is used effectively to simulate the response of moment-rotation effect of bolted joints with extended end-plate subjected to monotonically increased displacements. Standard tests were conducted to establish constitutive relationships, step increment size, number of integration points, kinematic descriptions and study the effects of different finite element types and discretization. The models included different constitutive laws for the flange, web, welds and bolt shank and simulations were conducted with elements C3D8, C3D8R, C3D8I. Finally, a three-dimensional non-linear FE model optimum for accurate analysis of extended end plate joint was proposed and validated.

Several numerical studies on T-stub component under monotonic loading have been developed during the last decade. In 2002, Swanson and Leon used ABAQUS software to perform a finite element analysis considering complex contact interface, non-linear material behavior and geometric characteristics (Swanson & Leon, 2002). Although good results in describing the experimental behavior can be attained with three-dimensional model but still due to the extensive computational cost in developing correct 3D model, a 2D simplified model was established to inculcate the effect of different pre-load levels in the bolts. The final results exhibited that initial stiffness is comparatively improved with increased pre-load force, but the ultimate failure load remained the same.

Experimental tests and numerical studies on welded T-stub component were conducted by Girão Coelho. In order to evaluate the advantages of designing steel-frame buildings with partial strength and semi-rigid joints (Girão Coelho and Simões da Silva, 2004) (Girao Coelho, 2013); several material and geometrical parameters were assessed. The FE models built using LUSAS provided accurate response of the T-stub behaviour up to fracture. The results showed that: (i) the deformation capacity primarily depends on the plate/bolt strength ratio and, (ii) the final collapse is governed by brittle fracture of the bolts, welds, or cracking of the flange near the weld toe.

Recently, numerical studies on the response of T-stub component subjected to quasi-static loading and impact loading have been carried out at University of Coimbra by Joao Ribeiro and Co-authors as part of National research project "ImpactFIRE" (Ribeiro *et al.*, 2014) (Ribeiro *et al.*, 2015). The behaviour of joints subjected to transient loads is uncertain and is not supported by current design strategies. A study was presented, which addressed these uncertainties by proposing a validated finite element model and establishing an analytical approach to assess non-linear response of the T-stub model exposed to impact loads. Welded T-stub with flange thicknesses of 10 and 15 mm (S335) bolted with M20's (8.8) are considered.

The T-stub model is used to describe the behaviour of components i) "column flange in bending" and ii) "end-plate in bending" present in a beam-to-column bending resistant connection. These components are responsible for the behaviour in the tension zone of joints, being able to provide ductility to a joint. The T-stub model is therefore a less complex model, when compared to a whole joint, yet it drives a joints' ductility capacity. Supplemented with a failure criterion describing the softening phase of the materials, the FE model captures the failure modes observed experimentally. Results show that the short transient loads applied induce elevated strain rates in the material enhancing its constitutive relationship, and therefore, enabling the T-stub to resist the maximum load observed in quasi-static cases with reduced displacement. Parametric studies show that stiffer T-stubs are less prone to develop elevated strain rates and therefore less keen to strength enhancement; on the other hand, the ductility capacity is reduced for rather flexible T-stub (T-10) comparing the quasi-static and the short transient dynamic response. The simplified approach established in the Eurocode to predict the resistance of T-stubs and a non-linear analytical model available in the literature, able to describe the post-limit regime, are improved to account for elevated strain rate effects. Once the non-linear routine was programmed, it allows faster derivation of the response than building finite element models.

Lemos and Co-authors, carried out an extensive investigation on an innovative type of connection proposed under the European Research program named "FREEDAM" (Lemos *et al.*, 2015). In order to ensure the buildings do not collapse even under strong seismic hazard the program focused to develop a new friction component dissipation mechanism employed within the beam-to-column joints in Moment Resisting Frames, which allow to release the induced energy of a catastrophic event by means of slippage of a friction damper material, without any damage in structural components. The study focused on developing three-dimensional numerical model of friction dampers subjected to monotonic tangential

loading and cyclic loading conditions using numerical software ABAQUS. The numerical modelling proposed a strategy for incorporating intricate frictional behaviour. Different frictional material along with varying geometrical configuration were assessed to conclude an optimum and best fit solution for the dissipative mechanism. Lastly, the complete beam-to-column connection equipped with friction dampers where assessed under monotonic and cyclic loading.

2.6 FREEDAM Research Project

FREEDAM research project (FREEDAM, Mid-term Report, 2017) aimed at development of a state-of-the-art design approach whose objective is to develop connections which are capable enough to sustain without any damage induced as a result of destructive seismic events. This type of new beam-to-column joints are facilitated with friction dampers located at the bottom flange of the beam at the junction of beam-to-column to dissipate the seismic induced energy. Till the mid-term report of the research properties of 8 different material for friction dampers have been investigated.

This novel approach is the transformation of the typical DST (Double Split Tee) connection by exchanging the bottom tee component with a friction device composed by an assemblage several of angles and pre-loaded friction pads, situated in an additional haunch which is equipped with slotted to permit the slippage of the friction damper as represented in the Figure 2.6.Under bending actions, the geometry offers the joint to rotates about the upper T-stub which allows the energy dissipation facilitated by the sliding of haunch flange on the friction pads. Therefore, making certain that under frequent and catastrophic events the only effected part are the friction pads.
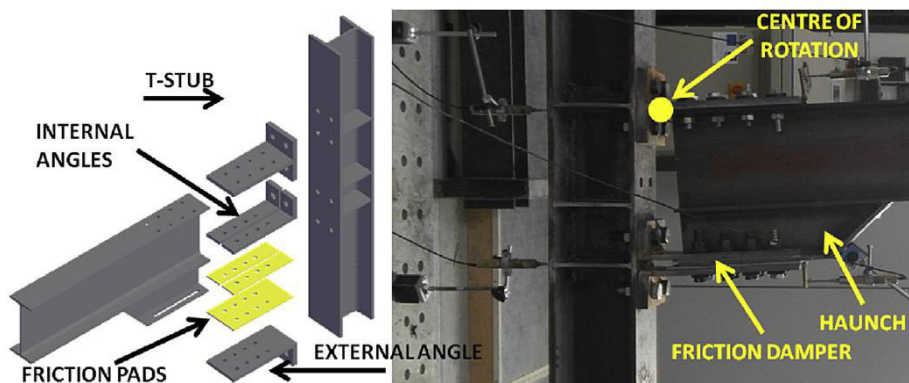
Figure 2.6 - FREEDAM Connection (Santos *et al.*, 2017)

Overall the research work on FREEDAM project can be comprehensively summarized into five work packages; The first work package (WP1) primarily focuses on the tribological characterization of material for friction dampers, which involves both static and impact testing along with the FEM simulation for the justification. The second package (WP2) emphases on the seismic response of beam-to-column joints equipped with frictions pads, which considers both the external and internal joints along with the finite element modelling. Also, the development of design guide for specifically these types of joints. The third work package (WP3) deals with seismic response of frames with friction joints, robustness and sustainability. The aim of this package is to carry out the impact test and verify the robustness of these joints. In addition, analysis of the design of 3D building mock-up. Then fourth work package (WP4) concentrate on development and fabrication of prototypes for industrial production. At last, the fifth work package (WP5) concludes the experimental analysis of a prototype building and dissemination of results.

The experimental testing was divided into work packages, which includes cyclic tests at low and high velocity, long term tests and impact tests, performed to identify the most appropriate friction material for damping. Regarding the cyclic tests, the results showed stable hysteresis response under cyclic loads (Lemos, 2015). Furthermore, till the mid-term report also a FE model for simulating the force-displacement conduct of the friction dampers has been developed. These models have been sequentially extended to the modelling of FREEDAM connections subjected to seismic loads. Although, most of the work is still in progress, the project is scheduled to be completed by the end of this year (FREEDAM, Mid-term Report, 2017).

3. MATERIAL CHARACTERIZATION

3.1 Introduction

In this reach work, finite element model of friction damper components, representative of the beam to column joint as dissipative member, were developed with an objective of energy dissipation behaviour under dynamic loading. Additional information is required regarding the characterization of each component, in order to accurately assess the behaviour at elevated strain rate. Typically, the description of the behavior of each component is defined by a force-deformation curve, which is either obtained from experimental tests or from numerical or analytical models. This chapter describes in detail the material properties required to characterize the behaviour of the joint and how to incorporate them for finite element assessment. Material properties were obtained from the coupon tests of the components carried out at University of Coimbra under FREEDAM project (FREEDAM Mid-term Report, 2017), which will be used for the calibration of model and also in the validation of results. In order to gain the necessary confidence in the model's response, average mechanical properties of components determined by quasi-static tension test were incorporated. Furthermore, uniaxial tensile response of the material is assessed by numerical approach along with the development of damage model.

3.2 Material Properties

The primary focus of this study is to evaluate the robustness of the suggested friction dampers, which eagerly proved the necessity to conduct the coupon tests for all the components of the assembly. Mild steel is macroscopically assumed as an isotropic material. Its inherent characterization, for most engineering applications, can be obtained through quasi-static tension tests, from which the elastic behavior (E) of the material along with the yield point (f_y) and the ultimate strengths (f_u) can be easily gathered. Following, were the listed components of the assembly and the method of material characterization which was necessarily used to extract their engineering properties.

1. External Plates S275JR (Experimental Testing)
2. Friction Pads (Friction Shims) S275JR (Experimental Testing)
3. Internal Stainless Plate AISI304 (Experimental Testing)
4. Bolts M20 – Class 8.8 (Experimental Testing)
5. Bolts M20 – Class 10.9 (Tri-linear stress-strain curve method)

3.2.1 Static Testing

Quasi-static uniaxial tension tests were conducted in accordance to the standard EN 10002-1 (EN10002-1, 2001) on a Universal Tensile Machine. Displacement control testing has been carried out at a reasonably slow rate (0.01 mm/s) in order to inculcate the static response of the steel plates. Tensile coupon tests for each component of the friction damper, namely friction pad (S275JR) steel plate, internal stainless (AISI304) steel plate and external (S275JR) steel plate were conducted. These mild steel specimens have been collected from the same steel batch as the material used to prepare the tested friction dampers. Figure 3.1 depicts the stress-strain curves obtained from the tensile coupon tests for each component of the friction damper (Santos *et al.*, 2017).
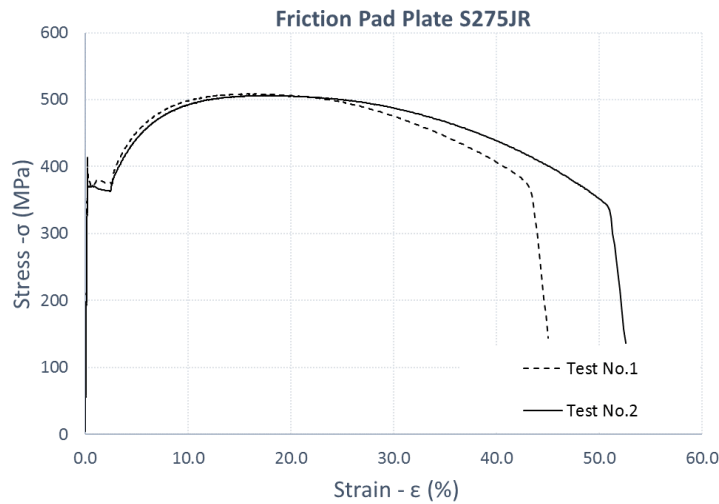
a)
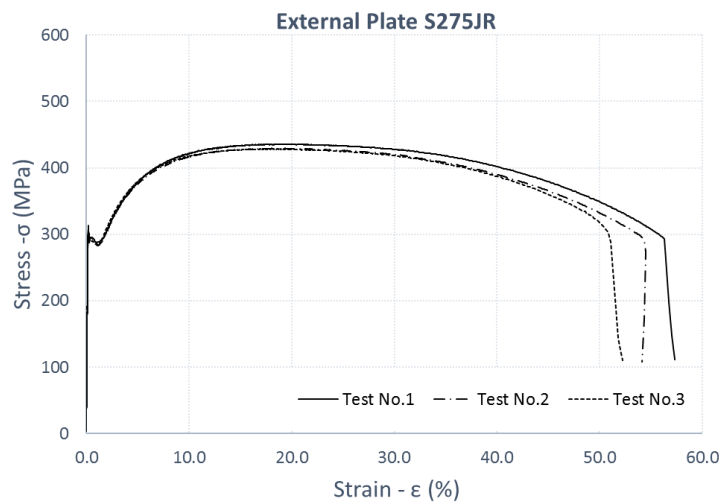
b)
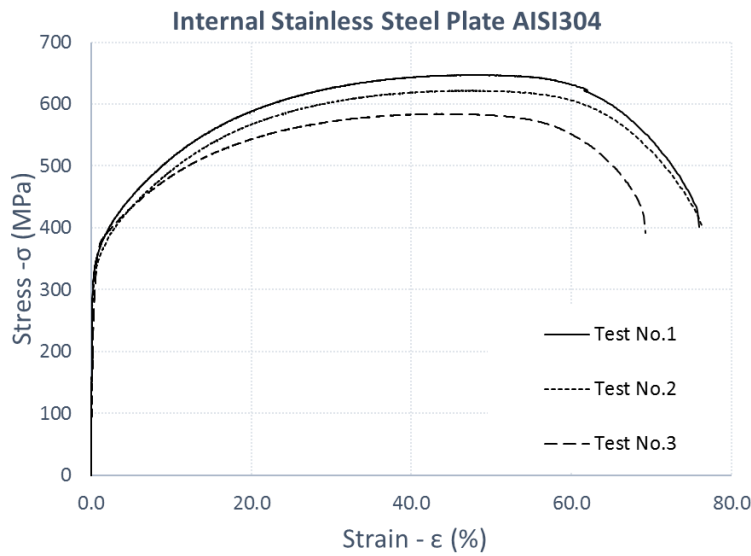
c)

Figure 3.1 - Engineering stress-strain curves: a) External plate (S275JR); b) Friction pad (S275JR); c) Stainless plate (AISI304) (Santos *et al.*, 2017)

Considering as example the stress-strain relationship for mild steel S275JR; it can be observed in Figure 3.2 that the response exhibits initially, a linear elastic development up to the yielding point where the elastic strength (E) is defined; afterwards the response is inelastic, meaning that the deformation is no longer recoverable, and the relationship becomes non-linear. This strain hardening phase is characterized by large deformations accompanied by the strength increase up to ultimate tensile strength (f_u). From this point onwards, the specimen undergo reduction in its area due to the growth and coalescence of voids, visible through necking of the cross-section until fracture occurs; this phase of the stress-strain relationship is often referred to as the softening phase.
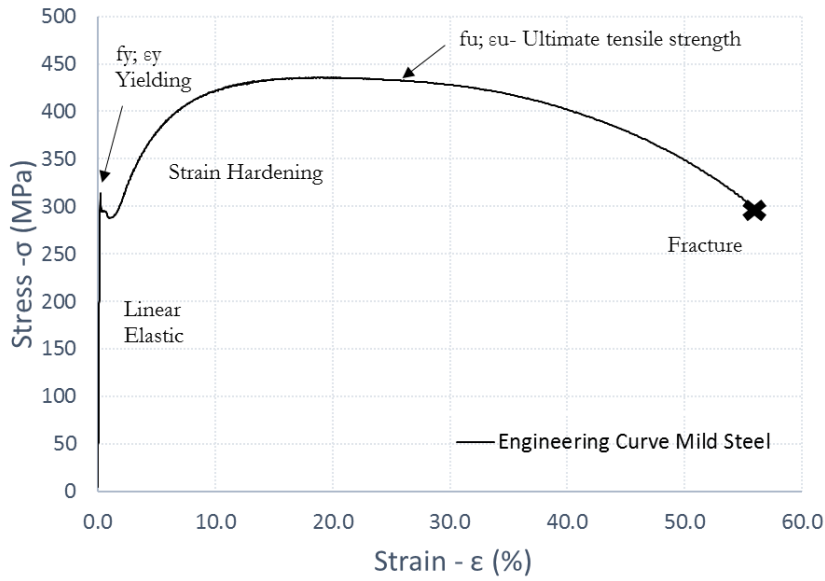
Figure 3.2 – Engineering Stress – Strain Relationship for Steel - S275JR

The Figure 3.3 exhibit the engineering stress-strain curve of the M20 bolt grade (8.8) obtain from the coupon test conducted at University of Coimbra (Ribeiro *et al.*, 2014) which presented a less ductile behaviour compare to the mild steel, as well as the absence of the yielding plateau.
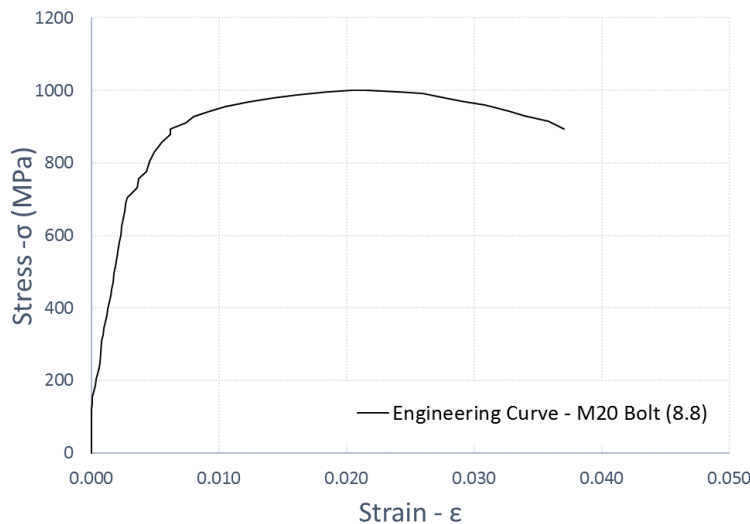
Figure 3.3 - Engineering Stress-Strain Curve Bolt M20 (8.8) (Ribeiro *et al.*, 2014)

3.2.2 Summary of Material Properties

To avoid the variance and uncertainties incurred in the coupon test results, mean value of the results is used to incorporate material properties in finite element model. The Figure 3.4 represents the conversion of test results into average results. Table 3.1 gives the average results of all the components from the test campaign.
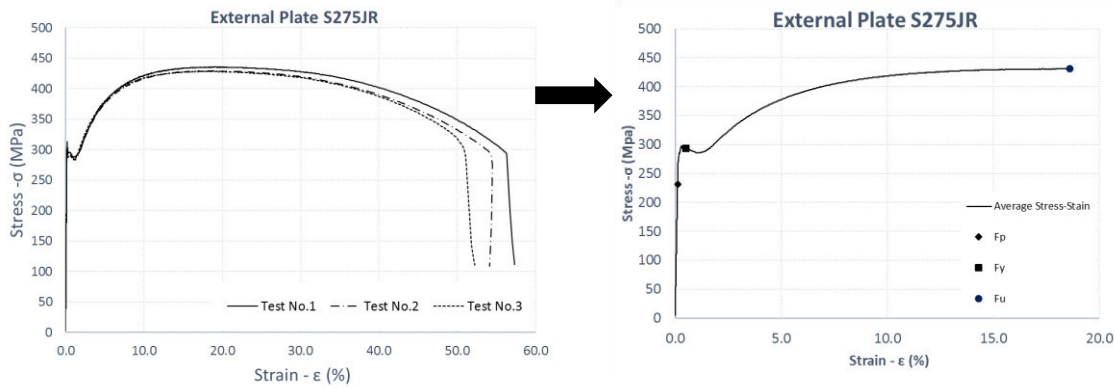
Figure 3.4 - Conversion of test results into average values

Table 3.1: Material Properties from Uniaxial Tension Test

Description	Material	E [GPa]	f_p [MPa]	f_y [MPa]	f_u [MPa]	ε_u [%]	ε_t [%]
Stainless Plate	AISI 304	181.76	-	302.83	617.9	45.80	73.82
External Plate	S275JR	197.67	234.90	291.72	431.31	18.58	54.55
Internal Plate	S275JR	198.13	299.76	374.01	507.49	16.96	47.09
Bolt (M20)	8.8 Gr	213.5	-	721.3	1002	2.3	3.75

3.2.3 Tri-Linear Stress-Strain Curve (Bolt 10.9)

M20 Bolt properties of grade 10.9 were not available from the coupon tests; therefore, in order to simulate the material non-linearities, tri-linear stress-strain curve is used. The tri-linear stress-strain model employed for the material behaviour is represented in Figure 3.5 (Tsavdaridis and Papadopoulos, 2016). The elastic Modulus for the elastic part (a) is $E = 210,000$ MPa and Poisson's ration, $v = 0.3$. The remaining two inelastic parts signifies the strain-hardening conduct of the material under tension loading with reduced stiffness:

- Part (b): $E_{h1} = E / C_{WH}$, with C_{WH} is the work hardening coefficient which is found to be equal to 50 from (Diaz *et al.*, 2011).

- Part (c): $E_{h2} = E_{h2}/10$, so as to avoid convergence shortcoming during the investigation.
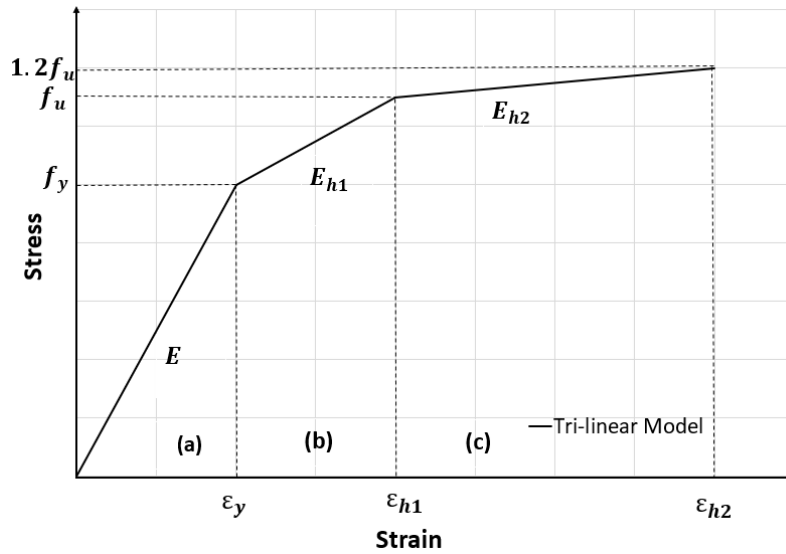
Figure 3.5 - Material tri-linear stress-strain curve (Tsavdaridis and Papadopoulos, 2016)

Strains ε_y, ε_{h1} and ε_{h2} were derived for each material using their yield and ultimate strengths and the corresponding Moduli of each region. The stress-strain curves for the M20 bolts class 10.9 is shown in the Figure 3.6.
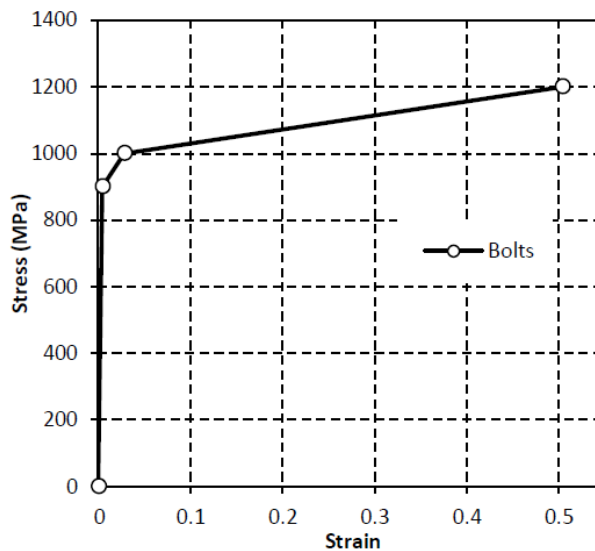
Figure 3.6 - Graphical representation of the bolt's stress-strain tri-linear curve (M20 Class 10.9) (Tsavdaridis and Papadopoulos, 2016)

However, later the bolt properties were calibrated according to the experimental results.

3.3 True Stress – True Strain

The engineering stress and strain are the original (measurement) dimensions of specimen which is represented by the curves obtain from the coupon test. However, length and cross-sectional area changes in plastic region therefore, to incorporate the material properties true stress and plastic strain are required. True stress is defined as instantaneous force acting on the instantaneous cross-sectional area. It is considered as the rate of instantaneous change in length. True stress-strain is used for accurate definition of plastic behaviour of ductile materials by considering the actual dimensions at specific instance. Because engineering Stress-Strain curve is based on original area, it descends after the maximum load as load bearing ability of the sample decreased due to reduction in area; while true stress – true plastic strain curve continues to go up till fracture as it based on actual area. All FEA simulations need to define True Stress – Strain curve.

Converting engineering stress into true stress:

$$\sigma_{tru} = \sigma_{eng} \left(1 + \varepsilon_{eng}\right) \tag{1}$$

Then, transforming engineering strain into true strain:

$$\varepsilon_{tru} = ln \left(1 + \varepsilon_{eng}\right) \tag{2}$$

Finally, changing true strain into true plastic strain:

$$\varepsilon_{pl} = \varepsilon_{tru} - \frac{\sigma_{tru}}{E} \tag{3}$$

Figure 3.7 represents the conversion of engineering stress-strain curve into true stress – plastic strain curve.
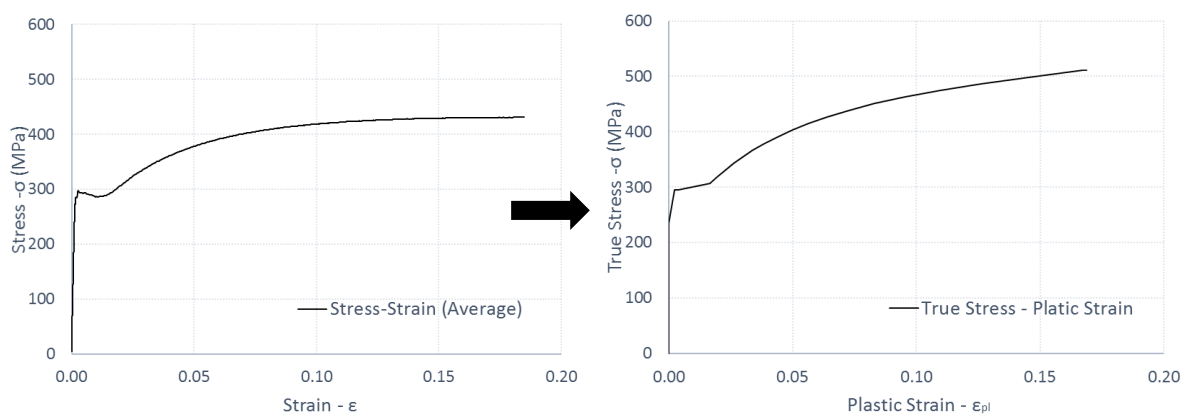
Figure 3.7 - Conversion of engineering curve into true stress – strain

3.4 High Strain-rate

Strain rate is defined as the variation in deformation of a material with respect to unit time. In order to evaluate dynamically loaded structures more precisely, it is essential to know the mechanical properties of the materials involved at the elevated strain rates to which the structural components are subjected. It is well known that the mechanical properties of most ductile materials are dependent to some extent by strain rate; as example, mild steel is known to have its flow stress affected (Nemat-Nasser, 1994). The effects of different strain rates on the stress-strain relationship of steel are illustrated in Figure 3.8. These true stress-logarithmic strain curves were obtained from an experimental campaign carried out at the University of Coimbra, using a Compressive Split Hopkinson Pressure Bar (SHPB) for the dynamic tests and the quasi-static tests. For the dynamic tests, an average strain rate around $\dot{\varepsilon} = 600 \text{ s}^{-1}$ was applied (Saraiva, 2012).

Relative comparison between quasi-static and high strain-rate results clearly depicts that:

i. Elastic modulus (E) of the material is independent of the loading rate,
ii. Yield strength (f_y) and ultimate strength (f_u) at elevated strain-rate approximately increased up to 1.5 times the results obtained at quasi-static loading,
iii. Ultimate strain on fracture (ε_u) is also decreased.
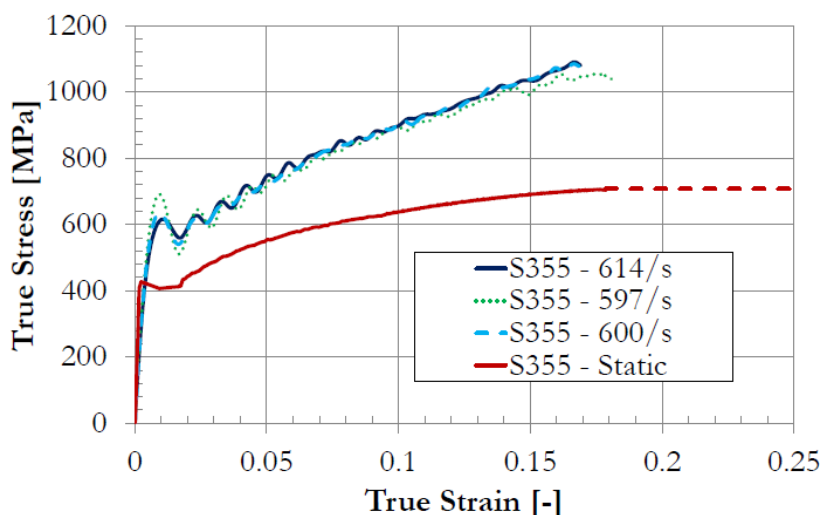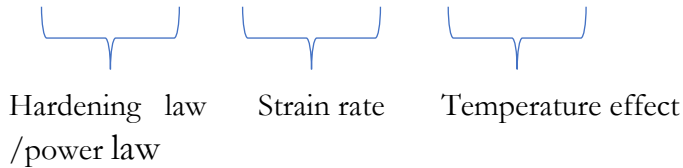
Figure 3.8 - True stress – plastic strain relationship of steel under high-strain rate for plate S355 (Saraiva, 2012)

A simplified way to consider high strain rate enhancement in the stress-strain material law is to adopt a dynamic increase factor (DIF), given by the relation (Eqn.4) of the dynamic strength, σ_{dyn} to the strength obtained under static conditions, σ_{static}:

$$DIF = \frac{\sigma_{dyn}}{\sigma_{static}} \qquad (4)$$

Finite element models aiming to simulate the behaviour of structural elements when subject to impact loads require a constitutive law representing the behaviour of materials for a range of strain rates. Amongst the most popular are the purely empirical Malvar model (Malvar and Crawford, 1998), Cowper-Symonds model (Cowper and Symonds, 1957) and Johnson–Cook model (Johnson and Cook, 1983). The latter accounts for the strain rate dependency and thermal softening behavior to establish the plastic behaviour. Its constitutive law assumes that the slope of flow stress, is independently affected by each of the mentioned variables.

$$\sigma = [(A + B\varepsilon^n).(1 + Cln\varepsilon^*).(1 - (T^*)^m)] \qquad (5)$$

Hardening law /power law Strain rate Temperature effect

Where: A is the yield stress, B is strain hardening parameter, n is the strain hardening exponent, C is the strain rate sensitivity parameter, m is the temperature exponent, ε is the accumulated plastic strain, $\varepsilon^* = \varepsilon/\varepsilon_0$ is a dimensionless strain rate and T^* is the dimensionless quantity depend upon the working temperature, room temperature and melting temperature, respectively.

The strain rate dependency for mild steel plates is determined using the second term of the Johnson-Cook's law which is stimulated by high strain rate and the experimental results gained from SHBT (Saraiva, 2012), the strain rate sensitivity parameter calculated is $C_{steel} = 0.039$ for the strain rate 600 s⁻¹. The strain rate dependency for bolt's material is accounted using earlier research. The impact tests carried out on A 325 bolts which were collected from the WTC debris exhibiting very low sensitivity to strain rate (Ellingwood, 2007) therefore, Chang and co-authors mentioned is their work that a dynamic increase factor $DIF_{bolt} = 1.1$ may be considered for the bolts (Chang et al., 2011). These values are initially employed in the current study, thus later the dynamic increase factor is being adjusted based on the experimental results obtained from the friction damper testing under static and impact loadings.

3.5   Tenacity and Toughness

Tenacity is defined as the amount of energy need per unit volume to cause breakage. The ability of a material to engross energy and deform plastically before going into rupture. This property plays an essential role in shock-absorbing potential of a structure. Thus, tenacity and toughness of a material can be described as the vicinity under the plastic zone of the stress-strain curve. Brittle materials have comparatively low toughness than ductile material (Dias da Silva, 2006). Mild strength steels, shown in red color in Figure 3.9, clearly depict the onset of yielding zone along with an evident visible zone of plastic deformations in the stress-strain diagram (Dias da Silva, 2006); whereas the absence of plastic deformation region eventually leads to a rather brittle behaviour.

The Eurocode provides assistance regarding the choice of the material to prevent any stiff response as a function of temperature. The characterization must be accomplished through Charpy and/or Izod impact tests on notched specimens measuring the breaking energy for a given temperature (EN 1993-1-10, 2005). The temperature dependence reduces as the material is exposed to elevated strain rate, so it can be clearly discerned that a better-quality steel should be employed in structures when high strain rates are imposed.

The developed numerical model, however, does not take any variability of the material toughness into account although elevated strain rates are expected. The stress strain relationship is merely enhanced following the dynamic increase factors presented in the previous section, and the damage modelling (next section) is not fitted to account for variability of the material toughness to the strain rate.
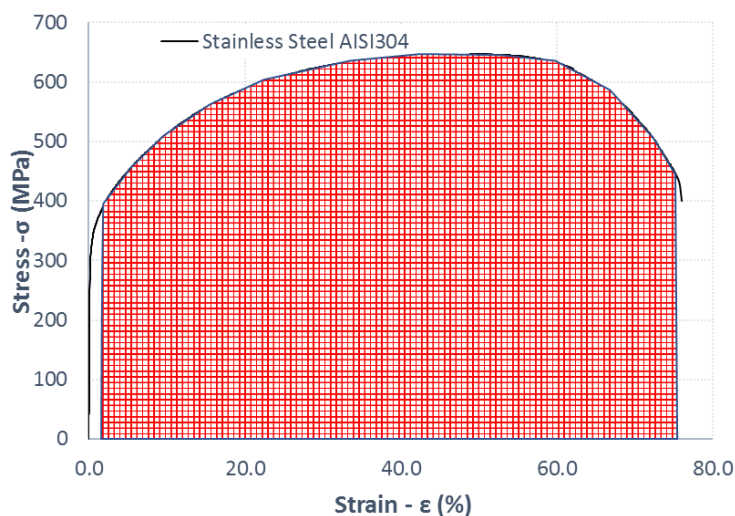
Figure 3.9 - Material toughness

3.6   Damage Consideration

The design of structures under severe loads demands to avoid the risk of failure. The failure of metals is an intricate phenomenon which often attributed with a term fracture. Most of the metals depict different types of mechanical failure i.e. fatigue, cleavage and ductile fracture. Materials which depict elastic-plastic behaviour when subjected to monotonic loading followed by the progression of isotropic hardening as for example the mild steel under quasi-static loading, then the failure of that material is categorized by a ductile fracture mechanism (Lemaitre, 1992). The stress-strain curve can be classified by ductile fracture when it yields from void nucleation followed by their growth and coalescence (Anderson, 1995).

ABAQUS provides an overall ability for simulating progressive damage and failure in engineering structures. Failure of a specimen means, the complete loss of load carrying capacity that results from the progressive degradation of the material. The progressive damage and failure of a component depends on the material definition as represented in Figure 3.10:

- Undamaged constitutive behaviour (e.g., the true stress- plastic strain)
- Damage initiation (point A)
- Damage evolution (from A-B)
- Choice of element removal (point B)
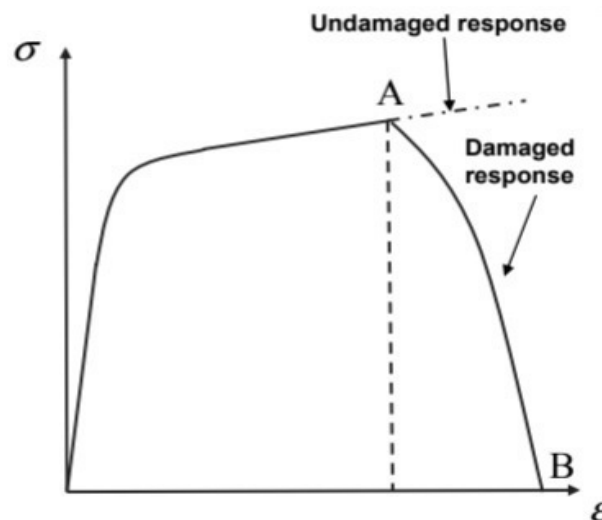
Figure 3.10 – Typical material response depicting progressive damage

Damage initiation criteria for ductile metals is based on the consideration of two key pertinent operations which can impart degradation of stiffness. First, the ductile

rupture principally occurs due to the nucleation seeding, and on the other hand shear fracture due to the localization of shear band. For this study, only ductile fracture model is incorporated, which considers that the equivalent plastic strain at the onset of the degradation is relying on the strain rate and stress triaxiality

$$\text{Stress triaxiality } \eta = \sigma_H / \sigma_{EQ} \tag{6}$$

Where: σ_H is the hydro static pressure and σ_{EQ} is the equivalent Von Misses stress

The ductile criterion can be defined with the Von Mises, Johnson-Cook, Hill, and Drucker-Prager plasticity models including equation of state. Hooputra and co-authors (Hooputra *et al.*, 2004) proposed the formulation of the failure models to depict the initiation of damage; it is already accounted in the numerical software ABAQUS (Abaqus, 2012).

Figure 3.11 presents the characteristic stress-strain behaviour of a material undergoing an impairment; the dashed curve denotes a basic material response without damage definition, whereas the solid line corresponds to the damaged stress-strain correlation. In this Figure 3.11, ε_0^{pl} is the equivalent plastic strain at the onset of damage, while ε_f^{pl} is the equivalent plastic strain at failure (Abaqus, 2012).
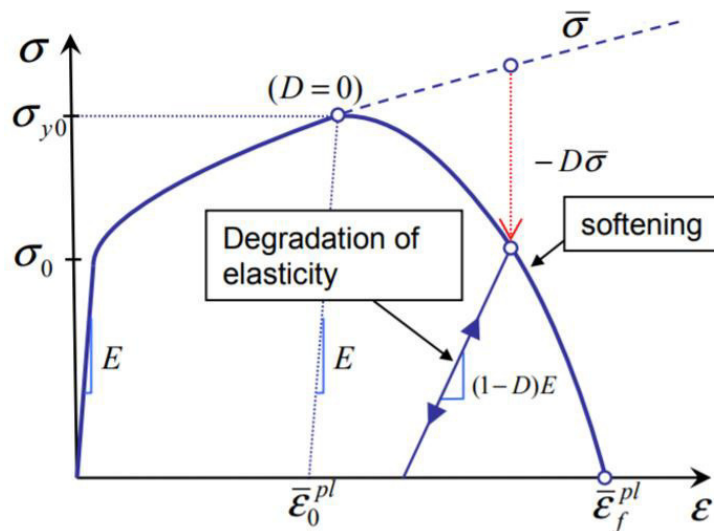
Figure 3.11 - Stress-strain curve with progressive damage degradation, adapted from (Abaqus, 2012).

In order to inculcate the actual response of the specimen assuming the load application is comparatively slow for a quasi-static analysis, strain rate can be exempted and material behaviour should incorporate the ductile failure modelling.

Therefore, an approach allows the setting of the equivalent plastic strain at the damage initiation, ε_0^{pl} for the stress triaxiality ratio for pure tension of $\sigma_H / \sigma_{EQ} = 1/3$. The equivalent plastic strain for other triaxial stress states have been interpolated along with the strain rate dependency, following the Eqn.7 included in the ductile damage failure model by Lemaitre (Lemaitre, 1992).

$$\bar{\varepsilon}_0^{pl}(\theta) = \bar{\varepsilon}_n^{pl} Exp[-1.5 . (\theta - 1/3)] \qquad (7)$$

Where: ε_n^{pl} is defined as true plastic strain at the very beginning of necking phenomenon obtain from the experimental coupon test results.

Finally, damage initiation criterion is established for the stainless steel (AISI304) plate as shown in the Figure 3.12 using the coupon test results.
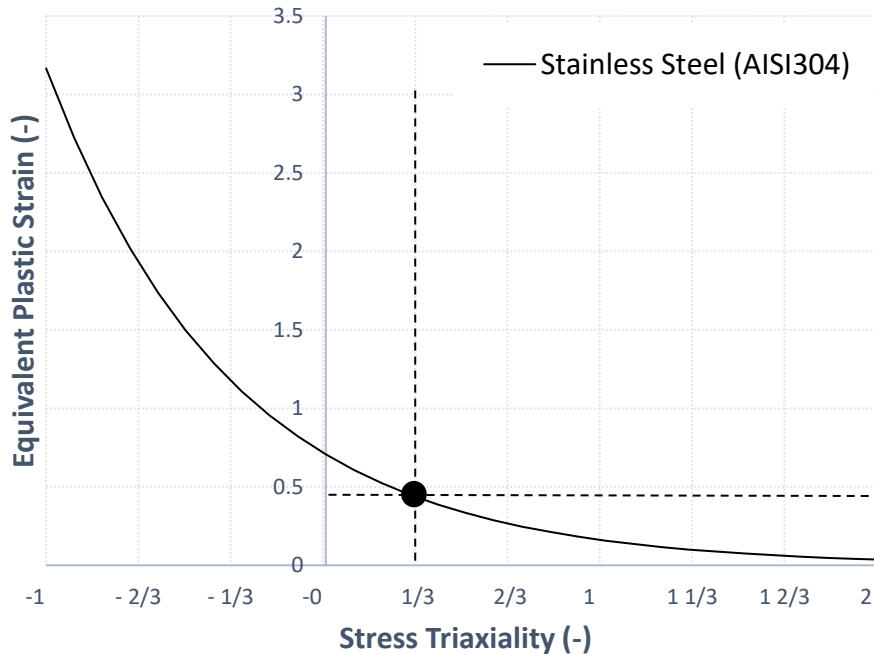
Figure 3.12 -Damage initiation criterion for stainless steel (AISI304)

Damage initiation does not essentially leads to complete damage until damage evolution state is not specified. Therefore, once the damage initiation criterion is established, then the damage evolution description is defined in the ductile damage material model. It describes the rate of degradation of the material stiffness once the initiation criterion is satisfied. The formulation is based on scalar damage approach with the following Eqn.8:

$$\sigma = (1 - D)\bar{\sigma} \qquad (8)$$

European Erasmus Mundus Master
Sustainable Constructions under natural hazards and catastrophic events
520121-1-2011-1-CZ-ERA MUNDUS-EMMC

ᒧᔕᒧᒪᒧᒧ

The overall damage variable D captures the combined effect of all active damage mechanisms. When damage variable $D = 1$, material point has completely failed (fracture occurs when D = 1). Damage evolution criteria based on linear displacement requires the definition of the effective plastic displacement $\bar{u}^{pl} = L.\bar{\varepsilon}_f^{pl}$, where $\bar{\varepsilon}_f^{pl}$ is the equivalent plastic strain at failure and L the characteristic length of the finite element. The progressive damage behaviour is entirely dependent on the meshing on the region located in the zone of necking development due to the strain localization (Abaqus, 2012). However, Hooputra and co-authors advise that the procedure is appropriate to predict crack initiation zones, but that element removal should be considered as the crack propagation mechanism (Hooputra et. al., 2004).

3.7   Failure Modelling

The ductile failure model mentioned in the earlier section is evaluated on a uniaxial quasi-static tensile test of a stainless AISI304 specimen with 15 mm thickness. The geometry of the finite element model follows the dimension of the tested specimen as shown in Figure 3.13. The experimental stress-strain curve (Figure 3.14) which depicts the material properties obtained from the mechanical extensometer with an initial gauge length $L_0 = 25$ mm.
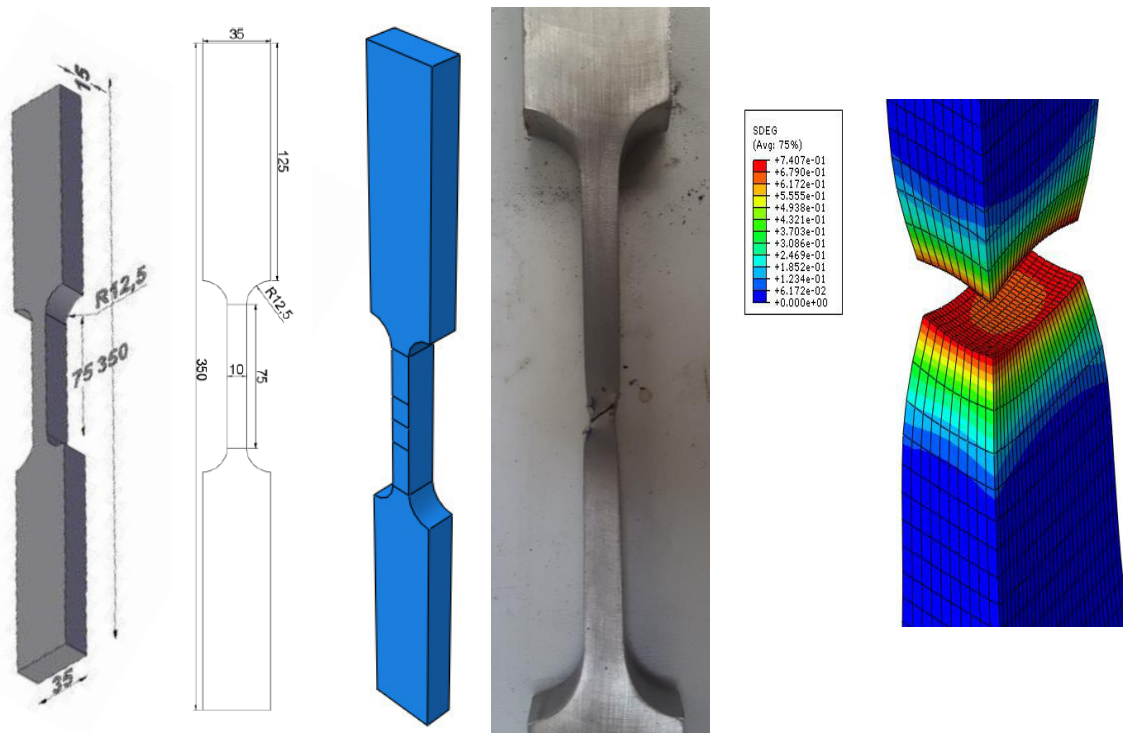
Figure 3.13 – Geometry and model of tested specimen with fracture

The finite element model is built with three-dimensional 8-noded linear brick solid elements C3D8R and an explicit dynamic analysis with displacement-based loading was carried out. This numerical model is able to describe the material behaviour and to predict the failure experimentally observed (Figure 3.14). This figure shows an increment within the softening phase with the damage scalar variable pattern (SDEG): elements with D ≥ 1.0 have been deleted, while the deformed mesh clearly exhibits necking in the specimen.

- Black curve – Represents the material curve obtained through the tensile test of the specimen obtained through the uniaxial quasi-static tensile test: Engineering – AISI-304
- Blue curve – Depict the strain-stress relationships obtained from the numerical model without any progressive damage definition: Numeric – No Damage.
- Red curve – Exhibit the strain-stress relationships obtained from the numerical model considering a strain at rupture of 48.13%. The damage evolution, as defined previously, has been set to follow a linear law with an effective plastic displacement of $\bar{u}^{pl} = 1.2$ mm. The numerical curve matches the experimental one very closely.
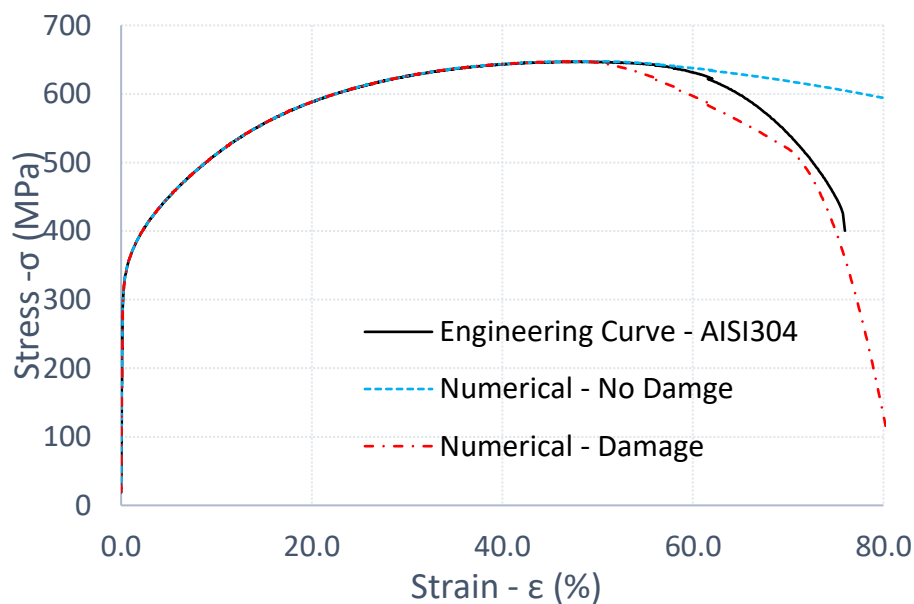
Figure 3.14 – Damage model assessment: Comparison of the stress-strain curve relationship obtained by numerical and experimental tests

4. NUMERICAL SIMULATION OF INNOVATIVE FREEDAM JOINT

4.1 Finite Element Method

4.1.1 Introduction

Nowadays, numerical methods are desired because analytical methods cannot meet up with the demand of real and complicated problems that are encountered within engineering. Whereas, setting up a real experimental arrangement is also quite expensive therefore, numerical method is the most preferred option. The finite element method is a numerical solving technique, usually used for approximation of specific problems in engineering and science. Due to its increased computational capacity, finite element analysis has become a cardinal tool in providing optimum solutions to intricate engineering issues. Given a system and its boundary conditions, its response can be estimated through the solution of algebraic equations governing its behaviour (Hutton, 2004). The fundamental of a static system calculation represents linear spring system therefore, the main equation can be reduced to Eqn.9:

$$F = K.\mu \tag{9}$$

Where: F is the external force applied, K is the stiffness matrix and μ the displacement vector.

One of the fundamental advantage in the finite element method is the discretization of the system's domain into number of finite-size domains; usually the smaller is the finite element size of domain, it will yield better approximation of the solution but at the cost of higher computational effort. There is a vast range of common applications of the finite element method in this modern world with complex scientific phenomenon.

This chapter deals with the general introduction to the finite element method and includes the description of basic concepts. Then, complete essentializing of FE model of FREEDAM joint with all the required steps are being discussed. Initially, the precise geometry of different parts of complete assembly was defined as per the design. Then, material's mechanical properties are introduced as recorded in the lab experiment, thereafter, well-articulated assembly is formulated according to the

experimental configurations. Later, the fine mesh, load step and boundary conditions are defined. More attention will be paid to the definition of the contact properties. For this, relations will be derived from the experimental tests and incorporated in the numerical model. Mesh sensitivity analysis with geometric and material non-linearity are duly considered to accurately evaluate the transient response of the friction assembly under quasi-static and impact loads.

4.1.2 Non-linear dynamic Analysis

Generally, the non-linear response of a system can be solved through the implementation of incremental procedure but in conventional incremental method error accumulates at each load step which will create incorrect results at the end of analysis. Though, Newton Raphson method (or any other modification method) governs by the reason of its quadratic convergence and establish the response of the studied system, as seen in the Figure 4.1. Although the number of Newton-Raphson iterations will increase, the overall computational time can be reduced.
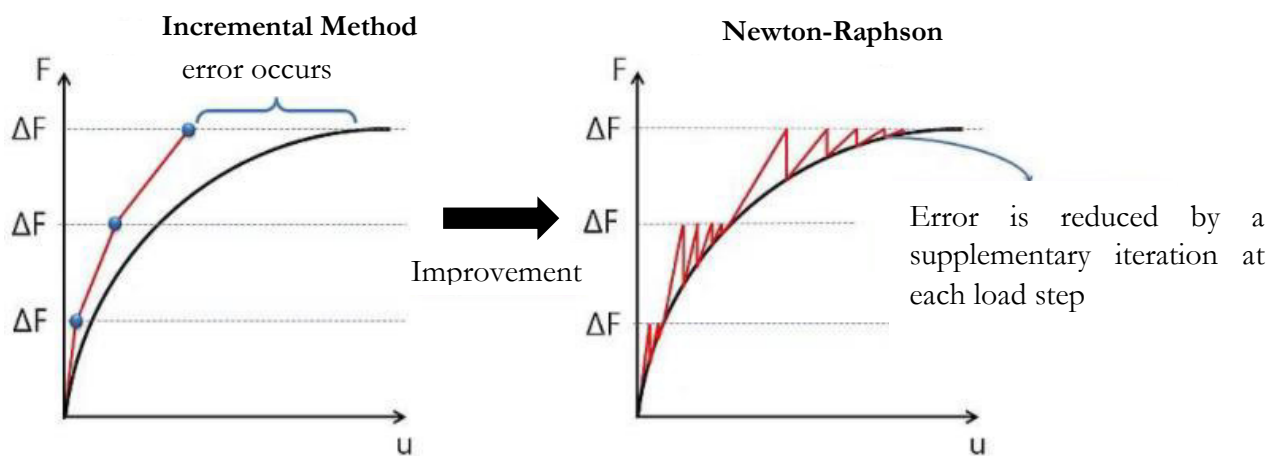
Figure 4.1 - Conventional incremental method vs Newton-Raphson method

During a non-linear dynamic analysis, the forces are applied as a function of time along with non-linear properties. The inertial effects of a mass cannot be ignored unlike in static conditions therefore, dynamic properties must be accounted along with acceleration and velocity. The transient behaviour description of a mass follows the Newton's 2nd law of motion $F = M.\ddot{u}$. In non-linear dynamic analysis field this equation is mostly transformed in the form of Eqn.10.

$$F = M.\ddot{u} + C.\dot{u} + K.u \qquad (10)$$

Where: M is the mass matrix, C the viscous damping and the K stiffness matrix, while $\ddot{u}, \dot{u}, u$ are the displacement, its first and second derivatives, velocity and acceleration, respectively, for each element.

4.1.3 Implicit vs. Explicit

The numerical simulation software ABAQUS-FEA, is ideally suitable for non-linear dynamic analysis. For a transient analysis geometric and material non-linearity needs to be considered in each incremental load steps. Towards the end of each iteration the geometry of the structures alters and possibly the material under gone the non-linearity if the material is already yielded. Therefore, both of them, geometry and material changes, should be incorporated in the stiffness matrix of the next increment. There are two solving techniques for non-linear dynamic analysis: implicit and explicit analysis. This section defines and gives an analogous aspect of both the strategies.

There are two distinct strategies to perform non-linear dynamic analysis, implicit and explicit solutions. The implicit solution entirely depends on the strategy of solution that requires a system of equations for assessment, although explicit solutions are those in which estimation can be directly yielded from the previous steps and do not depend on the solution of a system of equations, even the equation of motion is integrated in very small-time increment.

The Hilber-Hughes-Taylor (HHT) method also known as alpha-method is a well-renowned method in structural dynamics field for implicit numerical procedure for the direct integration of linear set of equations (Negrut & Ottarsson, 2006). The HHT approach provides dissipation combining the positive Newmark Υ-dissipation and negative α-dissipation methods, with enhanced characteristics ensuring dissipation of the higher frequencies, while the lower modes are not considered too effective. Moreover, the HHT algorithm is unconditionally stable with respect to time intervals whenever $-0.5 \leq \alpha \leq 0$, thus accommodating for relatively large time-increments (Hilber *et al.*, 1977).

In an implicit analysis, the displacement is not time dependent. Therefore, the velocities and accelerations factors are also considered as null and the mass and damping parameters can be ignored. The implicit method can be based on Newmark's method, Newton Raphson Method etc. In order to solve an FEM

problem using implicit method, inversion of stiffness matrix (k) is required. Very large deformation problems such as crash analysis can result in millions of degrees of freedom effectively increasing the size of stiffness matrix. Large stiffness matrix results in more computational time required for its inversion. Hence there is a need for an explicit method which would prevent the inversion of stiffness matrix.

In an explicit analysis, the displacements, velocities and accelerations of each node propagate clearly with respect to time. This means that the state of the model at the end of an increment is solely based on the displacements, velocities and accelerations at the start of the increment which is being operated by a central difference operator unlike implicit dynamic analysis, the integration operator matrix must be inverted and a set of nonlinear equilibrium equations must be solved at each time increment (Abaqus, 2012).

Considering a hysteretic analysis of bolted beam-to-column joints, differences in the use of both integration schemes have been addressed by Vegte (Vegte & Makino, 2004) in terms of: i) solution strategy; ii) computational time with respect to the model size; and, iii) convergence in non-linear contact. Vegte recommends the explicit procedure for solving large models with reduced computational cost and for handling non-linear contact with ease however, simulations run with very general contact definitions, equilibrium and contact constrains checks, do not need to be met.

i) Computational cost in explicit analysis arises linearly with the model size however, it arises rapidly with implicit analysis (Vegte *et al.*, 2004) (Abaqus, 2012). Therefore, with large models explicit approach is considered productive as represented in Figure 4.2.

ii) For non-linear contact analysis, explicit solution does not offer any convergence problems hence simulation runs efficiently (Vegte *et al.*, 2004).

iii) The explicit integration method is more efficient than the implicit integration method for solving extremely discontinuous events or processes.

iv) Explicit analysis does not require set of equations.

But one of the shortcoming of this technique is that you require very small increments for precision in terms of mass scaling, otherwise error will accumulate and result into incorrect solution. However, still all the benefits tend to favor explicit solver for non-linear dynamic analysis. Furthermore, the study involves the application of intricate frictional interactions at the contact interfaces and dynamic impact loading, therefore, taking in account all the advantages and

complexities, explicit approach is considered as the optimum choice for this study.
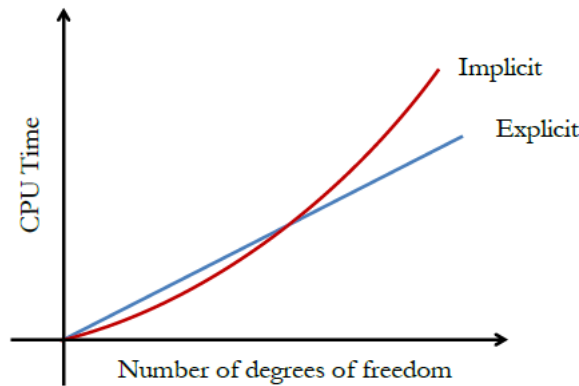
Figure 4.2 - Comparison of implicit and explicit solution

4.1.4   Finite Element Typology

The FE models of dissipative assembly are developed with solid brick elements. The C3D8R element is a multi-purpose linear brick element, with reduced numerical integration is generally considered for the modelling. The shape of C3D8R elements is shown in Figure 4.3, contain 8 nodes and 3 degrees of freedom per node with only one Guass integration point which follows the uniform strain formulation. ABAQUS is based on numerical techniques to integrate various quantities over the volume of each element. Using Gaussian quadrature for most elements, ABAQUS evaluates the material response at each integration point in each element, whereas in C3D8R element it has reduced integration to only one point.
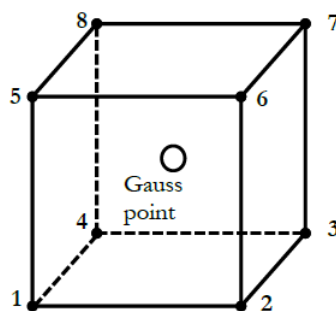
Figure 4.3 - 8 Node element with reduced integration

The strains are not obtained at the first-order Gauss point but are obtained as the analytically calculated average strain over the element's volume (Abaqus, 2012).

Following this formulation, first order reduced integration elements yield the exact average strain over the element volume simplifying the interaction with the non-linear constitutive routines.

Every finite element form has its own numerical integration complications (Bursi & Jaspart, 1998), (Sun, 2006). Fully integrated first order linear brick element when subject to bending may suffer from "shear locking" shortcoming and reduced integration elements are susceptible to "hourglassing" behavioural phenomenon.

Fully integrated linear brick elements when subjected to bending, should ideally transform into curved shape, however, elements are unable to bend to curves. They deliver a shape unable to maintain the rectangular angle, which results into introduction of incorrect artificial shear stress in the system. Therefore, the strain energy of the element is generating shear deformation instead of pure bending deformation. This overall effect is known as shear locking due to overly stiff under the bending moment (Sun, 2006).

To compensate the shear locking draw back and to improve the computational efficiency, a reduced integration element is employed, however, nothing is flawless. The reduced integration first order element suffers from its own problem called hourglassing as it tends to be overly flexible. Despite their nodal deformation remains similar to fully integrated first order brick elements, the lines passing in its integration point will remain unchanged Figure 4.4. In turn this means that normal and shear stresses are zero and that there is no strain energy generated by the deformation. Abaqus uses the artificial stiffness method and the artificial damping method controls the hourglassing in these elements (Sun, 2006), (Abaqus, 2012).
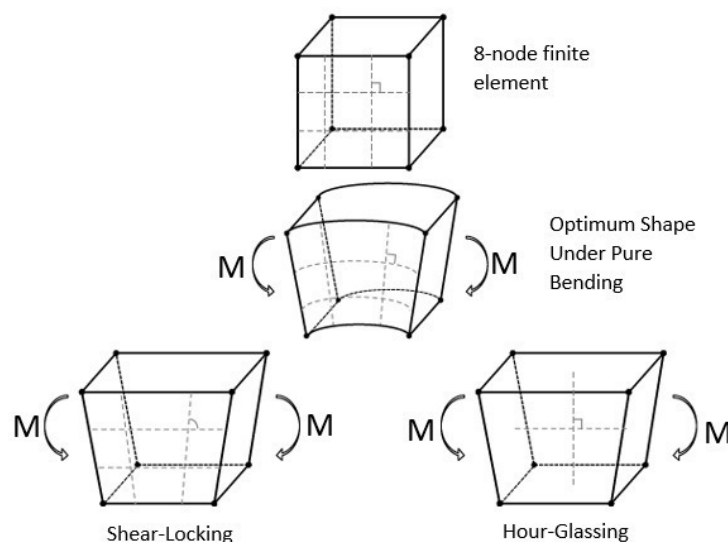
Figure 4.4 – Numerical integration problems of finite elements subjected to bending (Sun, 2006)

4.2 Description of Structural Model

The friction dampers model analysed is based on the study being carried out at the University of Coimbra under research project "FREEDAM" (Santos *et al.*, 2017). Two different test setups were established to carry out quasi-static and impact testing on the friction device. The test set up used for the static tests was the similar as used in the static tensile tests of the components (Figure 4.5). The tests have been made by both the force control and the displacement control, and force applied to the specimen has been read directly by the machine. The reason for using both displacement and force control was to study the influence on the variation of the slip force during the slip of the plates.

a)   b)
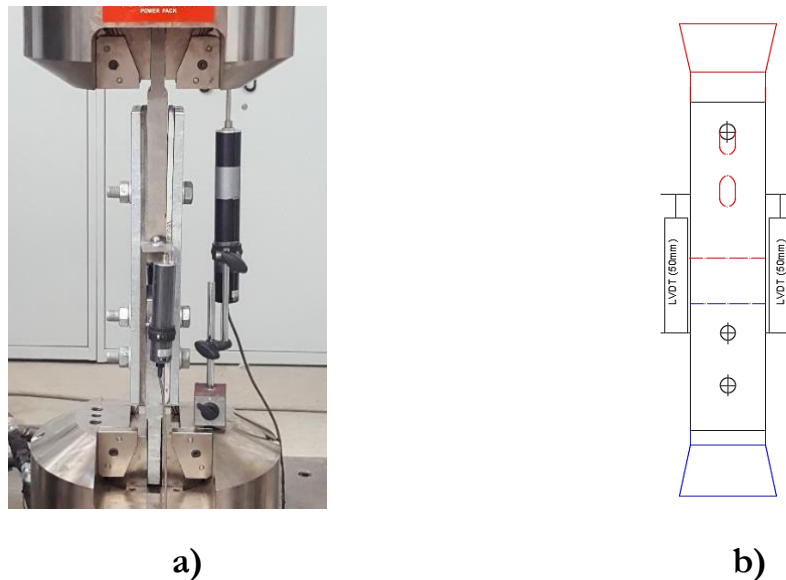
Figure 4.5 - a) Test Set-up for the quasi-static tests; b) LVDT's position (Santos *et al.*, 2017)

The experimental layout used on the impact tests is depicted in Figure 4.6 and further details can be found in (Santos *et al.*, 2017). It comprises of two HEB 500 beams which are placed horizontally and anchored to the floor slab. At one end, these two beams are orthogonally bolted to a rigid reaction frame built from two IPE 450. At the other end, they are connected to a HEB 650. The loading phenomenon is based on the principle of a 2nd class lever mechanism. The force is applied in the blue beam known as "flying beam". To ensure enough stiffness to the "flying beam" so that its deformation can be neglected, a welded HEM 240 made of steel (S355) has been used. In order to ensure that the assembly of friction damper only undergo axial tension loading, it is fastened to the layout by means of hinges to the flying beam and IPE 450 respectively. The specimen equipped with the deflection-meter

(for deformation measuring) ready for an impact testing; the measuring point is on top surface of the internal plate of the damper connected to blue beam.

The pneumatic cylinder is used to induce the impact loading in the assembly. This cylinder has been designed for a maximum operating pressure equal to 300 Bar (30 MPa) and, as the cylinder barrel has an internal diameter of 125 mm, results in a maximum applied force of 360 KN. During the tests force, displacements and accelerations are measured. Since this type of test occurs in very few seconds (around 0.1s), specific equipment with a large sample rate has to be installed to record the response. The dynamic equilibrium of the system is established by measuring the beam's acceleration and displacements, and the transient applied load. The instrumentation includes an accelerometer placed in the mass centre of the flying beam and another accelerometer, a load cell and a laser distance gauge located in the load application point of pneumatic cylinder.
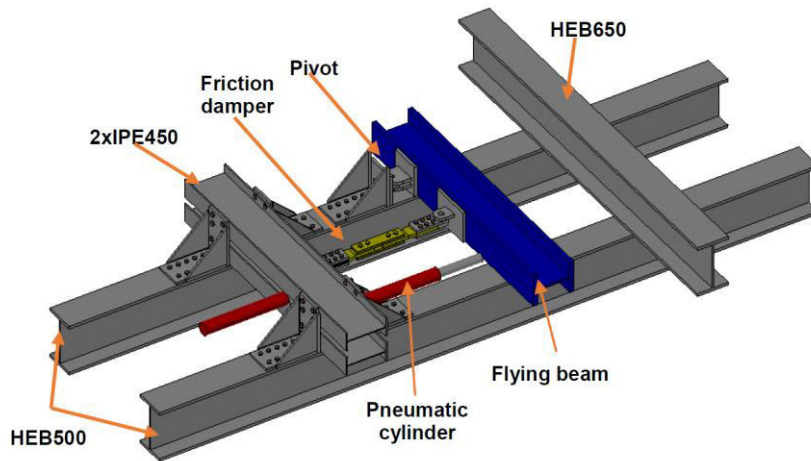
Figure 4.6 - Experimental test layout (Santos *et al.*, 2017)

4.2.1   Geometry of the Tested Specimens

The geometry of the friction dampers is presented in the Figure 4.7 (a). Overall, the assembly has a pair of 8mm steel plates (friction shims) pre-loaded with M20 bolt layered by application of thermal spray (friction material), slipping on a 30mm or 10mm AISI304 stainless steel plate (internal plate), slotted with one or two holes to allow the dissipation mechanism to dominate. Furthermore, to reproduce uniform distribution effect of the bolt preloading onto the interface, two 15mm steel plates (external plates) are provided under the bolt head and bolt nut respectively.
Three types of geometrical configuration of dampers were tested at University of Coimbra (Santos *et al.*, 2017) as depicted in Figure 4.7 (b). Different geometrical configurations were tested, in order to assess the non-linear response and different

failure modes under quasi-static and impact loading. Specimen A and C are quite similar in geometry but the thickness of the stainless steel AISI304 (internal plate) varies, which is done in order to highlight the shear and bearing failure of the bolt and plate respectively. In specimen B, a long-slotted hole is used to facilitate the slippage of plates to play dominantly with frictional damping due to abrasion between the interlayers.
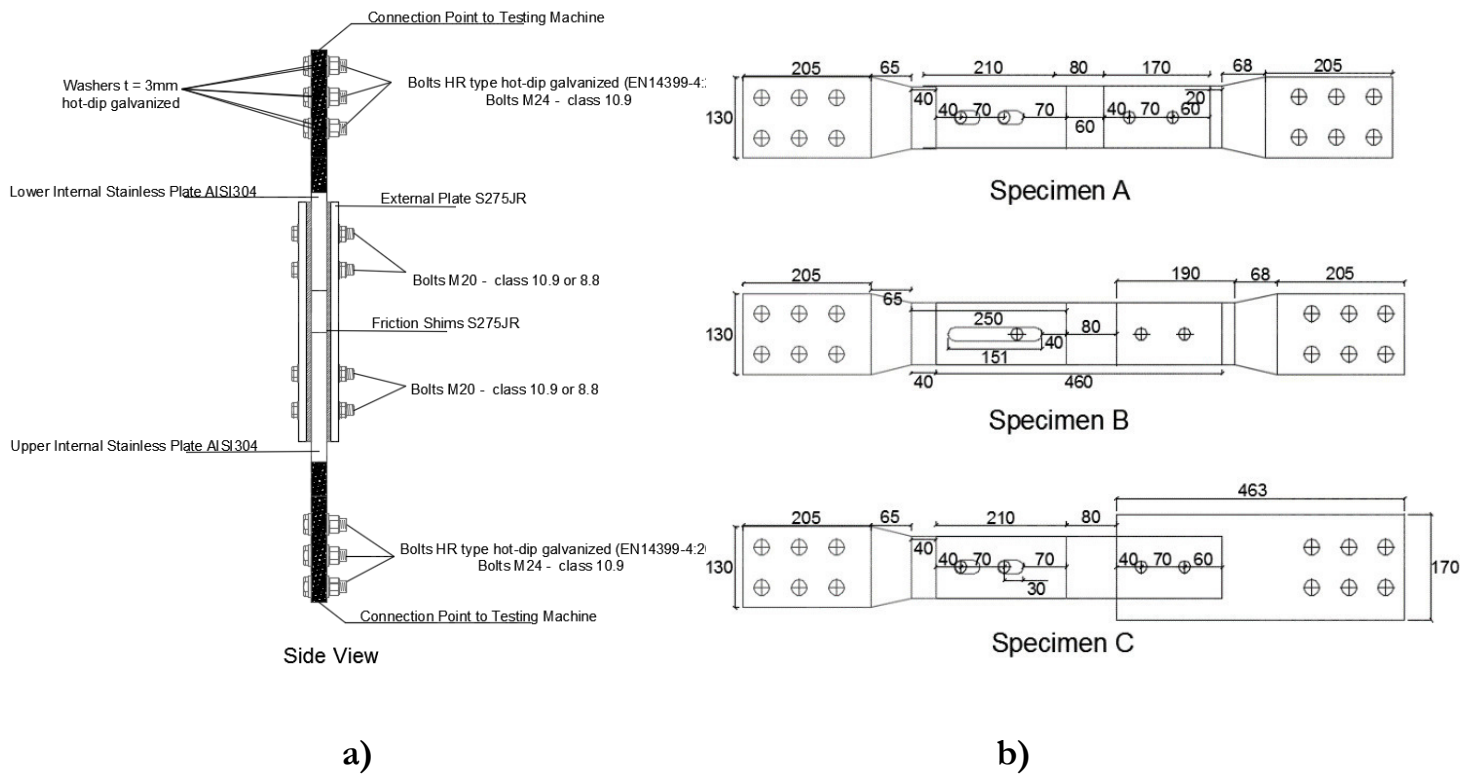
Figure 4.7 - Geometry of the connections of main interest to this work a) Friction damper side view; b) Geometrical configuration types of friction damper (Santos *et al.*, 2017)

4.2.2 Experimental Response of Friction Damper Under Dynamic Loading

The Figure 4.8 shows the typical experimental of quasi-static response of friction damping device. Initially, the device remains in elastic limit and shows micro-displacement. But as the loading keeps on increasing it results into the release of accumulation of shear force at point (A) by the slippage of lower internal plate of the assembly depicting stick-slip motion at a force know as slip force F_{slip}, which is followed by progressive frictional damping (B), till the bolt comes in contact with plate and in the end, it leads to the failure of joint either by bolt shear failure or plate bearing failure in phase (D) at a force know as collapse force $F_{collapse}$ at point (E), followed by a 2nd slip at point (C) which is due to the displacement of the bolts at

fixed plate because of bolt hole clearance and development of stick-slip phenomenon.
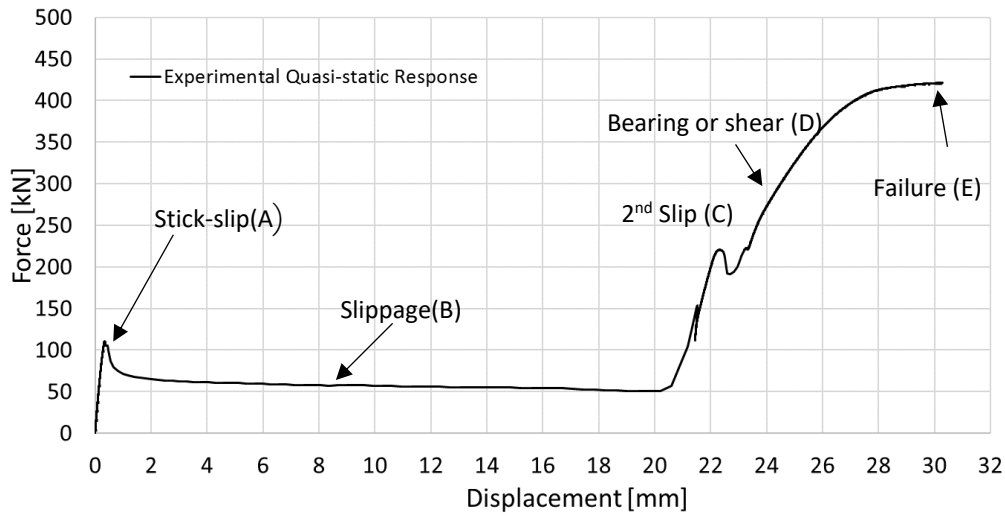
Figure 4.8 – Friction damper (FREEDAM joint) typical response under pull-out quasi-static loading.

The Figure 4.9 shows the typical experimental impact loading response of friction damping device. Initially, the device remains in elastic limit and shows micro-displacement. But the slip (A) took at a higher slip force F_{slip} due to the (*DIF*) dynamic increase factor. However, along the slippage there is no sign of frictional damping in phase (B). Then, the bolt comes in contact with plate and in the end, it leads to the failure of joint (either by bolt shear failure or plate bearing failure) at a force know as collapse force $F_{collapse}$ at point (D), which is comparatively higher than the collapse force in quasi-static test. There is also no evidence of 2nd slip in the impact response. It can also be depicted that the impact response leads to a brittle failure relative to static response.
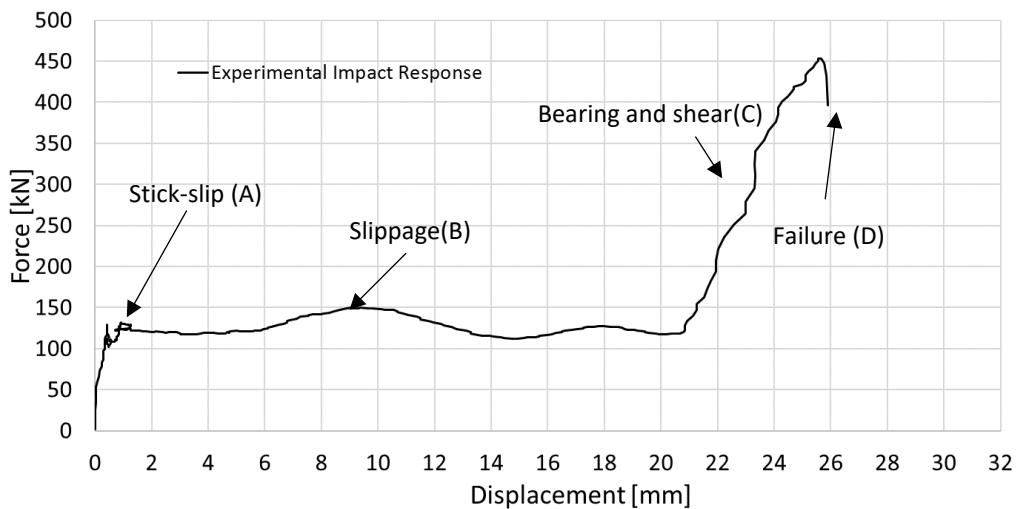
Figure 4.9 - Friction damper (FREEDAM joint) typical response under impact loading.

4.3   Finite Element Model Development

4.3.1   Description of Numerical Model

The simplified friction damper assembly is studied, which is the part of the additional haunch element of the beam-column joint. The different geometries of the damping devices are already explained in previous chapter, whereas Figure 4.10 illustrates an example and dimensions of one of a friction damper used in the study. Figure 4.11 shows the numerical model's boundary condition and mesh discretization.
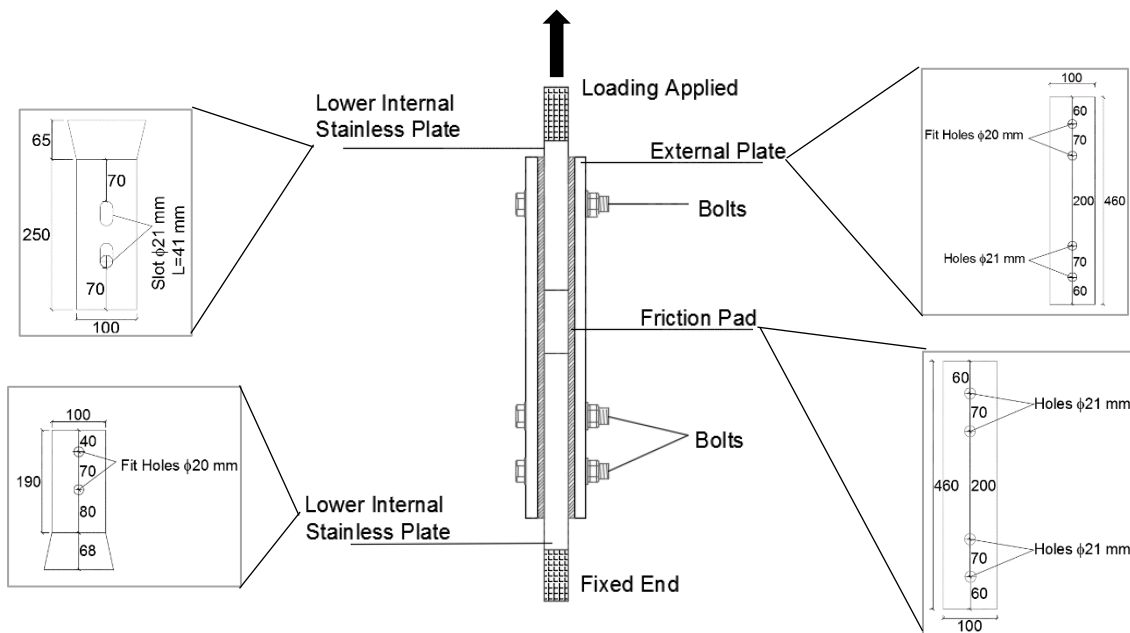
Figure 4.10 – Friction damper component details
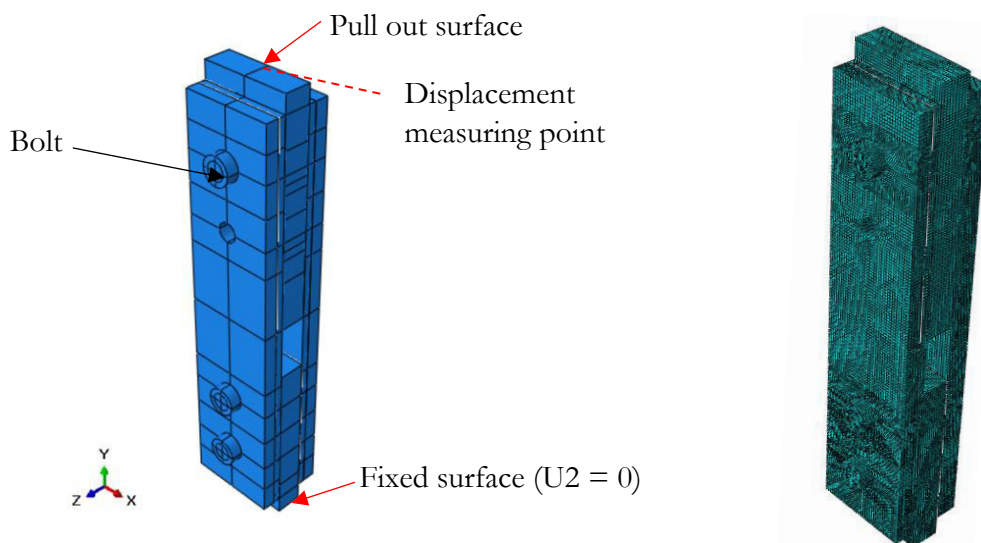
Figure 4.11 – Numerical model of friction damper, boundary condition and mesh

The FE analyses are conducted with the software ABAQUS (Abaqus, 2012). The FE model is based on the definition of five parts: (i) External Plate (attached with bolt head and friction shim); (ii) Friction Pad; (iii) Upper Internal Plate (Fixed end); (iv) Lower Internal Plate (pull out plate with slotted holes) (v) Bolt (head and shank as a single piece) as depicted in Figure 4.10

The friction device has been simplified by providing the rigid body constrain to the tip of the internal plates (displacing plate) so as to provide the required boundary conditions (Figure 4.11). No restraint is provided in the displacing plate, and on the other end the fixed internal plate is restraint in the direction of the application of displacement.

The model is generated with solid element type C3D8R (first order reduced integration continuum element), allowing for non-linear geometrical and material behaviour. Generally, a structured mesh technique with "Hex" element shape is used, except for the weld zone where a "Wedge" element shape is employed. Mesh sensitivity analyse was also conducted assuring that a discretization of elements through the thickness of plates and bolts, and a finer mesh around the bolt area to provide accurate results, while reducing the computation time and convergence problems. On the other hand, in zones where the strain gradients are negligible (near the end of the plates), a coarser mesh has been used.

4.3.2   Loading Steps

Loading was defined in two subsequent steps. The loading method corresponds to experimental testing, first the bolt preloading is done, then dynamic loading is applied in the form of quasi-static and impact loading. The application of loading steps in Abaqus is a function of time (Abaqus, 2012). Therefore, duration of loading steps in explicit quasi-static analysis was set similar to those in experimental testing but this will be time consuming; therefore, mass scaling is applied in order to simulate the same effects but with smaller time durations.

The displacement-controlled loading was applied on the tip of the lower internal plate and the tip of the upper internal plate was fixed as per the experimental test setup for quasi-static loading.

Appropriate smooth step was adopted for time dependent amplitude functions in all loading steps to avoid large inertia forces in case of quasi-static analysis. An example is shown in Figure 4.12, as time dependent amplitude function for the displacement controlled dynamic loading in model.
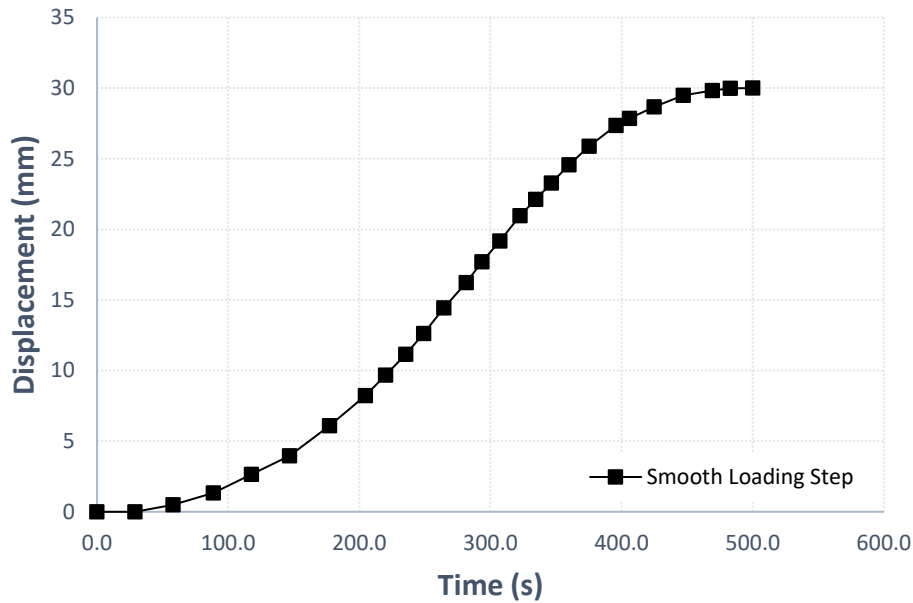
Figure 4.12 – Smooth loading step

4.3.3   Impulsive Load

Generally, structural classification is done through the static definition of loads, as the load duration is of no concern. The influence of static loading can easily be simulated, as the induced dynamic motion is neglected. Whereas, when the load duration is abridged to very small instant, the induced motion (accelerations and velocities) must be taken into account through the application of the impulse-momentum principle (Szuladziński, 2010).

Therefore, the effect of a short transient load is entirely dependent on the natural time period of the system. If a system is applied with a time shorter than 10% of the system's natural period, $(t_0 < 0.1\tau)$, are considered to as impact loads (Szuladziński, 2010). According to (Cormie and Smith, 2009) three regimes can be distinguished:

$$\text{Impulsive:} \quad t_0 < 0.1.\tau$$

$$\text{Dynamic:} \quad 0.1.\tau < t_0 < 10.\tau$$

$$\text{Quasi-Static:} \quad 10.\tau < t_0$$

Where: t_0 is the pulse duration and τ the natural period of the system.

There are four general types of blast and impact pulse load schemes as shown in Figure 4.13.
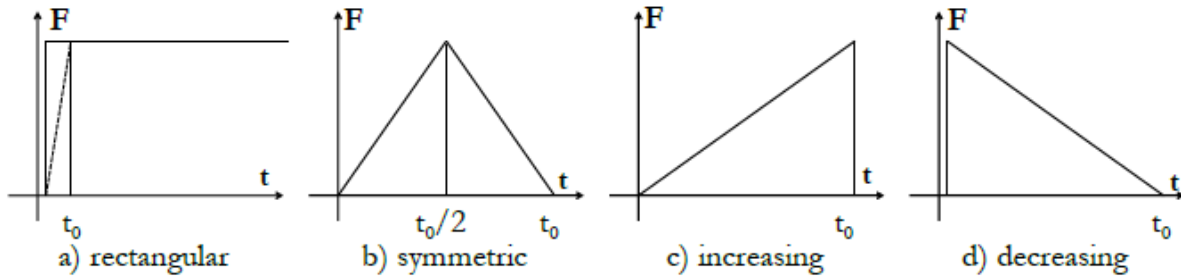
Figure 4.13 - Blast and impact impulsive load(Cormie and Smith, 2009), (Szuladzinski, 2010)

4.3.4   Bolt Preload Modelling

Bolted shear connection is such an assembly in which preloading is defined in bolts as the introduction of a self-induced normal load, prior subjecting to any shear loading in order to accomplish the friction grip at transfer interface, to make the joint more sustainable in terms of load carry capacity. The friction interface grip depends on two components one on the friction behaviour of material employed and on the other hand normal load transferred to the interlayers. There are several techniques mentioned in this study to simulate the application of preloading of bolts in Abaqus (Abaqus, 2012). Before each test, the bolts were tightening by means of a calibrated torque wrench in order to introduce a preload force (F_p) equal to $0.5 f_{ub} A_s$ (f_{ub} is the ultimate strength of the bolt and A_s is the tensile stress area of the bolt). The magnitude of torque applied to each bolt is dependent on the design preload value (F_p), the diameter of the bolt (d) and of the bolt *k-factor*. 122.5 kN and 98 kN preloads were applied in experiments to M20 Grade 10.9 and Grade 8.8, respectively.

Therefore, simplified models are created in order to study the optimum strategy for inducing preloading forces in finite element model for accurate assessment of friction dampers. Few simplified models were created as represented in Figure 4.14. Three different types of bolt hole geometries were analysed, with slotted hole, long slotted hole, and another is with nominal sized holes.

a)　　　　　　　　　b)　　　　　　　　　c)
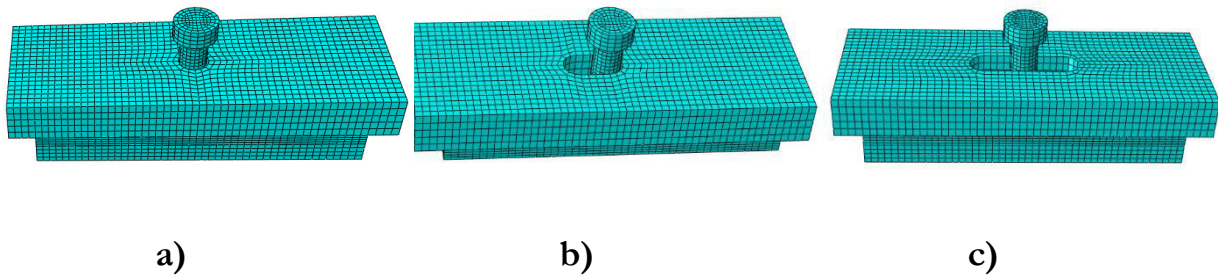
Figure 4.14 - Simplified model used for the evaluation of the application of preloading force in Abaqus: a) Model with normal holes; b) Model with slotted holes; c) Model with elongated slotted holes.

There are several methods that can be used to apply preloading step to use with explicit dynamic analysis. However, preloading for explicit dynamic analyses is not as easy as it is for implicit dynamic analysis. So, two techniques could be used to apply bolt preloading in the model. The first approach is based on application of preloading forces in bolts by using the "bolt load" option, presented in the load module using implicit solver. Second approach is based on the temperature induced preloading using explicit solver.

4.3.4.1　　　Preload with an implicit solver

The first strategy considers the application of preloading by using bolt load option which allows two methods: one as "concentrated" load while the second one allows a prescribed change in the bolt length as "adjust length". Due to convergence problems related with the first option, a change of the bolt length was applied. Figure 4.15 shows an example of the application of this type of load.
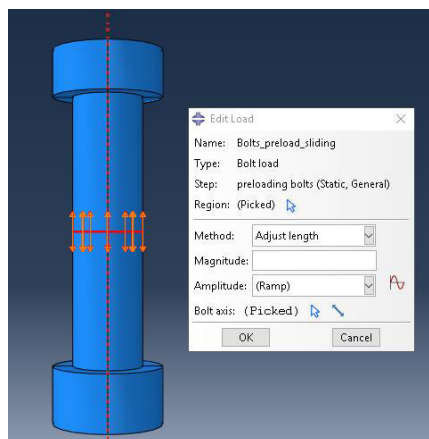
Figure 4.15 - Modelling a pre-tensioned bolt in Abaqus

The pretension is implemented by splitting the bolt body and applying a magnitude of adjusted length in the bolt-shank. At Abaqus/CAE are created the datum axes and the partition of the bolt body in the middle of the shank, then deformation is applied, calculated using elastic Eqn.11, in order to produce normal force equal to the preloading applied in experiments by means of a calibrated torque wrench.

$$\Delta_{bolt} = L_{bolt}\, \frac{\sigma_{bolt}}{E} \qquad\qquad (11)$$

However, in this case, a deformation is introduced into the shank part of the bolt instead of a force, but not all the imposed deformation is transferred to forces due to further deformation of the plates. Therefore, it is not enough to calculate the extension of the bolt that provokes a certain bolt pressure, considering the bolt in the elastic range.

After applying the pretension to the bolts, their length is fixed at their current position. This technique helps to avoid the problem with extensive elongation of the bolts under the loading. During the first two steps (preloading step and loading step), all three translational degrees of freedom (DOF) at the section of pretension are restrained. This degree of freedom served as the artificial boundary condition to prevent the numerical singularity error which occurs as a result of rigid body motion. After the preloading and activating the contact properties, this artificial boundary condition is then removed. High preload tension increases joint strength, creates friction between parts to resist shear, and improves the fatigue resistance of bolted connections.

In order to ensure that the applied deformation should impart the normal force equal to the force applied in experiment through torque wrench, identification of factors affecting the preloading force is necessary. The preloading force applied using bolt adjustment method, depend on several factors: the mesh quality, plate thickness, bolt length, and the geometry of bolt hole. Considering the mentioned factors, fifteen geometries were analysed through varying the plate thickness and subsequently the bolt length along with the bolt geometry and varying also the mesh; this results in ample number of models.

For a specific mesh quality and a specific bolt length (depending up the plate thickness), the magnitude of adjusted length can be calculated by an iterative method by comparing the numerical preload attained in the model, then altering the magnitude of change in length again, until the numerical preload attain is equal to experimental preload applied:

$$P_{num} = P_{acquired} \rightarrow P_{exp} \rightarrow \Delta L_{bolt}$$

From these analyses, it was concluded that:

1) It is also possible to infer that a finer mesh leads to more rigid elements and, accordingly, for the same adjusted length leads to higher stress in the bolt, in other words, greater preloading forces. It can be concluded that for a specific mesh, different calibration is required.

2) The geometry of the bolt hole also has a great impact on the results due to the contact area, as in case of slotted hole as shown in, comparatively smaller, results into greater deformation at the same extension.

3) The geometry of the hole has also a big influence on the results as the contact area is smaller in the case of slotted holes (see Figure 4.16), meaning the same extension of the bolt produces bigger influence in the surrounding of elongated holes, and, therefore bigger deformations. Furthermore, as the thickness of the plates decreases, this influence is better marked because the deformation in the thickness direction gains more influence. On the contrary, for both hole geometries, as the thickness of the plates increases, the tendency towards a strain plane problem occurs, and the deformation happening in the thickness direction of the plates is no longer significant.
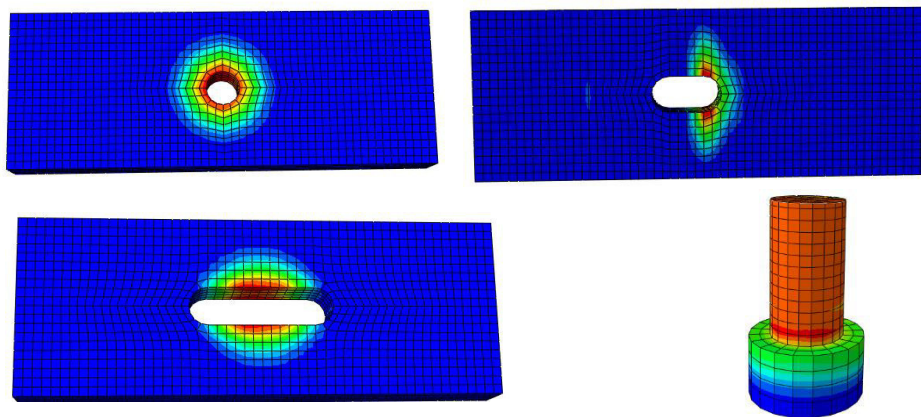
Figure 4.16 - Distribution of bolt stresses

4.3.4.2   Preload with an explicit solver

The principle of this approach is based on temperature gradient, inducing normal force in the bolt shank by varying temperature, which will produce deformation in the shank. This method used explicit solver to apply the temperature gradient and in order to make the bolt shank sensitive to temperature changes, the orthotropic expansion coefficient α for steel is defined in material properties only in the direction parallel to the bolt shank. Two material properties for bolt are created in order to apply the expansion coefficient only to the bolt shank so that, only shank will contract. Also, material orientation should be assigned to the bolt so that it should consider contraction only in the direction of shank. Negative temperature is applied to the shank of the bolt as a pre-defined field along with the clamping amplitude as a smooth step as shown in the Figure 4.17.

a)   b)
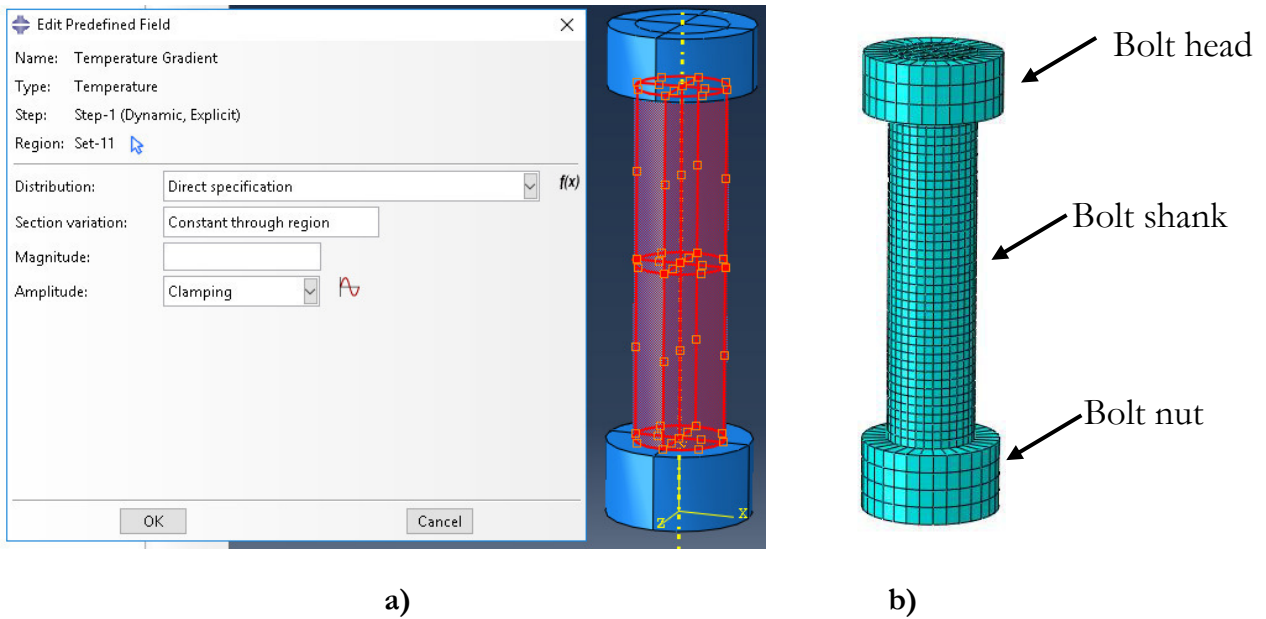
Figure 4.17 – a) Definition of temperature gradient; b) bolt parts

Negative temperature is defined to produce 122.5 kN and 98 kN preload applied in experiment to M20 Grade 10.9 and Grade 8.8 respectively (Santos *et al.*, 2017). Change in temperature (ΔT) can be calculated using the simple thermodynamics Eqn.12 and Eqn.13.

$$\Delta T = \frac{1}{\alpha} \frac{\Delta l}{l_{shank}} \qquad (12)$$

$$\Delta l = \delta_{joint} \cdot F_{s.Rd} \tag{13}$$

Where: $F_{s.Rd}$ is the bolt preload force, l_{shank} is the length of the bolt shank, α is the expansion co-efficient and δ_{joint} is the elastic resilience of joint.

To calculate the required change in length which can produce relevant preload, elastic resilience of the bolted joint is calculated by Eqn.14 according to the VDI Guideline (VDI Guideline, 2003). It consists of the elastic resilience of the preloaded bolt δ_{bolt} and the elastic resilience of clamping package (steel shells + cover-plate + nuts) δ_{cp}.

$$\delta_{joint} = \delta_{bolt} + \delta_{cp} \tag{14}$$

According to (VDI Guideline, 2003), the resilience of the bolt takes into account elastic deformation within the clamp length and any elastic deformations which occur outside this region and have effect on the deformation behaviour of the bolt in the joint. Thus, the geometry of the whole bolt has to be considered. The bolt shown in Figure 4.17 (b) consists of certain number of individual elements, which is substituted by cylindrical bodies of various lengths and corresponding cross sections.

Equivalent cylindrical elements of the bolt are arranged in a row, so that the total resilience of the bolt is given by Eqn.15.

$$\delta_{bolt} = \delta_{head} + \delta_{shank} + \delta_{nut} \tag{15}$$

Individual cylindrical elements of the bolt are: the head, the shank and the nut. Elastic resiliencies of these individual cylindrical elements are given in Eqn.16.

$$\delta_{bolt} = \frac{l_{head,shank,nut}}{E_{bolt} A_{nom}} \tag{16}$$

This is also a quasi-static method as smooth step is used for clamping amplitude. However, unlike implicit quasi-static methods, this uses an automated algorithm, where a large amount of mass-proportional damping is applied automatically and adjusted during the solution to remove dynamic behaviour. It periodically checks the kinetic energy of the system and the solution converges when this energy drops below a small percentage of the starting energy. The preloading is uniform and it does not depend on the bolt geometry and can be easily applied through this method.

Mesh and mass scaling sensitivity analysis with the smooth step was done to achieve the desired preload as per the experiment. The smooth clamping step for temperature gradient is applied for 50 sec which results into optimum preload in bolts.

Explicit typically yields the fastest solution when the preload analysis is not highly nonlinear. A preload solution that transfers only deformations to the explicit analysis will only be correct if the preload phase is linear and does not involve sliding contact. In cases where the preload phase is nonlinear or contains sliding contact, the preload solution must transfer contact status, velocity, stress and strain. This is typically a problem when the implicit code is different from the explicit code. In such cases, deformations are usually the only results transferred to the explicit code. Some codes, such as LS-Dyna for example, contain implicit solvers which will transfer all required data and therefore can be used for nonlinear preload analyses.

For this study preloading is applied using explicit solution as shown in the Figure 4.18. Both the bolts are preloaded according to the initial preload applied to the assembly
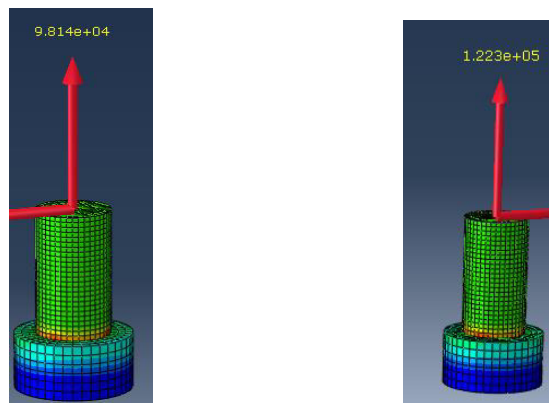
a) M20 Bolt (8.8)   **b)** M20 Bolt (10.9)

Figure 4.18 – Preloading of bolts using explicit solver

4.3.5   Sensitivity Analysis

Material and geometric non-linear dynamic analysis was conducted as quasi-static loading condition using the dynamic explicit solver, as it does not encounter common convergence problem which most likely observed in implicit solver. Cumbersome procedure of any explicit dynamic solver is defining the size of the smallest finite element in a model, since divided by a wave propagation speed it represents the maximum stable time increment for the integration. Computation

time of a real time quasi-static analysis can be extremely lengthy. Calculation speed can be increased either by a time scaling or mass scaling method. These methods tend to increase inertia forces in a model, sometimes leading to useless results. A compromise must be found between an acceptable computation time and quality of results, often by test analyses for each of the different model set-ups.

Mass scaling with desired time increment of 0.005 sec was used in these analyses. FEA code automatically increases masses of finite elements such that their stable time increment matches the desired time increment (Abaqus, 2012). Scaling was set to be variable (recomputed in every integration step) and non-uniform (different for each finite element) as it is the most efficient for the models with large spectra of elements sizes and damage included.

Quality of the results is verified by matching applied and reaction forces in a model for displacement-controlled loading. An example is shown in Figure 4.19 based on models presented. Linear matching curve with no fluctuations for the smallest analysed desired time increment proves that no inertia effects govern the results. The same matching curves for larger time increments (test analyses) are also shown for comparison. Loading time was reduced in order to achieve the same calculation time as for the satisfactory variable non-uniform mass scaling method with desired time increment of 0.005 sec, shown in Figure 4.19 along with the point of application of applied load and the reaction taken from the assembly.
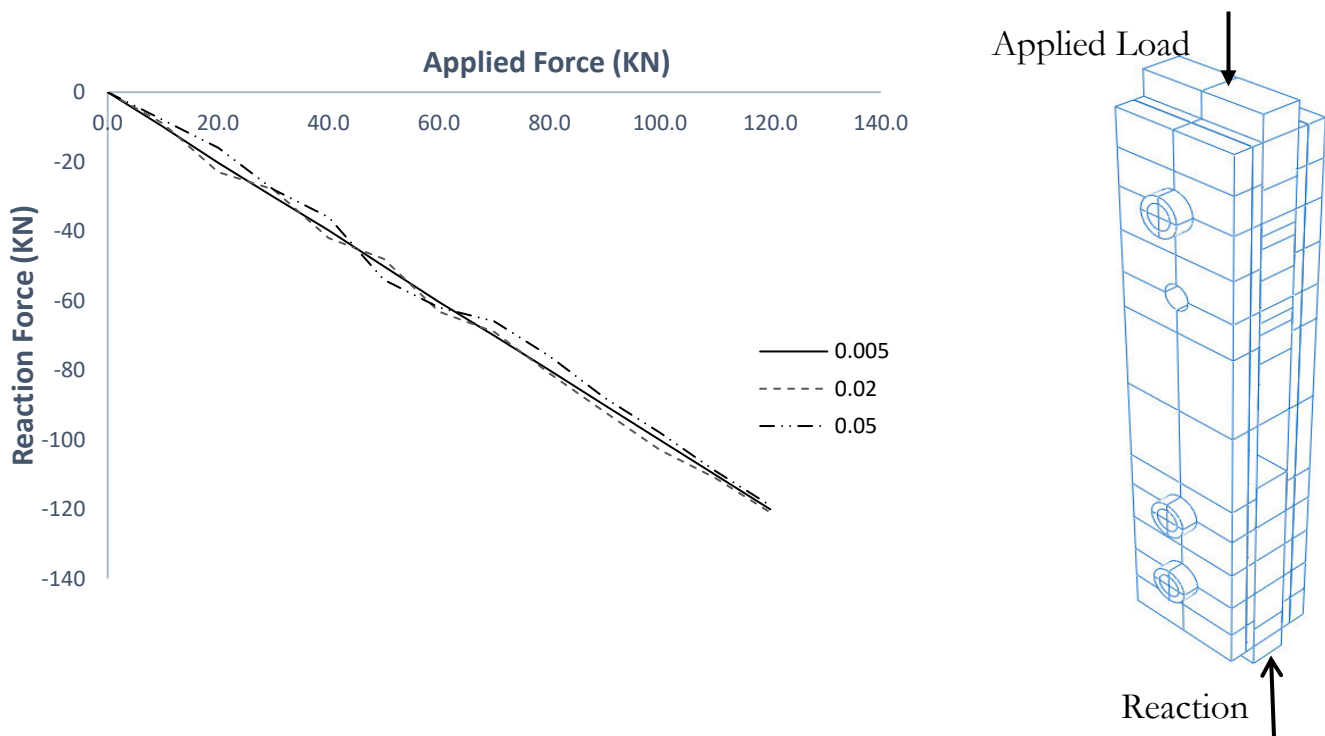
Figure 4.19 – Quality of quasi-static solution

European Erasmus Mundus Master
Sustainable Constructions under natural hazards and catastrophic events
520121-1-2011-1-CZ-ERA MUNDUS-EMMC

SUSCOS

4.3.6 Mesh Optimization

Based on the numerous analysis carried out, meshing is optimized to simulate the behaviour of the friction damper so that it should accurately depict the response under loading. A simplified damper assembly is subjected to quasi-static loading and by varying mesh size its force-displacement curve is developed as depicted in Figure 4.20
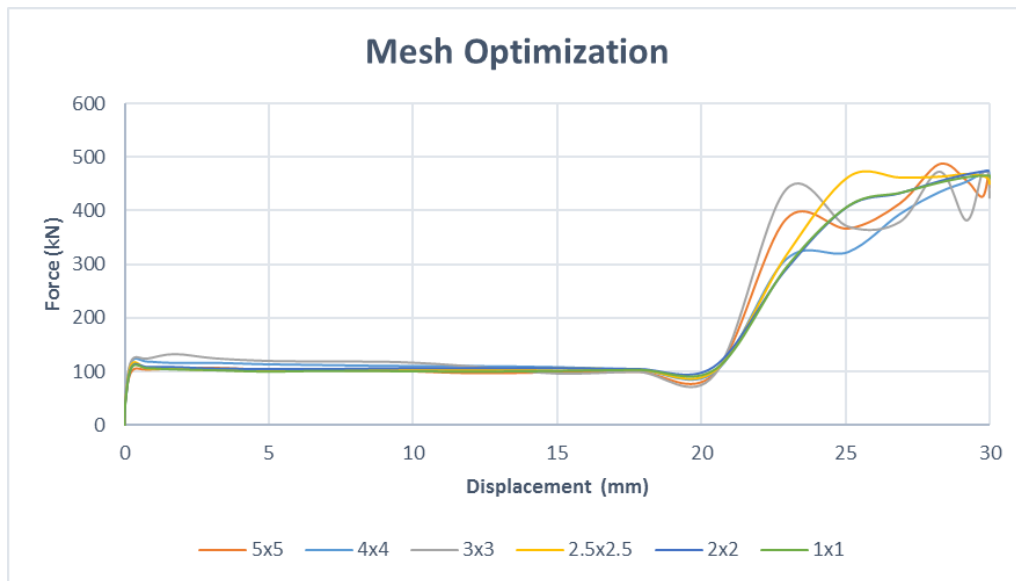
Figure 4.20 – Mesh optimization with varying size

Based on the above results finer mesh yields good results therefore, mesh size is used near the bolt holes to simulate better response of the assembly.

4.3.7 Interaction Properties

Modelling of bolted shear connection needs the precise simulation of the contact properties between the various connecting interfaces; the most fundamental concern in this studied connection (friction damper) is the interaction between the shearing surfaces and the interaction between the bolts and the bolt hole surfaces. The interface contact modelling is accomplished with ABAQUS (Abaqus, 2012) by providing surface to surface interaction (explicit) (Figure 4.21) with contact mechanical constrain formulation as plenty method along finite-sliding interaction between all the interacting surfaces. Interaction surfaces are applied through a surface to surface relationship, modelled between all the connecting parts namely:

(i) external plate with bolt head; (ii) external plate with friction pad; (iii) friction pad with internal plate (upper internal plate and lower internal plate) (iv) bolt holes with bolt shank. Whereas general contact properties are defined between all the surface to surface interactions except the interface between friction pads and internal plates, which is coated with thermally sprayed material also known as dissipative material having different coefficient of friction depending up on the experimental result.

Normal contact properties are accomplished with "hard-contact" property allowing for separation after contact; the tangential behaviour has been assumed with a friction coefficient of 0.2 following "penalty" formulation for the Coulomb frictional behaviour definition as steel to steel interaction. However, the tangential behaviour of the interface between friction pad with internal plates is defined by assessing the dynamic response of the friction assembly before the slip is allowed through experiments results, which is explained in detail in following sections. The slip, itself, is considered to be linear and isotropic (Abaqus, 2012).
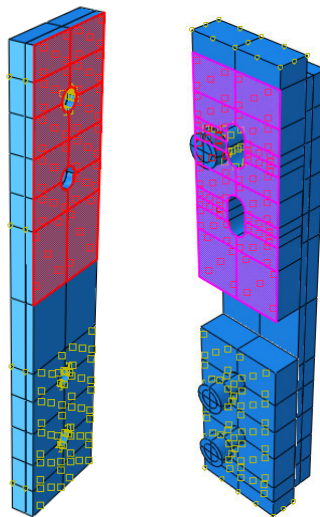
Figure 4.21 – Contact definition surface – to – surface.

4.3.8   Friction Modelling

Frictional mechanism is based on the materials coating used in the experimental campaign. For the purpose of various coatings, three different materials are used: i) two non-ferrous metals aluminium and zinc labelled as M4 and M1 respectively which are characterized for having a hardness much lower than the sliding stainless ("soft" materials) and ii) a carbide alloy Metco 70C-NS labelled as M6 which has a much higher hardness than the sliding stainless plate ("hard" materials). These

materials have been chosen from the investigation of the experimental tests of friction dampers (Santos *et al.*, 2017).

Friction dissipation is the fundamental mode of energy release and carries primary significance in the experimental campaign; therefore, before starting the finite element analysis of the damper assembly, delve understanding of the methods used to simulate complex phenomenon of friction by the ABAQUS software is required. In order to attain the real conditions, two basic simplified models were developed as represented in Figure 4.22, using similar geometry of the tested specimen with contact properties applied at the interface along with the introduction of normal pressure.
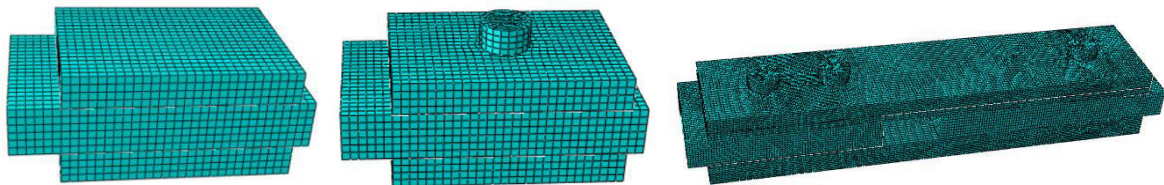
Figure 4.22 – Geometry of the simplified friction assembly a) without bolt, b) with bolt, c) complete model

There are two type of simplified models that was used to investigate the frictional behaviour. The first model was applied with a normal pressure on the outer plates and the inner plate was imposed with the displacements. The objective was to measure the sliding force required for initializing the movement. In the second model with preloaded bolt, the aim was to assess the slip force and to simulate the degradation of friction coefficient along the slippage through slotted bolt hole.

The external plates are considered to be made of steel S275 and internal plate is made of stainless steel AISI304. The pressure and apparent area of contact were modified and Amontons' and Coulomb's laws of friction for the generic cases of two metallic surfaces subjected to quasi-static tests were validated. The "laws of friction" cannot be applied for various cases. Therefore, to precise and validate the result values attained with FE methods in complex friction problems, comprehensive models, as well as experimentally determined coefficients of friction are required (Kloecke *et al.*, 2015).

It was clearly depicted from the simplified model results Figure 4.22, that the material behaviour introduced in the finite element model has no direct influence on the tangential behaviour while the plates sliding apart each other. The tangential behaviour introduced does not consider directly the plastic flow of the asperities,

their strain hardening, the adhesion and ploughing phenomena, the surface finish, and so on. For these reasons, the definition of the contact properties are of main interest for this work.

Most of the tribological interactions physically occurring are difficult to comprehend and not completely addressed by FE models. However, some approaches can indirectly introduce the friction coefficient variations. If the Coulomb approach is adopted as for simplified model, the input friction coefficient will remain constant as the load history proceeds as seen in the Figure 4.23:
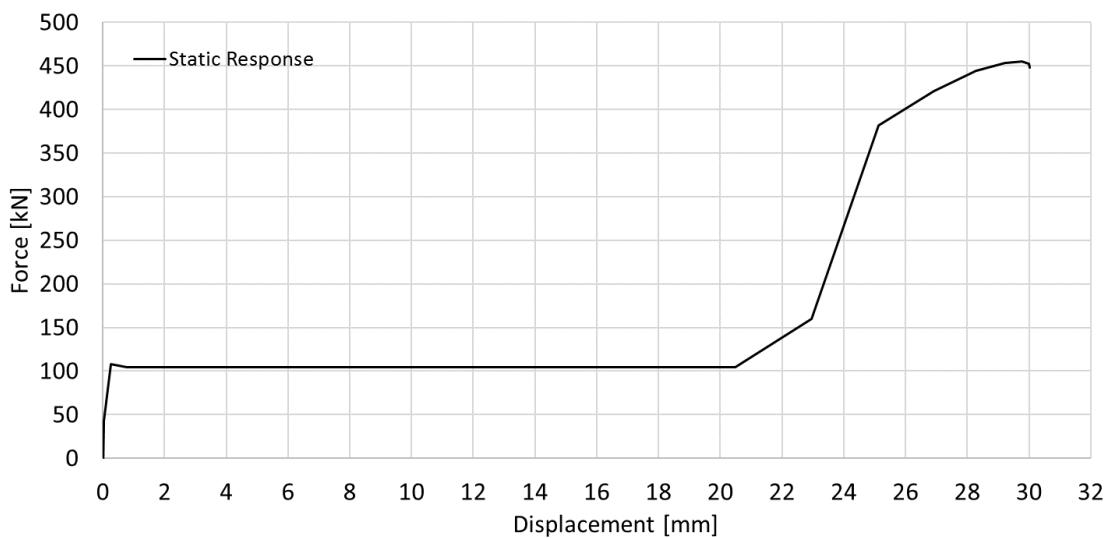
Figure 4.23 – Quasi-static response of damper with Coulomb's approach

- There is an occurrence of *stick-slip* phenomenon but not as it is depicted in the experimental results.
- The effect of significant *frictional damping* along the slippage is also not observed in the numerical results.
- No evidence of *2nd slip* was visible in numerical result.

In order to investigate the 2nd slip effect another approach was carried out with the implementation of distinct interaction properties to the lower and upper internal plates without any change in variables, as the slippage of both the plates occur at different moment. Therefore, separate interaction properties allowed to work at different instant of internal plate movement. Figure 4.24 clearly shows that the 2nd slip effect of the bolt in the fixed internal plate due to bolt hole tolerance and stick-slip motion.
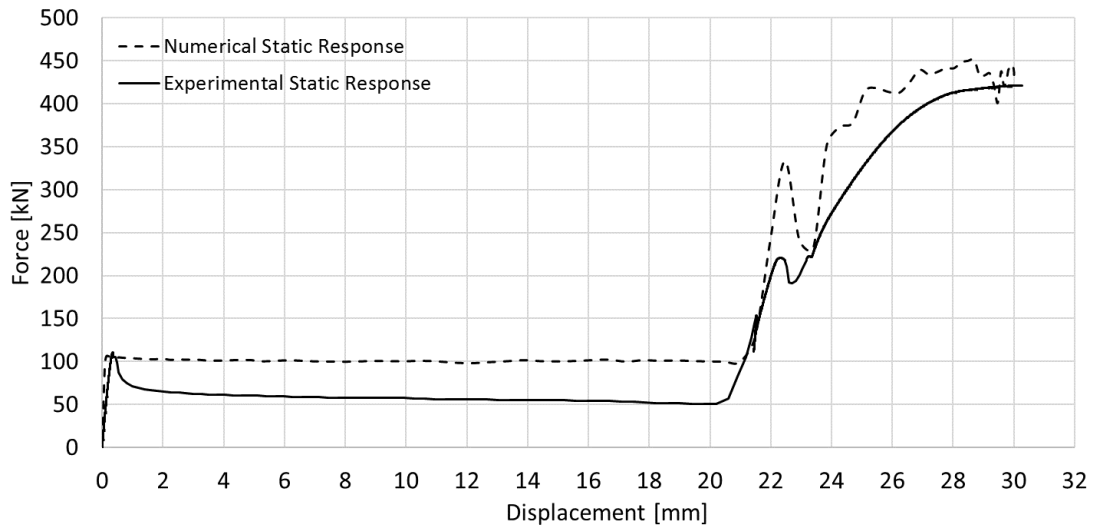
Figure 4.24 – Quasi-static response with 2nd slip

In order to incorporate all the concerns in finite element modelling, stick-slip motion and frictional degradation concept needs to be understood.

4.3.8.1 Stick – Slip Phenomenon

When two bodies are in contact with one another and one of them is compelled with tangential loading keeping the other body fixed, which results in sliding pass each other, intermittent vibration of relaxation phenomenon can be detected, specially at low driving velocities (quasi-static loading), this phenomenon is usually known as stick-slip motion (Bowden and Leben, 1939). Among the complex nonlinear behaviour of friction under dynamic systems are the nonlinear damping characteristics. *The essential condition for the occurrence of stick-slip motion is a decrease of the frictional force with increasing sliding speeds* (Oden and Martins, 1984).
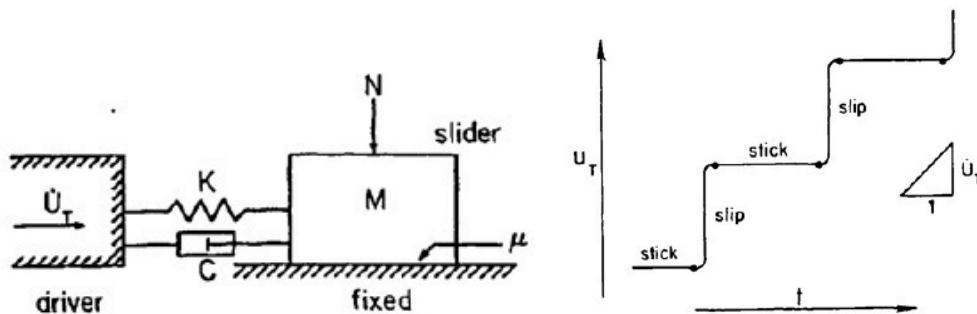
Figure 4.25 - Stick-slip response of a system (Oden and Martins, 1984)

Similarly, the experimental investigation describes the development of same phenomenon initially at the onset of the application of tension force microscopic sliding occurs. Then the continuous increment in the tangential force lead to the threshold value where the accumulation of forces reached to a point that stick and slip phenomenon takes place.

Stick-slip motion may be considered as an exhibition of dynamic instabilities integral in the bond of normal and tangential relative motions of contacting bodies. This phenomenon is not essentially an outcome of a decrease in the coefficient of friction with changes in sliding velocity, and can in fact be observed when the coefficient of friction is constant and equal to its so called static value.

It is possible to develop and to incorporate simple nonlinear interface models into a continuum model of elasto-dynamics which captures many fundamental features of dynamic friction. In particular, frictional damping can be depicted in such models in a natural and straightforward way.

Finite element approximations of the continuum models can be developed which feature consistently-derived frictional damping/stiffness matrices. These finite element methods, together with numerical schemes for solving associated systems of nonlinear ordinary differential equations, are capable of modelling stick-slip motion, dynamic sliding, friction damping, and related phenomena in a significant range of practical problems.

Therefore, this leads to the development of two approaches that have been employed in this study in order to simulate the effect of stick-slip phenomenon along with friction damping: i) static-kinetic exponential decay, ii) subscripting the decrease in preloading of bolts.

4.3.8.2   Static-Kinetic Exponential Decay

When stick-slips along with frictional damping transitions are relevant for the analysis, Abaqus provides a formulation that involves static-to-kinetic exponential decay. In order to induce a stick-slip phenomenon in the behaviour response of the friction damper, Abaqus also provides a model to specify a static and a kinetic friction coefficient directly. Experimental data show that the friction coefficient that opposes the initiation of slipping from a sticking condition is different from the friction coefficient that opposes established slipping (Figure 4.26). The former is typically referred to as the "static" friction coefficient, and the latter is referred to as the "kinetic" friction coefficient. Typically, the static friction coefficient is higher than the kinetic friction coefficient.

In this model it is assumed that the friction coefficient decays exponentially from the static value to the kinetic value according to the Eqn.17 (Abaqus, 2012).

$$\mu = \mu_k + (\mu_s - \mu_k)e^{-d_c \gamma_{eq}} \tag{17}$$

Where: μ_k is the kinetic friction coefficient, μ_s is the static friction coefficient, d_c is a user-defined decay coefficient, and γ_{eq} is the slip rate (Oden & Martins, 1985).
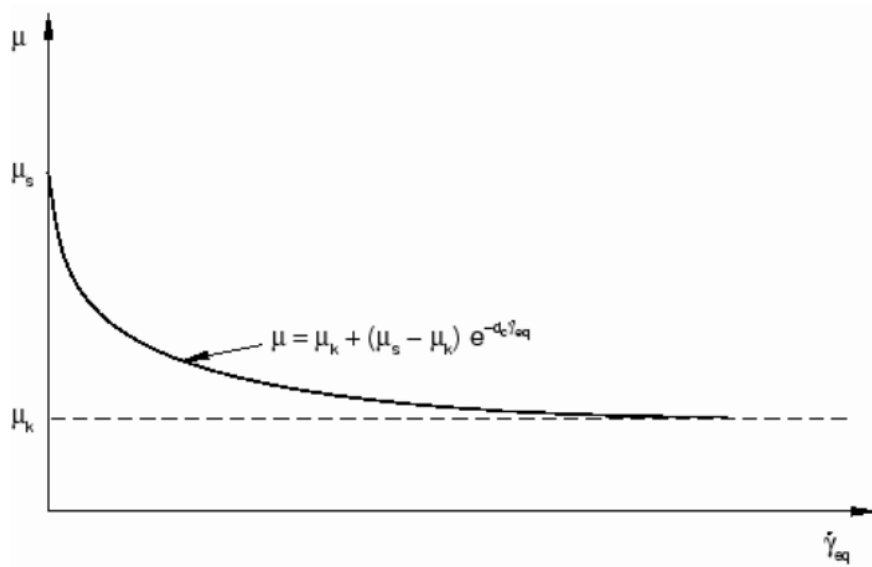
Figure 4.26 – Exponential decay friction model

To calculate the static coefficient, the kinetic coefficient and the decay coefficient experimental results are used to input the parameters in the static-kinetic exponential decay model. For calculation one of the quasi-static experiment result is used to depict the coefficients calculated by Eqn.18, Eqn.19 and Eqn.20.

$$\mu_s = F_{slip} / F_{preload} \tag{18}$$

Where: F_{slip} is the slippage resistance force and $F_{preload}$ is the normal load in the bolt.

$$\mu_k = F_{end} / F_{preload} \tag{19}$$

Where: F_{end} is the end slippage resistance force.

$$\gamma'_{eq} = \gamma / t \tag{20}$$

Slip rate is defined as the derivative with respect to time, which is calculated from experimental result. Whereas, the decay factor can be calculated by calibrating the experimental frictional coefficient values over the slippage with the value calculated from the static-kinetic exponential decay model as shown in Figure 4.27. Several iterations must be done to approximately calculate the decay factor with which friction model looks similar to the experimental curve.
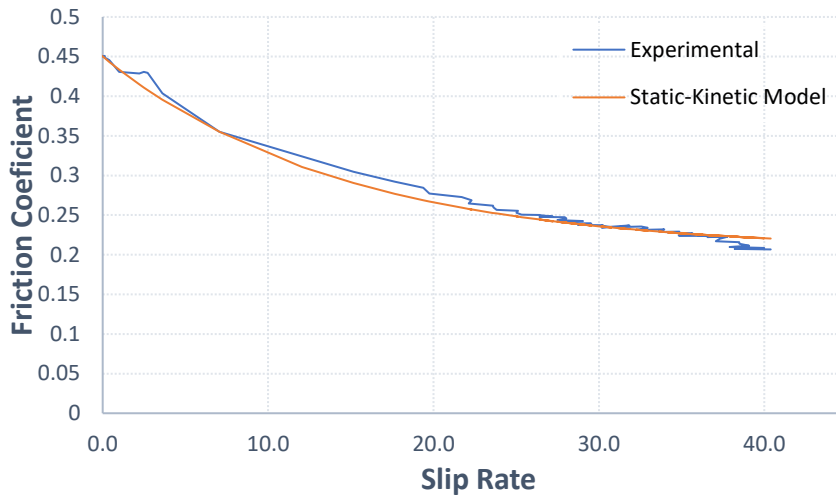
Figure 4.27 – Development of decay coefficient

Even after the use of static-kinetic model and providing the threshold kinetic friction, the results (Figure 4.28) obtain does not matched quite accurately to the experimental curve of quasi-static analysis. Therefore, further investigation was required using bolt preload relaxation.
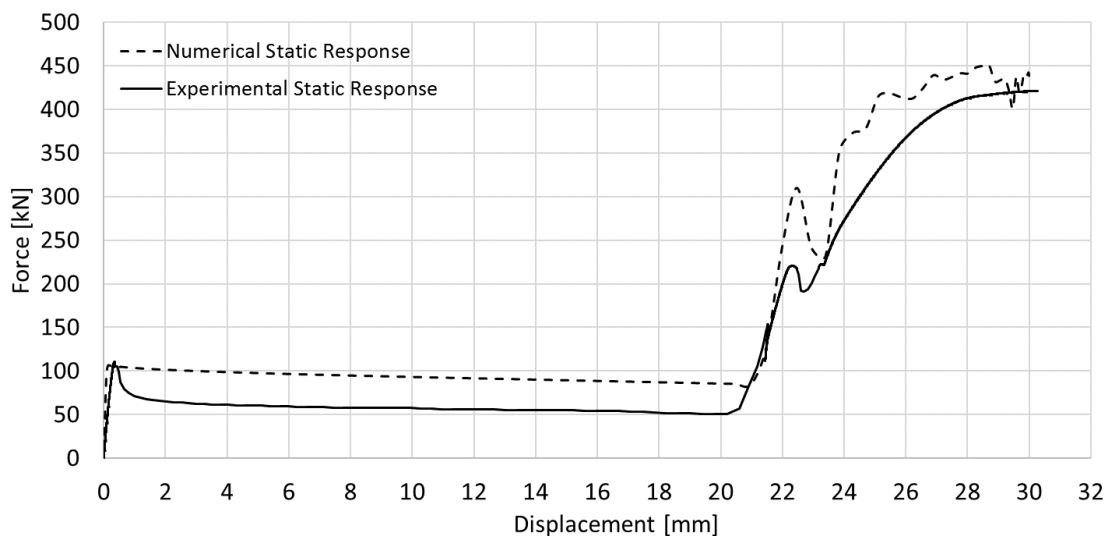
Figure 4.28 – Numerical results under quasi-static loading with static-kinetic decay model.

4.3.8.3   Preload Relaxation

The effect of friction damping is more significant when there is relaxation of clamping force due to the sudden slip takes place which is reported by sterling and co-authors (Sterling *et al.*, 1965). Therefore, the degradation of friction coefficient along the slippage can also be interpreted as the loss of preload normal force, which will ultimately reduce the friction grip while the frictional damping is applied. In order to do so subscripting is done by introducing degradation of clamping force indirectly in terms temperature field, applied in lieu of clamping amplitude in the second step of dynamic analysis developed in relation with experimental slip rate.

$$\mu = \frac{F_{slip}}{F_{preload}} \tag{21}$$
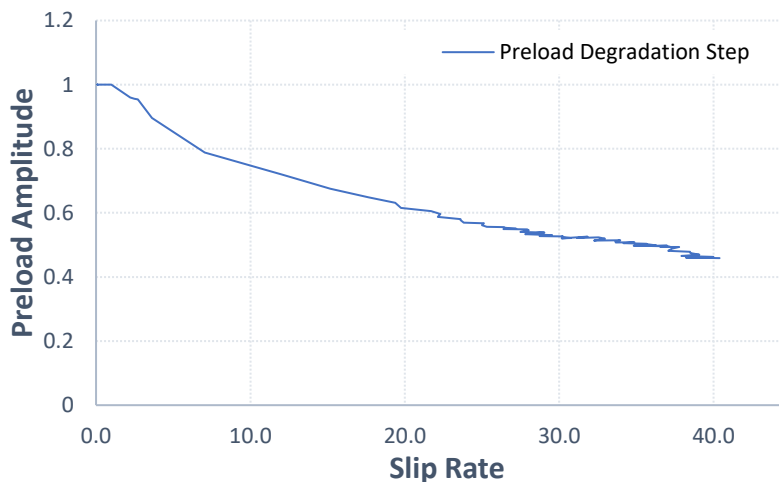
Figure 4.29 – Preload relaxation with the slip rate

Preloading is applied by dynamic explicit procedure in first step with a smooth clamping amplitude, which remain fully preloaded until the slippage take place in the pull-out plate. At the very onset of slip behaviour, the model will incorporate the degradation amplitude of preloading only in the bolt in slotted hole, as it is the only bolt experiencing the slippage, along with the friction damping with the slippage is incorporated by the method static-kinetic exponential decay. The moment the second slip take place along the bolts of fixed end plate the preloading degradation is also applied in those two bolts as well. The result (Figure 4.29) shows that the concept of this degradation and slip phenomenon exactly matches the experimental results. After incorporating the preload relaxation in the model, the final static

response in the Figure 4.30 depict that the immediate bolt preload relaxation provides the facilitation of friction damping as well.
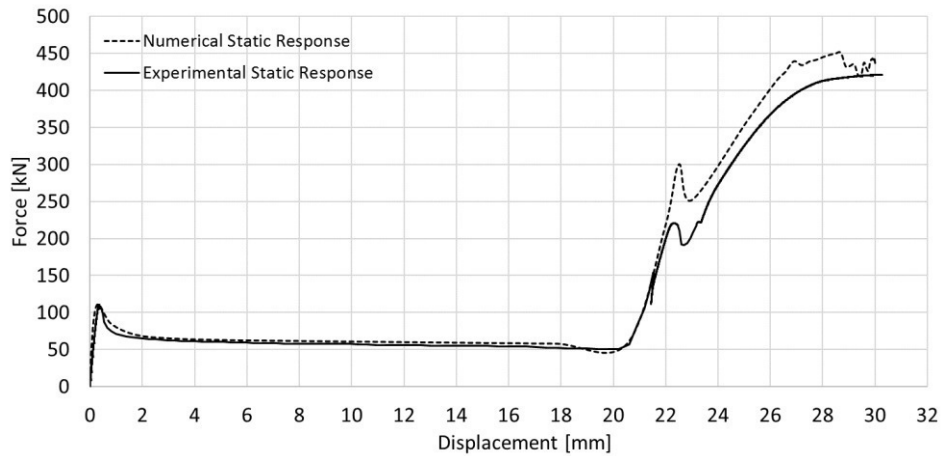
Figure 4.30 – Numerical results of quasi-static loading with frictional decay and preloading relaxation.

4.4   Discussion on Numerical Modelling

In order to simulate complex phenomenological problems, a full characterization of the tangential behaviour of the surfaces has to be performed and friction coefficients determined from experiments. These friction damping can then be introduced in more complex geometries, in which the same friction behaviour is expected, by using static-kinetic exponential decay model and by introducing preload relaxation in accordance with considerations related to energy.

The friction simulation completed in the present work resulted in the expected outcomes, making it possible therefore to introduce the same approach to the all the friction damping assembly, using these friction models. However, the time required to run such analysis is not compatible with this work. Even, this approach has no effect in the impact analysis of the friction damper connection.

5. DAMPERS UNDER STATIC AND IMPACT LOADING – NUMERICAL APPROACH

5.1   Experimental Programme – Static Loading

The validation of the numerical models establishing the non-linear response of friction device is based on the experimental results extracted from Santos and co-authors (Santos *et al.*, 2017). There were total of 8 quasi-static tests that have been executed as the part of experimental programme. Which were divided in three groups as represented in Table 5.1: Testing group A, using the specimen configuration A (Figure 4.7(b)), in which the performance of M20 class (10.9) HV bolts in shear is verified; Testing group B, using the specimens configurations A, in which the performance of a M20 class (8.8) SB in shear is conducted and Testing Group C using the specimen configuration C (Figure 4.7(b)), in which the behaviour of the plates in bearing was studied by using a lower thickness for the internal plates (10 mm). In addition, the three different friction surface treatments referred above have been used in tests (Santos *et al.*, 2017). In group A five quasi-static tests have been performed: three under force control (0.2 kN/s) using each of the selected coating materials and two under displacement control (0.01 mm/s). The reason to conduct both force control and displacement control is to assess the behaviour of slip resistance due to the variation in loads.

Table 5.1 - Experimental programme for Test Group A, B and C (Santos *et al.*, 2017)

(ID-Test: Tn°- X- Tt – Pt: Tn°=Test number- X=ID Coating Material (M4, M1, M6) – Tt=Test type: static (Static) – Pt=Internal plate thickness [mm])

Test Group A				
ID - Test	Specimen	Bolts class	Design value of Preload	Test Procedure
T8-M4-Static-30				Monotonic force control: 0.2KN/s
T8- M6-Static-30				Monotonic force control: 0.2KN/s
T8-M1-Static-30	A	M20 10.9 HV	$0.5 f_{ub} A_s$=122.5 kN k-factor =0.13 Mt =350 Nm	Monotonic force control: 0.2KN/s
T10-M4-Static-30				Monotonic displacement control: 0.01mm/s
T11 –M4–Static 30				Monotonic displacement control: 0.01mm/s
Test Group B				

T7-M1- Static-30	A	M20 8.8 SB	$0.5f_{ub}A_s = 98$ kN	Monotonic force control: 0.2kN/s
T7-M6-Static-30			Mt =370 Nm	Monotonic force control: 0.2kN/s
Test Group C				
T9-M1-Static-10	C	M20 10.9 HV	$0.5f_{ub}A_s = 122.5$ kN Mt =500 Nm	Monotonic force control: 0.2kN/s

5.2   Validation Under Static Loading

Friction dampers are validated against the experimental results which are classified according to group.

Group A

From the force-displacement curve shown in Figure 5.2, three different phases of behaviour can be observed under a quasi-static response. Initially, the force increases with no significant movement (micro displacement) until the achievement of the slip resistance force. This phase is categorized as "elastic phase" (Figure 5.1(a)). It dependents on the friction coefficient, which is extracted from the experimental results. Coefficient of friction is governed by the critical shear stress (τ_{crit}) and the normal load applied in terms of preload (F_b). Critical shear stress is the threshold stress develop at the interface, after that the assembly will start experiencing the slippage (2nd phase). In numerical model this phase is entirely based on the friction coefficient extracted from the experimental results and the preload applied in the bolts.

a) Elastic	b) Slip motion	c) 2nd slip	d) Failure
(1st phase)	(2nd phase)	(3rd phase)	(3rd phase)
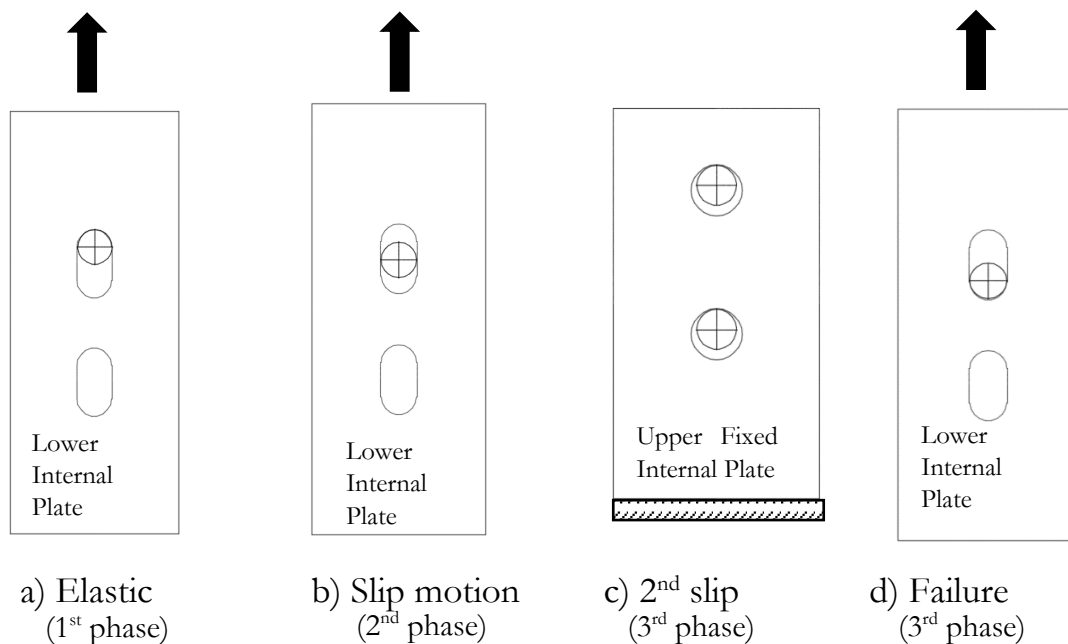
Figure 5.1 – Position of the bolt during the test

Second phase is the slippage of slotted plate over the friction pads (Figure 5.1 (b)), which begin immediately after the maximum slip force is achieved. The force experiences an immediate degradation, which is already justified in the chapter 4 that the bolt under goes "preload degradation". This degradation entirely depends on the initial magnitude of the preload applied. Then the force starts to decrease with the increase of slip until it reaches the force corresponding to the kinetic friction coefficient. This phase can be categorised as the "friction damping". For the preload degradation part, subscript is devised in terms of temperature gradient amplitude as mentioned earlier whereas, friction damping is incorporated by the static-kinetic exponential decay model (Abaqus, 2012).

Finally, the plate and bolt come in contact and subjected to shear and bearing until the attainment of the failure (3rd phase) (Figure 5.1 (d)). According to the design of specimen A, the assembly will fail due to the bolt shank in shear. In addition, before the achievement of the ultimate resistance, a second reduction of the force is visible (Figure 5.2) This phenomenon is explained by the stick-slip motion, as stated by Blok (Blok, 1940), soon after the bolt reaches the end stroke of the hole, the movement is restraint and a sticking behaviour takes place allowing the concentration of shear forces in the upper internal plate, followed by a second slip. However, this second slip is facilitated by the bolt hole tolerances in the fixed plate approximately on a load twice the load of first slip. In the end the bolt fails in shear so, this phase is based on the bolt material properties.
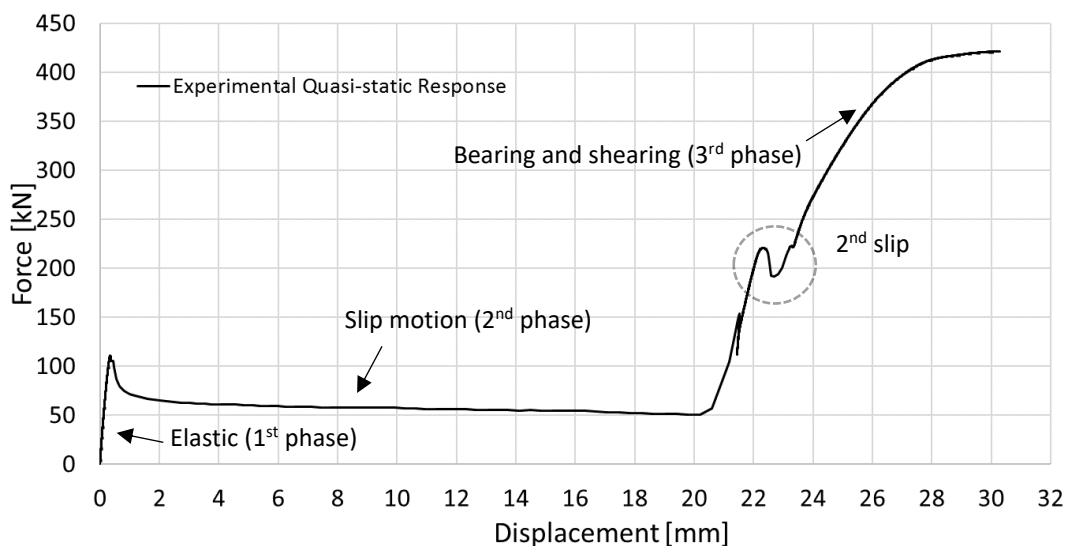
Figure 5.2 - Friction damper typical response under quasi-static loading of Group A

Group B

Correspondingly, the force-displacement curve depicts (Figure 5.3) a similar response as for the group A. The only evident difference lies in the second phase of friction damping and bolt preload degradation part. Which is not very imminent as it was in the group A. The reason for it is the use of M20 bolt (8.8) with lower strength and correspondingly the preload applied is also comparatively low, that results in such a slip even at a lower critical shear stress. This behaviour is also incorporated in the finite element modelling as the preloading degradation is subscripted as the function of temperature amplitude which would result a lower degradation in this case. Likewise, in the third phase of shearing, there is no such eminent slip observed, which was also due to the a very low degradation resulted by the slip of the bolts in the fixed plate. Ultimately the shear failure of bolt occurs at a comparatively, lower force due to the low strength bolt being used in the assembly.
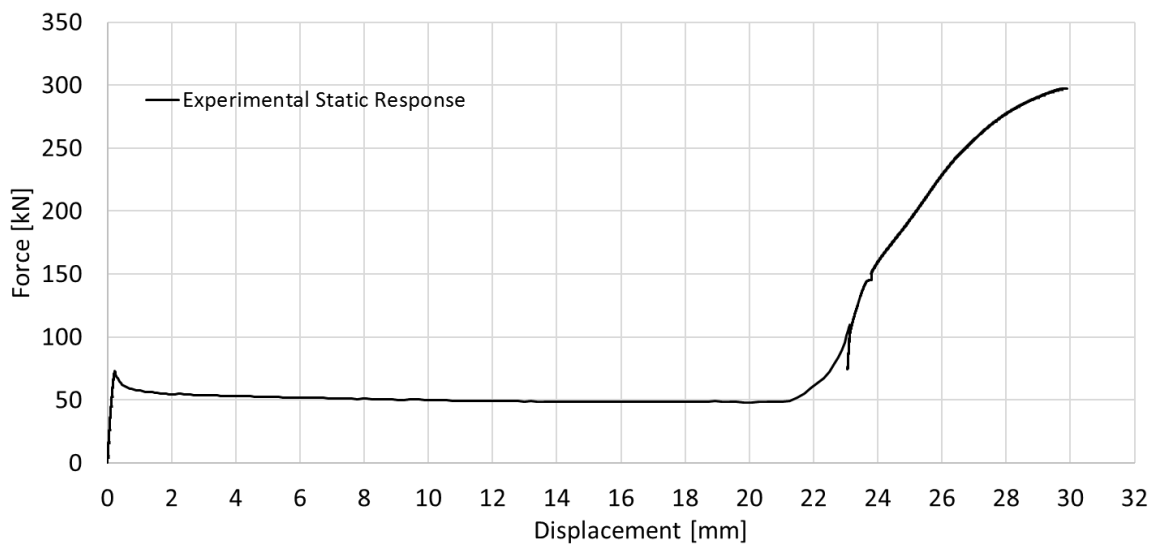
Figure 5.3 – Friction damper typical response under quasi-static loading of Group B

Group C

The whole force-displacement curve of specimen C is presented in Figure 5.4. From the quasi-static response four phases can be depicted in the Figure 5.5. First two phases are of same nature as explained in the earlier test groups, however the two failure modes can be discerned in the later phases. At first when the bolt slides on to the hole reaches the end stroke (Figure 5.5 (b)), the plate starts deformation in bearing. Pushing the hole to tear apart, as the plate thickness is 10mm. After this failure plate bearing, then almost immediately, the bolt reached the edge of the adjacent hole and the plate fails by plate net section in tension (Figure 5.5 (c) and

(d)). In order to simulate the ductile damage behaviour of the stainless steel AISI304 plate the damage model (as explained in chapter 3) is incorporated to evaluate the response. It should be noticed that only the first failure mode was possible to be achieved on the impact tests due to attainment of the maximum rotation of the layout. For this reason, only the force-displacement response up to the bearing of the plate hole (bearing failure of the curve Figure 5.4) will be considered in order to compare with the results from the impact tests.
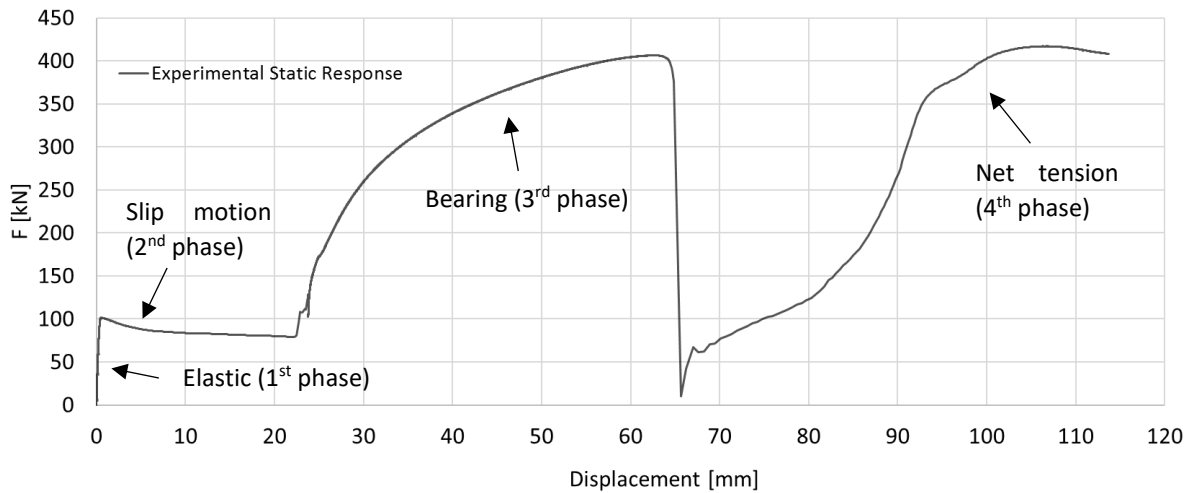
Figure 5.4 - Friction damper typical response under quasi-static loading of Group C

a) Elastic
(1st phase)

b) Slippage
(2nd phase)

c) Bearing Failure
(3rd phase)

d) Net Tension
(4th phase)
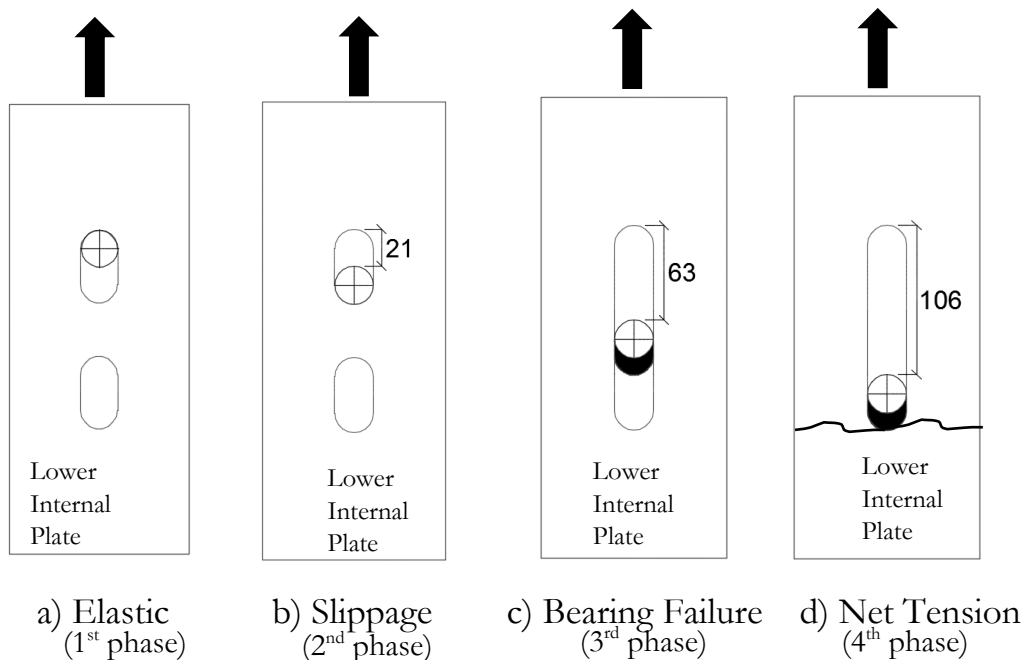
Figure 5.5 – Position of bolt during the test

European Erasmus Mundus Master
Sustainable Constructions under natural hazards and catastrophic events
520121-1-2011-1-CZ-ERA MUNDUS-EMMC

rusros

5.2.1 Numerical vs Experimental Results – Quasi-Static

Group A

The experimental results regarding the testing group A are presented in the Table 5.2. The force-displacement curves for the quasi-static tests using Aluminium, Tin and METCO 70C NS are reported in Figure 5.6. In these tests the slippage force was 156kN, 121kN and 110kN for materials TIN, Aluminium and METCO 70C NS, respectively; which corresponds an initial friction coefficient equal to 0.65, 0.49 and 0.45. After slippage, the failure happens for the bolt in shear in all tests for an ultimate resistance equal to 450KN, 470KN and 421KN. In addition, in all the cases the ultimate resistance achieved in numerical results showed some difference compare to the experiments; as it depends on the material properties of the M20 bolt (10.9) which was derived from trilinear model of material properties. Furthermore, the analytical method (EC-3) conservatively calculates the ultimate design force.

Table 5.2 – Experimental, Numerical and Analytical Results for Test Group A

(ID-Test: Tn°- X- Tt – Pt: Tn°=Test number- X=ID Coating Material (M4, M1, M6) – Tt=Test type: static (Static) – Pt=Internal plate thickness [mm])

		F_{slip} [kN]	μ	F_{ult} [kN]	δ_{max} [mm]	Failure Mode
T8 - M1 - Static-30	Analytic-EC3	-	-	377	-	
	Experimental	156	0.65	450	30.17	Bolt in shear
	Numerical	160	0.65	457	30.1	
T11- M4 - Static-30	Analytic-EC3	-	-	377	-	
	Experimental	121	0.49	470	31.34	Bolt in shear
	Numerical	125	0.49	455	30.2	
T8 - M6 - Static-30	Analytic-EC3	-	-	377	-	
	Experimental	110	0.45	421	30.28	Bolt in shear
	Numerical	108	0.45	452	30.02	
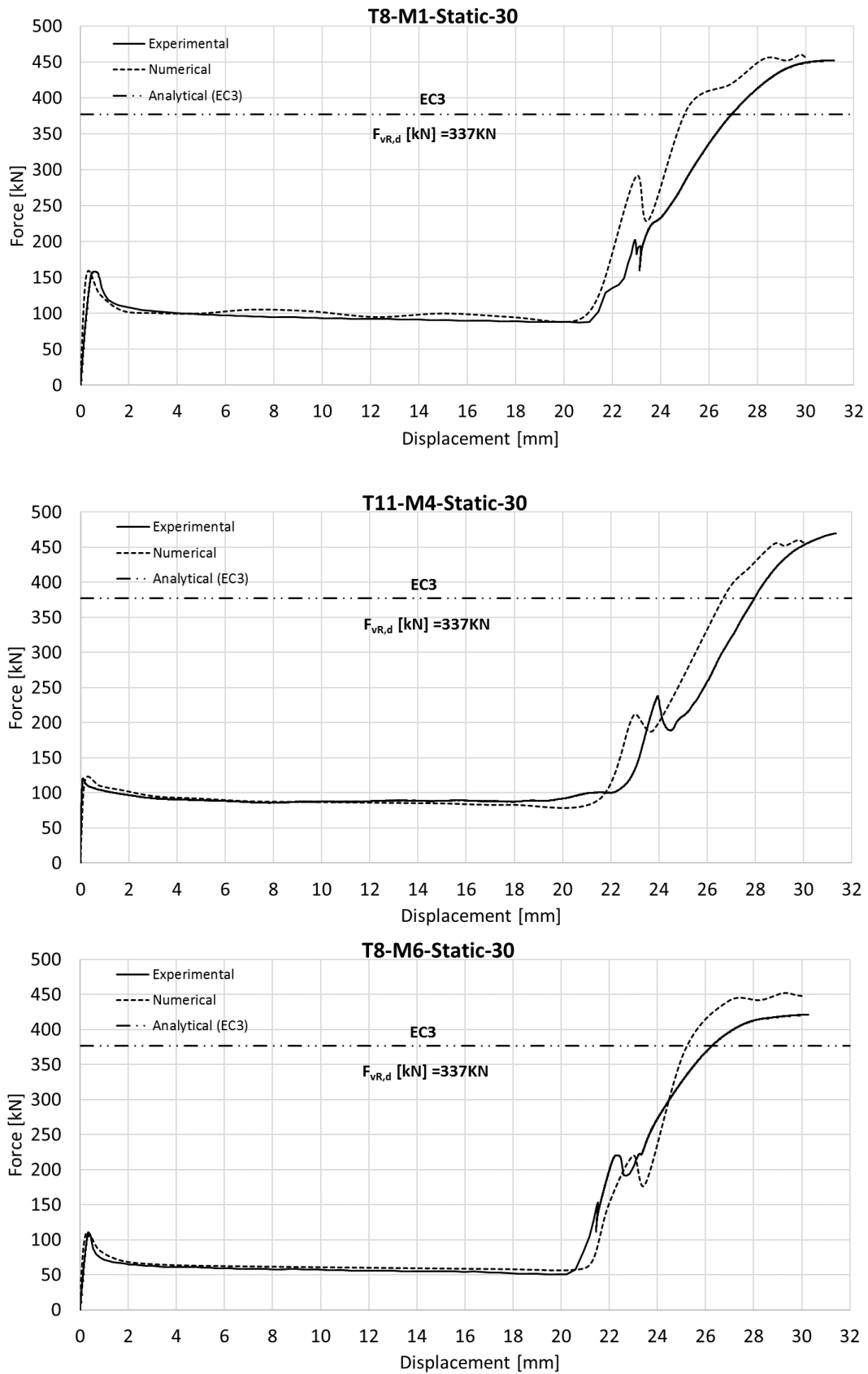
Figure 5.6 - Experimental and numerical quasi-static response of group A

a) Critical shear stress at 1st slip

b) Slippage initiation

c) Critical shear stress at of 2nd slip

d) Ultimate shear failure

Figure 5.7 – Static response of specimen A

Comparing the global response for the assemblies, it can be observed that the damper undergoes bolt shear failure, resulting into a stiffer behaviour failure which occur at comparatively lower distance. Although, all specimens were bolted with the same M20 (10.9) bolts and even the failure mode was also similar however, the friction material used for the dissipation differs which result in difference in slip resistance of the specimen, but overall ultimate resistance remains somewhat similar.

Group B

The experimental results concerning the testing group B are presented in the following section. The force-displacement curves for the quasi-static tests Tin and METCO 70C NS are reported in Figure 5.9. In these tests the slippage force was 65kN and 75kN for materials TIN and METCO 70C NS, respectively; which corresponds an initial friction coefficient equal to 0.33 and 0.38. After slippage, the failure happens for the bolt in shear in both tests for an ultimate resistance equal to 290KN and 297KN. In addition, in both cases the ultimate resistance achieved in numerical results was significantly higher than attained experimentally, which could be dependent on the material properties of the M20 bolt (8.8). Furthermore, in both cases the ultimate force achieved was significantly higher than the one given by the code (Table 5.3).
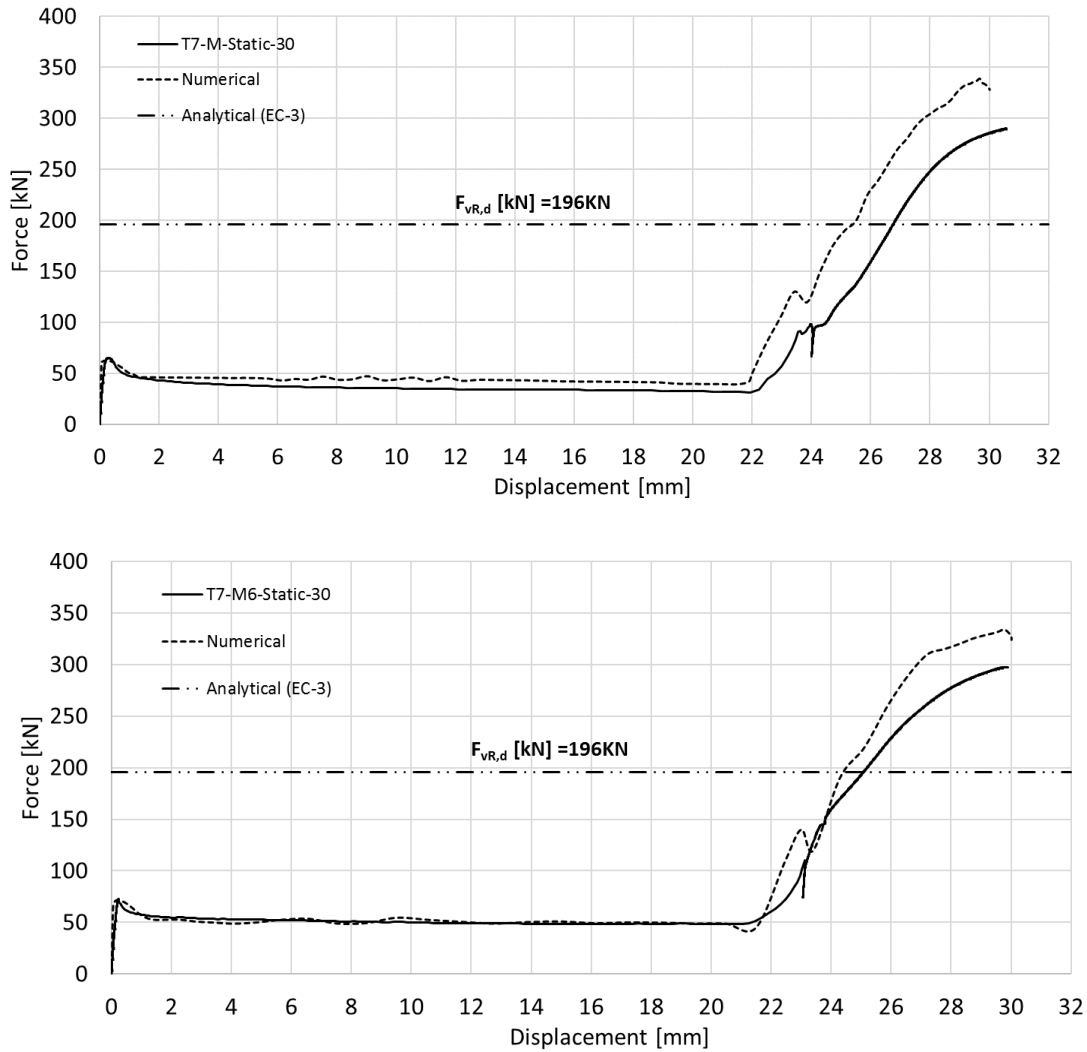
Figure 5.8 – Force displacement curve for monotonic loading: Numerical versus experimental results.

Table 5.3 – Experimental, Numerical and Analytical Results for Test Group B

		F_{slip} [kN]	μ	F_{ult} [kN]	$δ_{max}$ [mm]	Failure Mode
	Analytic-EC3	-	-	196	-	
	Experimental	65	0.33	270	30.58	Bolt in shear
T7 – M1- Static-30	Numerical	62.3	0.33	337	30.1	
	Analytic-EC3	-	-	196	-	
	Experimental	75	0.38	297	29.89	Bolt in shear
T10 - M6- Static-30	Numerical	71	0.38	334	30.01	

a) Slippage   b) 2nd Slip
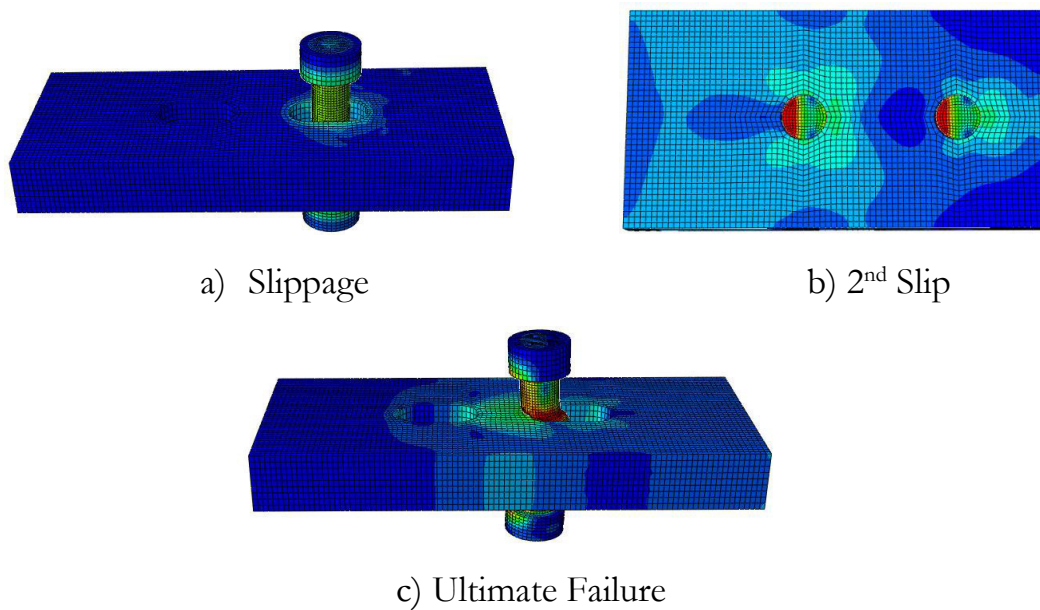
c) Ultimate Failure

Figure 5.9 - Static response of the group B

Comparing the global response of both assemblies, it can be observed that the bolt undergoes shear failure, stiffer behaviour is observed due to the bolt shear failure which occur at a lower ultimate strength compare to group A as M20 bolt (8.8) is used in group B. Although both specimens were bolted with the same M20 (8.8) bolt and both failed through the bolt shear failure but the friction material used for the dissipation diff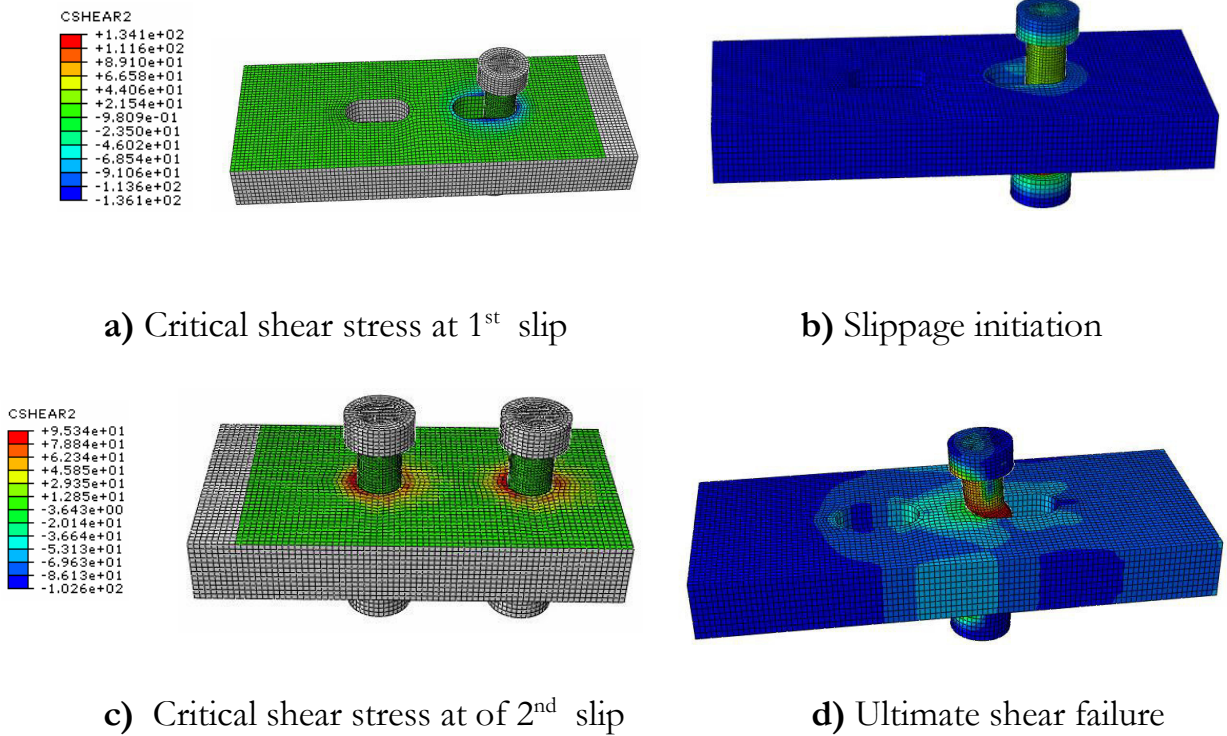ers which result in difference in slip resistance of the specimen. The Figure 5.9 shows the numerical model and response at different phases.

Group C

The experimental result concerning the testing group C are presented in the following section. The force-displacement curve for the quasi-static tests Tin is reported in Figure 5.9. In this test the slippage force was 100kN which corresponds an initial friction coefficient equal to 0.41. After slippage, the failure happens in bearing of internal plate AISI304 for an ultimate resistance equal to 406KN. In addition, the ultimate resistance achieved in numerical results was approximately same, which depends on the material properties of the stainless-steel plate AISI304. Furthermore, ultimate force achieved was significantly higher than the one given derived from the code (Table 5.4).
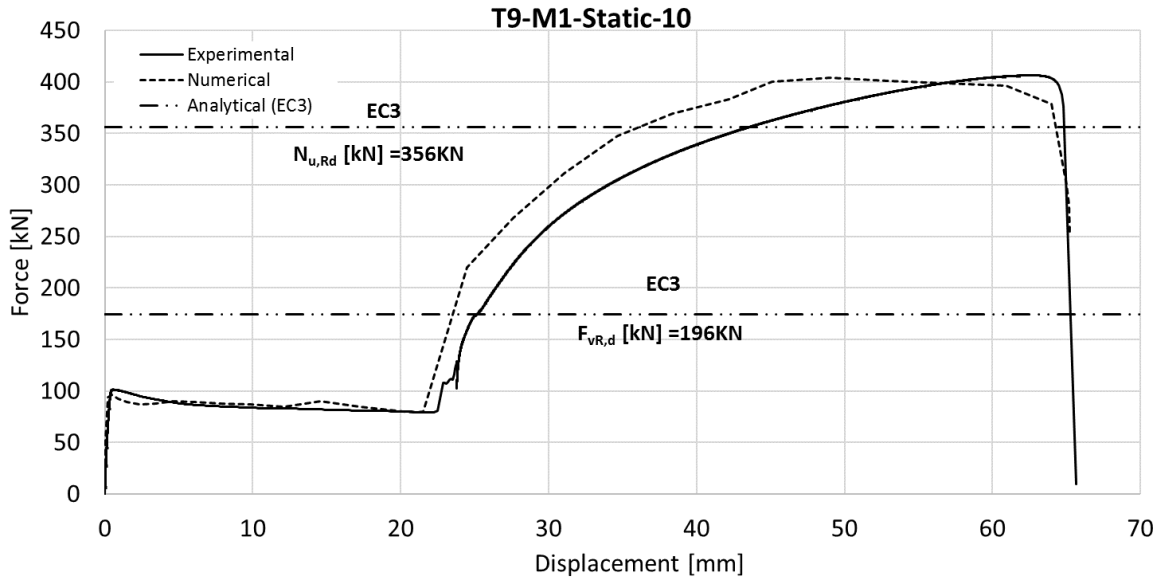
Figure 5.10 - Force displacement curve for monotonic loading: Numerical versus experimental results.

Table 5.4 –Experimental, Numerical and Analytical Results for Test Group C

		F_{slip} [kN]	μ	F_{ult} [kN]	δ_{max} [mm]	Failure Mode
T8 - M1 - Static-30	Analytic-EC3	-	-	356	-	Plate in bearing / net section in tension
	Experimental	100	0.41	406	62.5	
	Numerical	96	0.41	400	61	

The assembly depicted ductile behaviour, which lead to a failure mode due to the bearing of plate.

Figure 5.11 shows the damage onset of the plate due to bearing. Necking is also observed in the experimental test similarly it can be seen in the numerical model. Damage model is just used to define the onset of cracking however, accurate crack propagation cannot be predicted from this damage model.
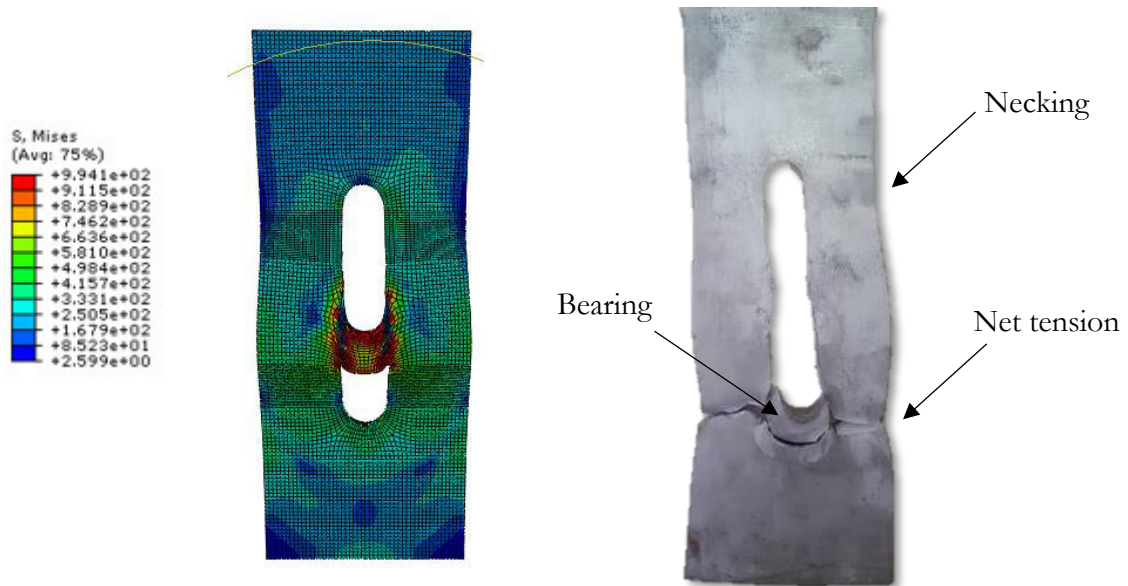
Figure 5.11 – Bearing failure in the internal plate.

5.3   Experimental Programme – Impact Loading

The validation of the numerical models establishing the non-linear transient response of friction device is based on the experimental results extracted from Santos and co-authors (Santos *et al.*, 2017). A total of 32 impact tests have been carried out. Similarly, like quasi-static testing, the experimental programme is divided into three testing groups (Table 5.5). Concerning the impact tests, two types of impact have been considered: sequential impact and full impact. In the sequential impact tests, the specimen is loaded and unloaded with an additional impact until the failure of the specimen, while in a full impact test the specimen is loaded with the collapse load. The sequential tests are used in order to determine an approximate value of the impact loading needed to achieve the failure. In addition, the unloading phase is also used to determine the elastic stiffness, which is difficult to define during the initial phase due to parasite displacements in the system. However, for the numerical study only full impact testing is considered, to determine the non-linear response of the assembly. In group A, two full impact tests have been executed, with

impact (pressure 100Bar and 80Bar) being applied in a very small-time period (0.1s) by piston.

Table 5.5 - Experimental programme for Test Group A, B and C

(ID-Test: Tn°- X- Tt – Pt: Tn°=Test number- X=ID Coating Material (M4, M1, M6) – Tt=Test type: Sequential (SI), Full Impact (FI), static (Static) – Pt=Internal plate thickness [mm])

ID - Test	Specimen	Bolts class	Design value of Preload	Test Procedure
Test Group A				
T4- M1- FI-30	A	M20 10.9 HV	$0.5f_{ub}A_s$=122.5 kN k-factor =0.13 Mt =350 Nm	1 Impact: #100Bar
T4- M6- FI-30				1 Impact: #100Bar
Test Group B				
T2-M1- FI-30	B	M20 8.8 SB	$0.5f_{ub}A_s$ = 98 kN Mt =370 Nm	1 Impact: #80
Test Group C				
T5-M4- SI-10	C	M20 10.9 HV	$0.5f_{ub}A_s$ =122.5 kN Mt =500 Nm	5 Impacts: #50Bar; #80Bar; #100Bar; #120Bar; #150Bar

5.4 Validation Under Impact Loading

5.4.1 Loading application Procedure

The numerical validation under impact loading conditions consider specimens, for two different load level input according to the experimental layout described in chapter 4: gas pressure of 100 Bar (Impact #1 of T4) and 80 Bar (Impact #1 of T2) (Santos e*t al.*, 2017). Each load level induces a transient displacement curve represented in Figure 5.12; the maximum displacement values are reached in approximately 100 milli-seconds. These experimental displacement fields are applied as a boundary condition in the "pull-out surface" of the numerical model and the generated reaction forces on the fixed surface" extracted. However, later velocity is applied as the boundary condition in order to induce the impact loading which yielded good results.
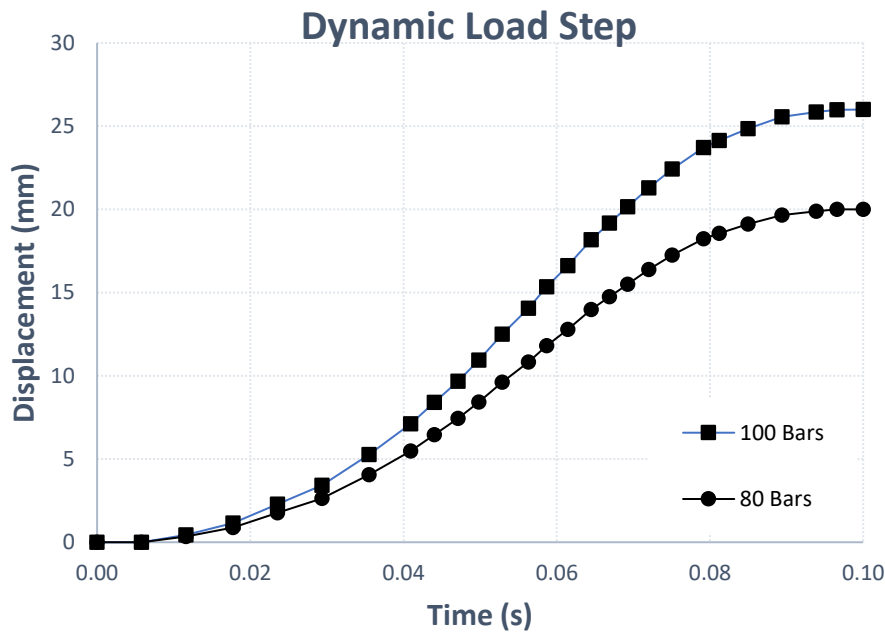
Figure 5.12 - Friction damper displacement curves used for dynamic loading application in the FEA.

Group A

The impact tests performed on the specimen A are represented in Table 5.6 and compared with the reference quasi-static test. The force-displacement curves for the impact tests using Tin and METCO 70C NS are shown in Figure 5.13. It can be clearly observed, that due to the elevated strain rate, not only the material strength properties are varied, but also the initial friction coefficient is dynamically increased. In the tests, slippage force was amplified to 170kN and 120kN respectively, which corresponds to an increase of the initial friction to 0.7 and 0.49. Although, failure mode remains, the same as it was in quasi-static test but the response became stiffer (Figure 5.14). The M20 bolt (10.9) undergoes shear failure although at a higher ultimate resistance but at a lower displacement, which depict the brittle behaviour due to the high strain rates. In numerical model the Johnson – Cook law is employed based on the experimental test performed at elevated strain rate. Therefore, the numerical results depict a close approximation of the experimental results. Mechanical properties of the material at elevated strain rate as explained in Chapter 3, which are incorporated along with the elevated friction coefficient, extracted from the experimental test. The fluctuations observed in the response during the slippage are due to the high velocities induced in the test and inertial force come into play. Contrarily, to what observed in the static tests, the degradation of the force is less significant. However, in the finite element modelling the initial friction coefficient

was taken from the experimental results but even after the application of friction damping through static-kinetic decay model, like in quasi-static model, no appreciable damping was observed. This type of behaviour has been also stated by Blok, which stated that for higher velocities, the initial friction coefficient is closer to the kinetic coefficient, which remains similar during the slip (Blok, 1940). Concerning the ultimate resistance force, a value is increased by dynamic increase factor which is higher than the one observed in quasi-static tests. Conversely, for both impact tests the ultimate deformation has decreased approximately 13% compared to the quasi-static. The fluctuating response of the force is due to the high velocities applied in the numerical model which also take into account the inertial forces.

Figure 5.13 - Force displacement curve for impact loading: Numerical versus experimental results.

Table 5.6 – Experimental vs Numerical results for Test Group A

		F_{slip} [kN]	μ	F_{ult} [kN]	$DIF_{collapse}$	δ_{max} [mm]	$\delta_{colapse\_imp}$/ $\delta_{colapse\_static}$	Failure Mode
T4 - M1-FI-30	Static	156	0.65	450	-	30.17	-	Bolt in shear
	Experimental	170	0.7	479	1.06	25.85	0.87	
	Numerical	180	0.7	475	1.05	26	0.867	
T4- M6- FI-30	Static	110	0.45	421		30	-	Bolt in shear
	Experimental	120	0.49	453	1.08	25.67	0.856	
	Numerical	127	0.49	465	1.09	26	0.867	

F_{slip} – the initial slippage force; μ - initial friction coefficient; $F_{collapse}$ – ultimate resistance of the friction damper; DIF – dynamic increase factor, DIF = $F_{collapse\_imp}$/ $F_{collapse\_static}$; δ_{max} – ultimate deformation of the friction damper;

a)   b)
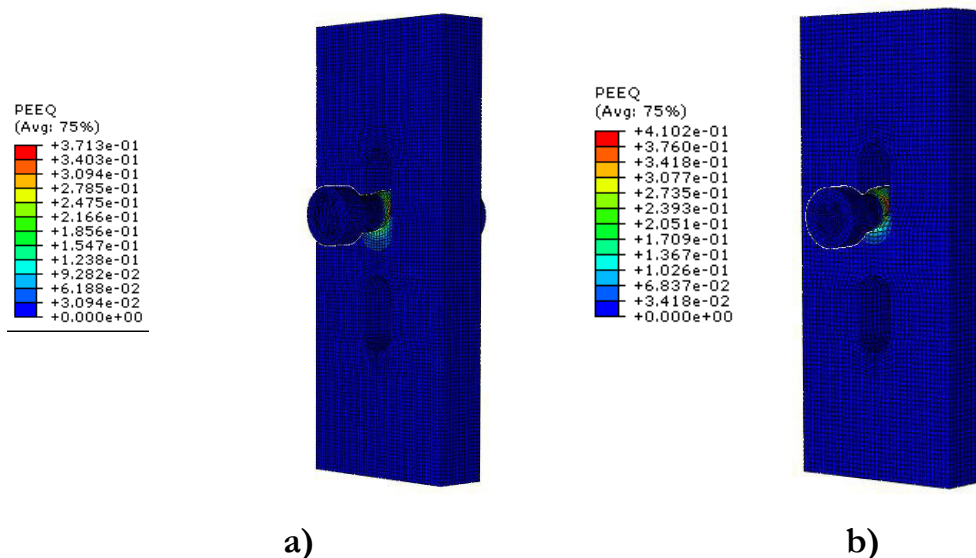
Figure 5.14 - Equivalent strain patterns (PEEQ) [-] – a) Impact Vs. b) Quasi-Static

Group B

The impact tests performed on the specimen B are represented in Table 3.1 and the force-displacement curves for the impact tests using METCO 70C NS are shown in Figure 5.15. In this case no experimental quasi-static test was carried out. In the tests slippage force was amplified to 150kN, which corresponds to the initial friction coefficient of 0.77. The bolt geometry used in this case is elongated hole as specified in the specimen B, which allows the dissipation along the slippage. The M20 bolt (8.8) was used in this assembly which resulted in a shear failure at a very low strength, showing the brittle behaviour under high strain rates. In numerical models the Johnson – Cook law is employed based on the experimental test performed at elevated strain rate. Numerical results in this case was not very close to the experimental results, probably because due to the bolt properties used, as they were not from the same batch of the tested bolts. The Figure 5.16 shows the friction assembly undergoes shear failure.
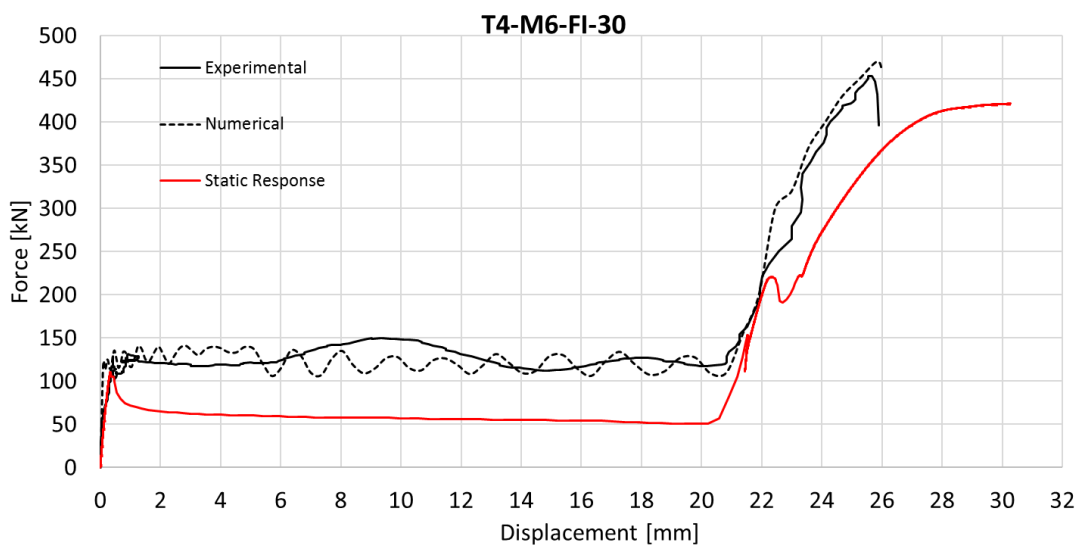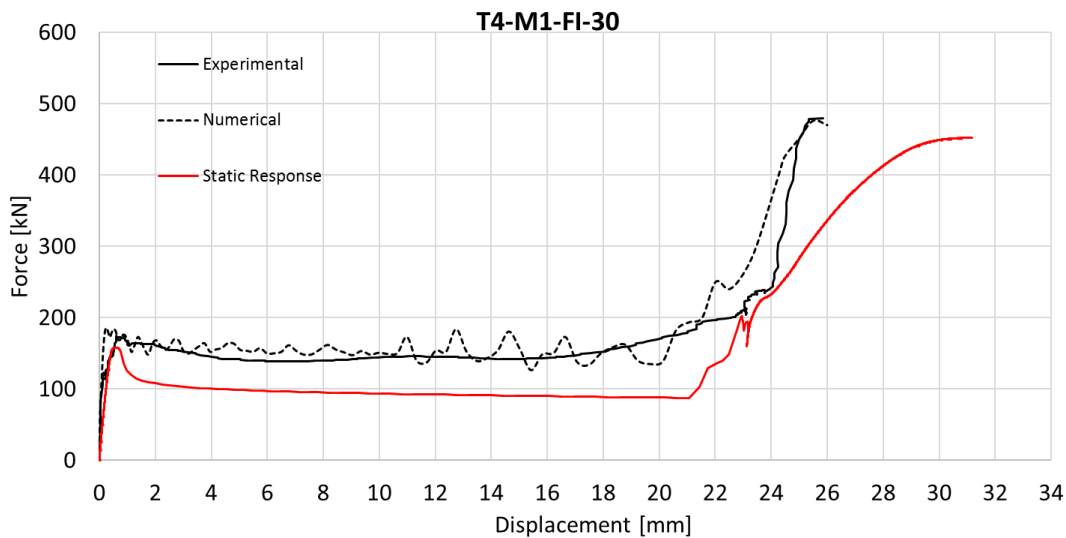

Figure 5.15 - Force displacement curve for impact loading: Numerical versus experimental results.

Table 5.7 - Experimental and numerical results for Test Group B

		F_{slip} [kN]	μ	F_{ult} [kN]	$DIF_{collapse}$	$δ_{max}$ [mm]	$δ_{colapse\_imp}/$ $δ_{colapse\_static}$	Failure Mode
T42- M6-FI-30	Static	-	-	-	-	-	-	
	Experimental	150	0.77	315	-	35.38	-	Bolt in shear
	Numerical	155	0.77	398	-	34.4		

F_{slip} – the initial slippage force; μ - initial friction coefficient; $F_{collapse}$ – ultimate resistance of the friction damper; DIF – dynamic increase factor, DIF $=F_{collapse\_imp}/F_{collapse\_static}$; δ_{max} – ultimate deformation of the friction damper;
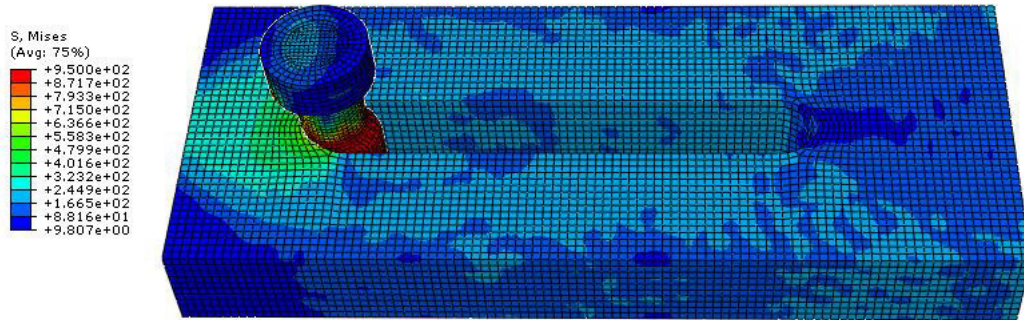

Figure 5.16 – Stresses developed at the interface due to shearing

Group C

The numerical impact tests performed on the specimen C are represented in Table 5.8 with the reference of the quasi-static test and sequential impact test. The force-displacement curves for the experimental sequential impact tests using Tin are compared with numerical full impact test as shown in Figure 5.17. It can be clearly observed due to the elevated strain rate; the damper depicts the brittle behaviour and undergo bearing failure of the displacing internal plate. However not only the material mechanical properties are varied but also the initial friction coefficient is augmented by dynamic increase factor (DIF). Although in this test slip force is barely amplified, failure mode remain same as it was in quasi-static test but the response became stiffer. The stainless steel AISI304 internal plate fails in bearing at a higher ultimate resistance but at a lower displacement. Therefore, the numerical results depict a close approximation of the experimental results. The fluctuations observed in the response during the slippage are due to the high velocities induced in the test and the abrasion resistance provided by the slipping surface. Concerning the ultimate resistance force, a value 9% (DIF$_{colapse}$=1.09) higher than the one found for the quasi-static one is observed. Conversely, for both impact tests the ultimate deformation has decreased approximately 30% compared to the quasi-static.
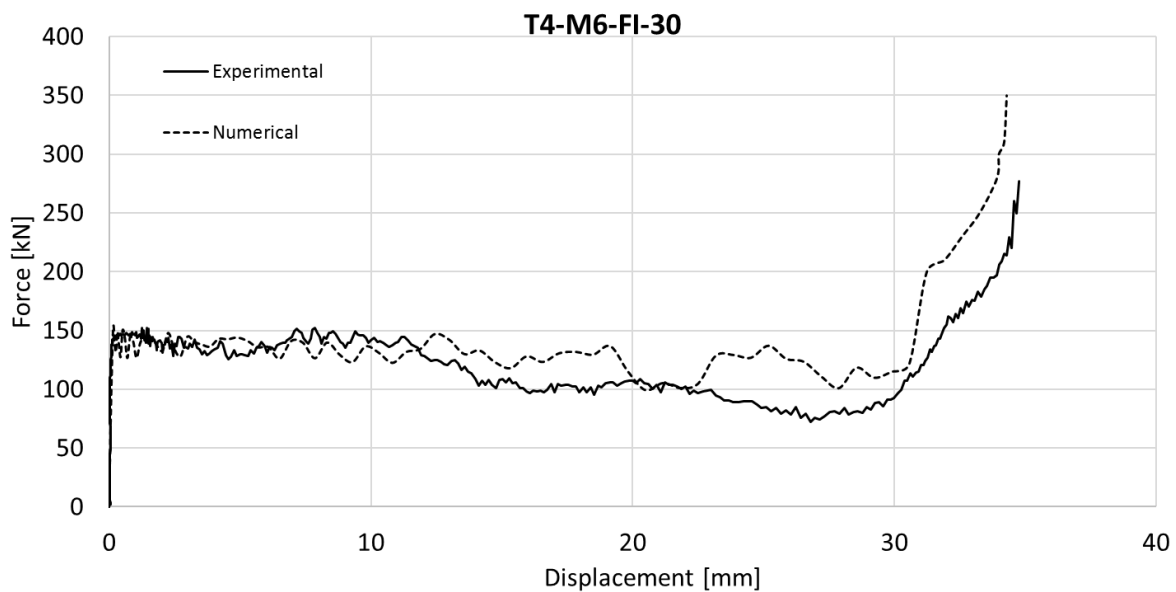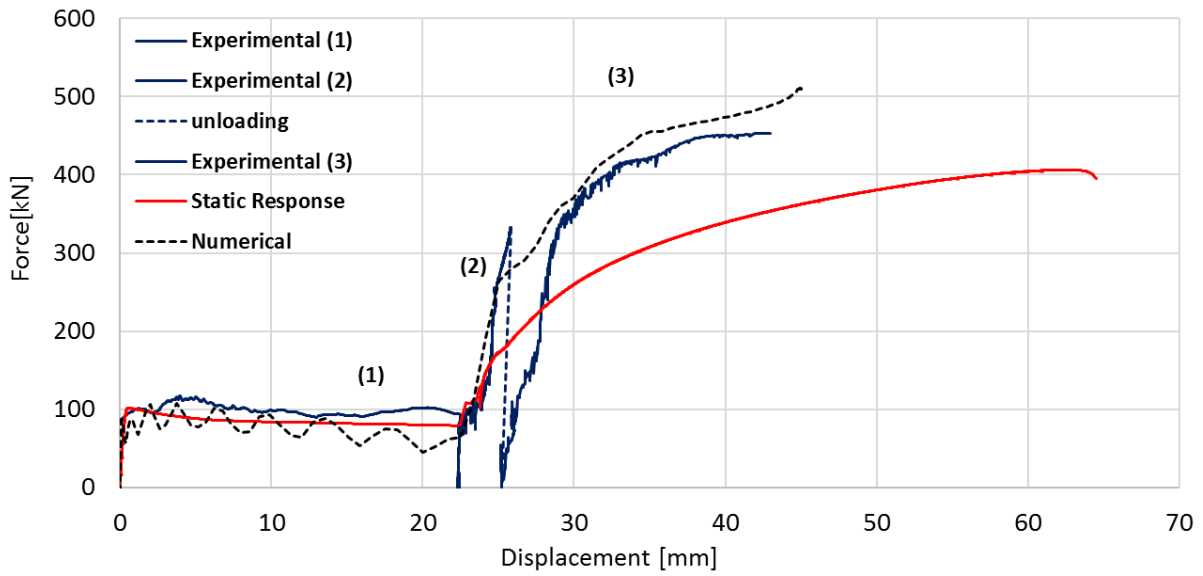
Figure 5.17 - Force displacement curve for impact loading: Numerical versus experimental results.

Table 5.8 - Experimental and numerical results for Test Group C

		F_{slip} [kN]	μ	F_{ult} [kN]	$DIF_{collapse}$	δ_{max} [mm]	$\delta_{colapse\_imp}/\delta_{colapse\_static}$	Failure Mode
T5 - M1-SI-10	Static	100	0.41	406	-	62.5	-	Plate in Bearing
	Experimental	100	0.41	443	1.09	43	0.69	
	Numerical	100	0.41	510	1.25	45	0.72	

F_{slip} – the initial slippage force; μ - initial friction coefficient; $F_{collapse}$ – ultimate resistance of the friction damper; DIF – dynamic increase factor, DIF =$F_{collapse\_imp}/F_{collapse\_static}$; δ_{max} – ultimate deformation of the friction damper;


a)   b)
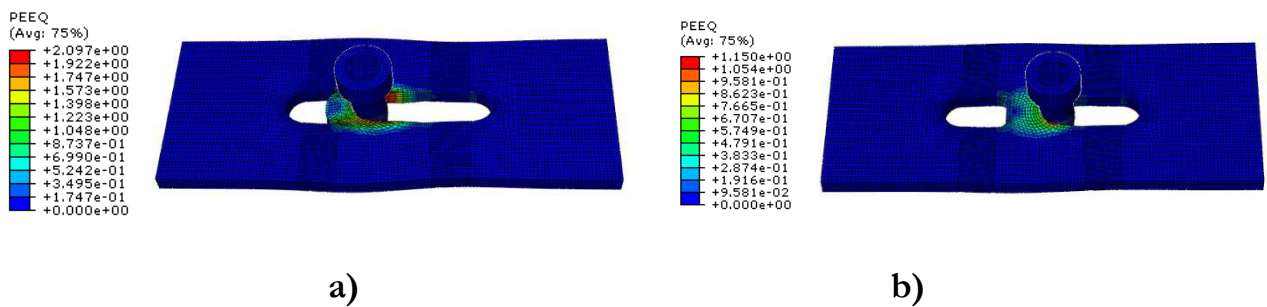
Figure 5.18 - Equivalent strain patterns (PEEQ) [-] – a) Static Vs. b) Impact

5.4.2   Concluding Remarks

In this chapter, the numerical models were validated with the experimental campaign concerning the behaviour of the friction dampers under quasi-static loading and impact loading along with the detail results explanation. Some conclusions can be deduced regarding the complex behaviour of friction material and the non-linear behaviour of the different geometries.

It can be concluded from the tests results

- Specimen A undergo M20 bolt (10.9) shear failure, which depict a brittle behaviour as the failure was entirely dependent on the bolt properties. At elevated strain rate the material undergoes even sudden failure but at a higher ultimate force.
- Specimen B is equipped with elongated slotted hole which facilitates with the dissipative mechanism along the slippage of the slotted hole. However, the ultimate failure even in this case is also dependent on M20 bolt (8.8) shear failure, which depicts a brittle response even at an ultimate force lower than the specimen A.
- Specimen C which is similar to specimen A but the internal plate thickness is reduced from 30 mm to 10 mm. This reduction in the thickness of the internal plate lead to a change in failure mode from shear to bearing. In this case the response of the assembly is based on the stainless steel internal plate which depicted according to the material properties, ductile behaviour. Due to the material ductility it provides 62.5 mm dissipation under quasi-static loading whereas, under impact loading the response became stiffer but still facilitated with 45 mm of dissipation.
- In impact test the response of the friction degradation was not appreciable as compared to the quasi-static test, because the initial friction coefficient is considered as the kinetic coefficient. The time period of execution of impact test is very small which does not allow the development of any imminent sticking and slipping behaviour due to which the degradation of friction is also not very clearly visible, instead there is fluctuation of the force-displacement curve during the slippage depicted due to high velocities.
- The failure modes remained unaffected due to transient loading condition. The failure modes depicted under impact loading were similar as depicted in quasi-static conditions however, the failure response became stiffer due to the elevated strain rate.

6 CONCLUSION AND RECOMMENDATIONS

6.1 Conclusion

The present study entails the non-linear dynamic response of dissipative joints exposed to accidental conditions. The friction damper model is used as the "component method" to describe the behaviour of components able to facilitate dissipation to beam-to-column connections. Compared to a complete connection, it is still a kind of intricate model when incorporating dissipation behaviour and preloading in the bolts, thus a suitable approach is developed to assess the response under impulsive loads. This proposition anticipates with this concerned subject by investigating the non-linear behaviour of the friction dampers under quasi-static and impact loads by means of a numerical and analytical (EC-3) approach. Initially, pertinent features are explored and incorporated in a numerical models: i) high strain rate influence on material properties ii) developed a damage model criteria to predict the damage initiation; iii) selection of suitable numerical algorithm to simulate the frictional behaviour along with the preloading application; iv) then, the numerical model is validated against quasi-static and impact loading experimental evidences and finally, v) evaluation of factors that affect the dynamic behaviour of the friction damper are stated.

Developed detail finite element models considering a incorporating the damage model and validated them against quasi-static experimental test results gathered from research project "FREEDAM" carried at the University of Coimbra; the results from the experimental campaign showed that the numerical model is reliable to predict the force-displacement response, displacement capacity and the ultimate resistance. Elevated strain rate effects on the damper are considered following the Johnson-Cook model, established considering the results from Split Hopkinson bar tests performed on mild steel specimens and the initial friction coefficient calculated form the impact test of the dampers carried by (Santos *et al.*, 2017)

The benefit of using implicit and explicit solutions were discussed; taking in account of non-linear dynamic analysis, simulation of complex friction behaviour along with the preloading solution and convergence issue discerned, the explicit methodology to be the most favourable and optimum for the concerned study. The use of an explicit solver removes the numerical singularities with ease and reducing computation costs. However, results obtained using the explicit algorithm also revealed that defining contact algorithm may require delve expertise to obtain a valid solution, which was efficiently dealt.

Furthermore, a comprehensive numerical model was developed for the connection equipped with a friction device using three different material at the friction interface, capable of simulating both the monotonic and impact loading of the connection. The numerical model was validated using the experimental results available and proved capable of providing accurate results. Whereas, the experimental results proved to be very essential in defining the behaviour of damper material and providing friction and bolt properties.

For the friction interface in Abaqus (Abaqus, 2012) static-kinetic exponential decay model was employed by validating the decay factor from the experimental results for each material which led to the degradation of the forces under slip rate simultaneously, to facilitate the applied prestressing thermal gradient technique is used to induce preloading in bolts.

Finally, some general considerations can be made. The possibility of using slip resistance connections could lead to a higher efficiency of present frame structures as no structural parts would suffer damage in the consequence of a severe accident. Elongated slotted holes may be used in the friction devices in order to provide an appreciable dissipative mechanism and avoid the bending mechanism of general joints for abnormal loading conditions. Additionally, the flexural strength obtained for these joints is greater than the plastic resistance of the associated beam, so that, almost full-strength connections can be utilize without any damage to the beam element.

6.2 Future Recommendations

The finite element model of the dissipative joint developed in this work has established to be a reliable resource in evaluation of the non-linear dynamic behaviour of the friction dissipative joints. However, there is still a scope of improvement, that can be achieved through material characterization of all the components, even at elevated rate as well. Particularly the material characterization of the bolts should be done in future in order to accurately simulate the post slippage behaviour. The implemented damage model needs to be refined and considered for all the component failure criterion. Deeper understanding of damage models available in the literature (or development of new) establishing accurate behaviour of mild steel with minimum dependency on the finite element size, could enable finite element models to establish a joint's ductility with reduced cost.

Furthermore, in order to depict the accurate behaviour of dampers, a complete model of the joint equipped with component model of friction damper, needs to be studied. A prototype was developed as part of this study shown in Figure 6.1.
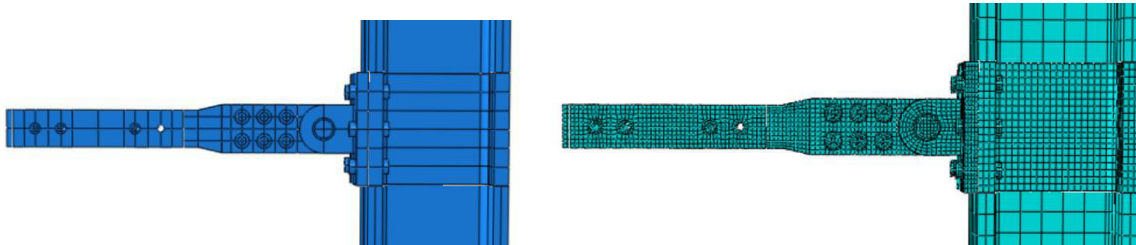
Figure 6.1 – Complete model of joint

There is also a dire need of bolt load to be tested experimentally by introducing load cell in bolts to evaluate the influence of slip on the normal force acting on the sliding surface containing the slotted holes. Long-term tests are also important in terms of evaluating the influence of the relaxation effects that occur over the period of time. These tests should be helpful in deciding the best structural design strategy, that should be adopted to preserve the tightness of the bolts. Naturally, the influence of the adjacent preloaded bolts and of external loads should also be analysed.

Furthermore, the development of an analytical approach to evaluate such joints, capable of addressing the non-linear behaviour of friction dampers under short transient loading, which would be a great asset for the industries and particularly structural engineers in design the structures.

European Erasmus Mundus Master
Sustainable Constructions under natural hazards and catastrophic events
520121-1-2011-1-CZ-ERA MUNDUS-EMMC

ーuーc=ー

REFERENCES

(Abaqus, 2012) Karlsson, & Sorensen, I. U., (2012). *Abaqus Theory Manual, v.6.12.*

(Al-Rifaie *et al.*, 2017) A. Al-Rifaie, Z.W. Guan, S.W. Jones, Q. Wang, Lateral impact response of end-plate beam-column connections, *Engineering Structures* 151 (2017) 221–234

(Anderson, 1995) Anderson, T.L., (1995). *Fracture mechanics: fundamentals and applications. Boca Raton,* FL: CRC Press.

(Arup, 2011) Arup (2011). *Review of international research on structural robustness and disproportionate collapse.* Tech. rep., Department for Communities and Local Government.

(Barata *et al.*, 2014) Barata, P., Santiago, A., Rodrigues, J.P., & Rigueiro, C., 2014, "Experimental behaviour of T-stub component subject to impact loads, *EUROSTEEL 2014*, Naples, 2014.

(Bowden and Leben, 1939) Bowden, F.P. & Leben, L., The nature of sliding and the analysis of friction, *Proc. Roy. S~.* London A 169(1939)

(Bruneau *et al.*, 1998) Bruneau, M., Uang, C. M., and Whittaker, A. [1998] Ductile Design of Steel Structures, McGraw-Hill, New York.

(Bursi & Jaspart, 1998) Bursi, O.S. & Jaspart, J.P., (1998) Basic issues in the finite element simulation of extended end plate connections. *Computers & Structures*, 1998. 69(3): p. 361-382.

(Blok, 1940) H. Blok, Fundamental mechanical aspects of boundary lubrication, *S.A.E. J.* 46(2) (1940) 54-68

(Chang & Tyas, 2011) Chang, L. H., & Tyas, A., (2011). Numerical simulation of steel bolted beam-column connections subjected to dynamic loading. *Applied Mechanics and Materials*, 82, 314-319.

(Cormie and Smith, 2009) Cormie, D. M., & Smith, P., (2009). *Blast Effects on Buildings, 2nd edition.* Thomas Telford.

(Davidson, 2011) Davidson, J., (2011) "Investigating the Robustness of Steel Beam-to-Column Connections," *in 10th International Conference on Steel, Space and Composite Structures*, Cyprus.

(Dias da Silva, 2006) Dias da Silva, V., (2006). *Mechanics and Strength of Materials.* s.l.:Springer-Verlag.

(Diaz *et al.*, 2011) Díaz, C., Victoria, M., Marti, P., and Querin, O. 2011. FE Model of Beam-to-Column Extended End-Plate Joints. *Journal of Constructional Steel Research.* vol. 67, pp. 1578-1590.

(Ellingwood, 2007) Ellingwood, B. S. (2007). *Best Practices for Reducing the Potential for Progressive Collapse in Buildings.* NISTIR 7396.

(EN 1990, 2002) EN 1990, (2002) Eurocode - Basis of structural design. Brussels: European Committee for Standardization.

(EN 1991-1-7, 2006) EN 1991-1-7, (2006). Eurocode 1: Actions on structures. Part 1-7, General actions - Accidental actions. Brussels: European Committee for Standardization

(EN 1993-1-8, 2005) EN 1993-1-8, (2005). Eurocode 3: Design of steel structures Part 1-8: Design of joints. Brussels: European Committee for Standardization

(EN 1993-1-10, 2005) EN 1993-1-10, (2005). Eurocode 3: Design of steel structures Part 1-10: Material toughness and through-thickness properties. Brussels: European Committee for Standardization.

(EN10002-1, 2001) EN10002-1, (2001). Metallic – Tensile testing Part 1: Method of test at ambient temperature, Brussels: European Committee for Standardization.

(Faella et. al., 2000) Faella, C., Piluso, V. & Rizzano, G., Structural Steel Semi-Rigid Connections. Boca Raton: *CRC Press*, 2000.

FEMA 352 [2000] "Recommended post-earthquake evaluation and repair criteria for welded steel moment-frame buildings," Federal Emergency Management Agency, Washington, D.C.

FEMA 350 [2000] "Recommended seismic design criteria for new steel moment-resisting frames," Federal Emergency Management Agency, Washington, D.C.

FEMA 351 [2000] "Recommended seismic evaluation and upgrade criteria for existing welded steel moment-frame buildings," Federal Emergency Management Agency, Washington, D.C.

(FREEDAM, Mid-term Report, 2017) FREEDAM, FREE from DAMage Steel Connections, Mid-term Report, 1st july 2015 – 31st December 2016, University of Salerno, University of Coimbra, FIP Industriale, University of Liege, University of Naples, O Feliz Metalomecanica, March,2017

(Girao Coelho, 2013) Girão, A., (2013). "Rotation capacity of partial strength steel joints with three-dimensional finite element approach", *Computers and Structures*, vol. 116, pp. 88-97

(Girão Coelho and Simões da Silva, 2004) Girão Coelho, A. B., & Simões da Silva, L. (2004). Experimental assessment of the behaviour of bolted T-stub connections made up of welded plates. Journal of Constructional Steel Research, 60, 269-311.

(Grismo *et al.*, 2015) Grismo, E., Clausen, A., *Langseth*, M., and Alberg, A., "An experimental study of static and dynamic behaviour of bolted end-plate joints of steel," *International Journal of Impact Engineering*, vol. 85, pp. 132-45, 2015.

(Grecea et al., 2004) Grecea, D.; Dinu, F.; Dubină, D. (2004). "Performance criteria for MR steel frames in seismic zones". Journal of Constructional Steel Research, Vol. 60, pp.739–749.

(Hilber *et al.*, 1977) Hilber, H.M., Hughes., T.J.R. & Taylor, R.L., (1977). Improved numerical dissipation for time integration algorithms in structural dynamics. Earthquake engineering and structural dynamics, 5, 283-292.

(Hooputra *et al.*, 2004) Hooputra, H., Gese, H., Dell, H., & Werner, H., (2004). A comprehensive Failure Model for Crashworthiness Simulation of Aluminium Extrusions. International Journal of Crashworthiness, 9(5), 449-464.

(Hu et. al., 2012) Hu, J. W., Leon, R.T & Park, T., (2012). Mechanical modelling of bolted T-stub connections under cyclic loads, Journal of Constructional Steel Research, Vol. 78, pp. 45-57, 2012.

(Hutton, 2004) Hutton, D. V., (2004) Fundamentals of Finite Element Analysis, McGraw-Hill.

(Iannone *et al.*, 2011) Iannone, F.; Latour, M.; Piluso, V.; Rizzano, G. (2011). "Experimental Analysis of Bolted Steel Beam-to-Column Connections: Component Identification". Journal of Earthquake engineering, Vol. 15, pp. 214-244

(Inoue *et al.*, 2006) Inoue, K.; Suita, K.; Takeuchi, K.; Chusilp, P.; Nakashima, M.;M.ASCE; Zhou, F. (2006). "Seismic-Resistant Weld-Free Steel Frame Buildings with Mechanical Joints and Hysteretic Dampers". Journal of Structural Engineering, Vol. 132, pp.864–872.

(Izzuddin, 2012) Izzuddin, B., A., (2012) Structural systems analysis for robustness assessment, Department of civil and environmental engineering, Imperial College of London.

(Jaspart, 1991) Jaspart, J., (1991). Etude de la semi-rigidité des noeuds poutre-colonne et son influence sur la resistance des ossatures en acier. Ph.D. dissertation, University of Liége, Belgium.

(Jaspart *et al.*, 1994) Jaspart, J.P. and Maquoi, R. (1994) Prediction if the semi-rigid and partial-strength properties of structural joints, Proceedings of the Annual Technical session, SSRC Lehigh, USA, June 29 1994, pp. 177-192.

(Johnson & Cook, 1983) Johnson, G.R. & Cook, W.H., (1983). A constitutive model and data for metals subjected to large strains, high strain rates and high temperatures. Proceedings of the 7th International Symposium on Ballistics, The Hague, The Netherlands, (pp. 541-547).

(Kishiki *et al.*, 2006) S. Kishiki, S. Yamada, K.Suzuki, E. Saeki, and A. W. (2006). "New ductile Moment-Resisting Connections Limiting Damage to Specific Elements at the Bottom Flange". Proceedings of the 8th U.S. National Conference on Earthquake Engineering, California, Paper No. 852.

(Kloecke *et al.*, 2015) Kloecke, F.; Trauth, D.; Shirobokov, A.; Mattfeld, P. (2015). " FE-analysis and in situ visualization of pressure, slip-rate, and temperature dependent coefficients of friction for advanced sheet metal forming: development of a novel coupled user subroutine for shell and continuum discretization". *Advanced Manufacturing Technology* (author's personal copy).

(Koetaka *et al.*, 2005) Koetaka, Y., Clusilp, P., Zhang, Z., Uno, N. (2005). "Mechanical property of beam-to-column moment connection with hysteretic dampers for column weak axis". Engineering Structures, Vol. 27, pp.109–117.

(Koccaz et al., 2008) Koccaz, Z., Sutcu, F., Torunbalci, N., (2008). "Architectural and structural design for blast resistant buildings". *The 14th world conference on earthquake engineering*, Beijing, China

(Latour *et al.*, 2014) Latour, M.; Piluso, V.; Rizzano, G. (2014). "Experimental analysis on friction materials for supplemental damping devices". *Construction and Building Materials*, Vol. 65, pp.159–176.

(Latour *et al.*, 2015) Latour, M.; Piluso, V. ;Rizzano, G. (2015). "Free from damage beam-to-column joints: Testing and design of DST connections with friction pads". *Engineering Structures*, Vo. 85, pp. 219–233.

(Lemaitre, 1992) Lemaitre, J., (1992). A course on damage mechanics. Berlin/Heidelberg: Springer-Verlag.

(Lemaitre, 2001) Lemaitre, J., (2001). Handbook of Materials Behaviour Models, Vol. I, Deformations of Materials, Academic Press

(Lemos, 2015) Lemos, A. S. S, (2015) Numerical simulation of connections designed for seismic actions, MSC. dissertation, Univ. of Coimbra, Coimbra, Portugal

(Mazzolani and Piluso, 1996) Mazzolani, F. M. and Piluso, V. (1996) Theory and Design of Seismic Resistant Steel Frames, E&FN Spon, London.

(McAllister, 2002) McAllister, T., (2002). *World Trade Centre building performance study: data collection, preliminary observations and recommendations*. Federal Emergency Management Agency, Federal Insurance and Mitigation Administration, Washington, D.C.

(Moore *et al.*, 1999) Moore, K. S., Malley, J. O., and Engelhardt, M. D. [1999] Design of Reduced Beam Section (RBS) Moment Frame Connections, AISC Structural Steel Educational Council, Moraga, CA.

(Newmark, 1959) Newmark, N.M., (1959). A Method of computation for structural dynamics, Journal of the Engineering Mechanics Division, Procedings of the ASCE, pp. 67-94.

(Oh et al., 2009) Oh, S.-H., Kim, Y.-J., & Ryu, H.-S. (2009). "Seismic performance of steel structures with slit dampers". Engineering Structures, Vol. 31, Issue 9, pp. 1997–2008.

(Pilluso & Rizzano, 2008) Piluso, V. & Rizzano, G., (2008). Experimental analysis and modelling of bolted T-stubs under cyclic loads, Journal of Constructional Steel Research, vol. 64, 2008, pp.655-669.

(Ramhormozian & Clifton, 2014) Ramhormozian, S., & Clifton, G. C. (2014). "The Asymmetric Friction Connection with Belleville springs in the Sliding Hinge Joint". Proceedings of the NZSEE Conference.

(Rahbari *et al.*, 2014) Rahbari R, Tyas A, Buick Davison J, Stoddart EP. Web shear failure of angle cleat connections loaded at high rates. J Constr Steel Res 2014; 103:37e48.

(Report for AISC, 1994) Engelhardt MD, Sabol TA, Aboutaha RS, Frank KH. AISC Northridge moment connection test program. Report for AISC, 1994.

(Ribeiro *et al.*, 2014) Ribeiro, J., Santiago, A., and Rigueiro, C., (2014) Assessment of the T-Stub component subject to high strain-rate, Conference: EURODYN'2014 – 9th European Conferece on Structural Dynamics.

(Ribeiro *et al.*, 2105) Ribeiro, J., Santiago, A., Rigueiro, C., and Silva, L. S., (2015) Analytical model for the response of T-stub joint component under impact loading, *Journal of Constructional Steel Research,* 106 23-34.

(Sabuwala *et al.*, 2005) Sabuwala, T. L., & Krauthammer, T., (2005). Finite element analysis of steel beam to column connections subjected to blast loads. *International Journal of Impact Engineering*, 31, 861-876.

(Santos *et al.*, 2017) Santos, A. F., Santiago, A., Silva, S. L., Latour, M., and Rizzano, G. (2017) Experimental assessment of friction dampers under impact loading, Proceedings of EUROSTEEL Conference, Vol. 1, Pages 711-720

(Saraiva, 2012) Saraiva, E., (2012). Variação das propriedades mecânicas do aço relacionadas com problemas de impacto em estruturas. Master's thesis, Master Thesis at University of Coimbra.

(Sterling *et al.*, 1965) G. H. Sterling, J. J. Wallaert and J. W. Fisher, "What happens to bolt tension in large joints?," *Fritz Laboratory Reports,* Vols. Vol. 20, No. 3, 1965.

(Sun, 2006) Sun, E. Q., (2006). Shear locking and hourglassing in MSC Nastran, ABAQUS, and ANSYS., MSC Software

(Swanson & Leon, 2002) Swanson, J.D. & Leon, R., (2002). Advanced finite element modeling of bolted T-stub connection components. Journal of Constructional Steel Research, 58 (5-8), 1015-1031.

(VDI Guideline, 2003) VDI Guideline – Part 1, Systematic calculation of high duty bolted joints – Joints with one cylindrical bolt, *VDI-Handbuch Konstruktion*, Verlag GmbH, Berlin: Beuth, 2003.

(Vegte & Makino, 2004) Vegte, G. J. v. d. and Makino, Y., (2004). Numerical simulations of bolted connections: the implicit versus explicit approach. Connections in Steel Structures V. Amsterdam, Netherlands, pp.89-94, 2005.

(Ronan point, 1968) (Ronan point, London – accidental gas explosion, 1968) http://en.wikipedia.org/wiki/ Ronan_Point

(WTC, 2001) (World Trade Centre Attack, 2001)

https://en.wikipedia.org/wiki/September_11_attacks

Journal manuscript submitted for publication:

Santos, A., F., Santiago, A., Maqbool, U., and Rizzano, G., (2018) Friction dampers subjected to impact loading: Experimental assessment, *Engineering Structures* (Submitted)